Synthesis and Photophysical Properties of Tricarbonyl Rhenium(I) Complexes Having Arylborane Charge Transfer Units

Department of Chemical Sciences and Engineering,
Graduate School of Chemical Sciences and Engineering,
Hokkaido University

Yuanyuan Kang

Contents

Chapter 1. Introduction

1-1 Artificial Photosynthesis

Recently, energy shortage from fossil fuels and pollution of the environments have been the central issues among the important problems we face, and a large number of researchers have been trying to find highly recyclable and durable ways for energy storage and distribution.[1–8] While alternative methods like solar panels, tidal-, wind- or hydroelectric-power plants providing the electric power are already utilized widely, storage and transport of electricity are still difficult and, thus, it does not compete successfully with that from fossil fuels. Therefore, a chemical form of energy carriers is highly desirable as a possible candidate.[5,9–13]

Among various energy sources, solar energy is the only abundant, renewable and environmentally clean energy source available in the earth. It is known that the annual global consumption of energy corresponds roughly to one hour's solar energy that reaches the earth. In other words, if 10% solar energy at 0.3% land surface is converted, it would suffice to exceed the projected energy that needed in 2050.[5] In nature, plants and other organisms successfully convert solar energy into chemical energy mainly as a form of carbohydrate molecules from carbon dioxide and water with oxygen emission as a byproduct.[14] In the system of the natural "photosynthesis", two light-harvesting units, photosystem I (PSI) and photosystem II (PSII), which are principally coupled with hydride addition and water oxidation reactions, respectively, play quite important roles. Scheme 1-1 shows a schematic illustration for electron transport in the natural photosynthesis: so-called Z-scheme.[10] In the Z-scheme, a photon excites chlorophyll P680 in PSII by light absorption and, then, the excited electron is transferred to another

chlorophyll P700 in PSI via electron transfer. The oxidized P680 is reduced to the original form by electron transfer from the oxygen-evolving complex (OEC). On one hand, the excited electron in P700 is also transferred sequentially to other pigments and, finally, reduces $NADP^+$ to NADPH catalyzed by a $NADP^+$ reductase. Multiple cycles of such charge separation reactions result in CO_2 reduction to carbohydrates and oxygen evolution in the natural photosynthesis.[12,15–19]

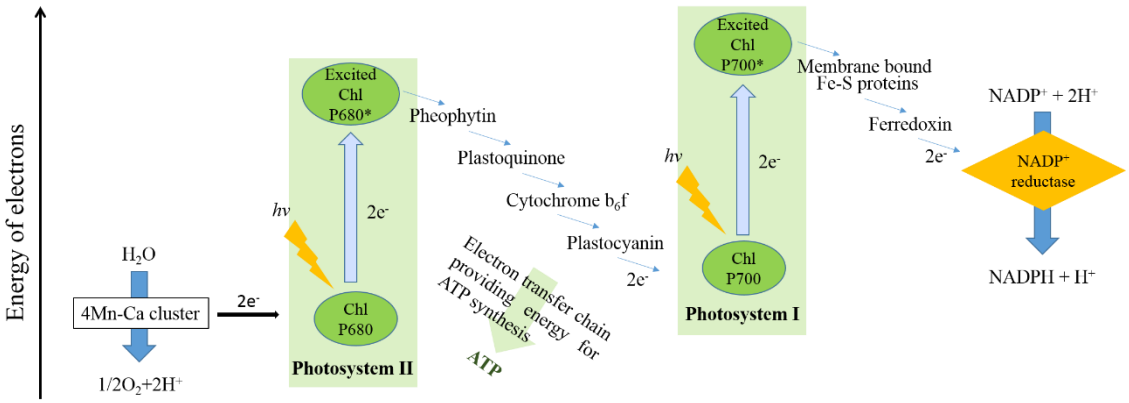

Scheme 1-1 Schematic illustration for the Z-scheme in the natural photosynthesis.

Replicating the concept of the natural photosynthesis artificially is one of our continual and important tasks. The requirement and possibility to achieve "artificial photosynthesis" was first proposed by an Italian chemist, Giacomo Ciamician, in 1912,[20] who proposed a switch from the use of fossil fuels to that of solar energy by technical photochemistry devices. 60-years later, in 1972, the publication by Fujishima and Honda on light-driven water splitting by TiO_2 opened the new research area on artificial photosynthesis.[21] In their paper, an electrochemical cell, in which a TiO_2 electrode was connected with a platinum black electrode through an external circuit, successfully split water into molecular oxygen and hydrogen on TiO_2 and platinum

black electrodes, respectively, under light irradiation with a small external bias. After their report, artificial photosynthesis received much attention by many groups for water oxidation,[22,23] hydrogen evolution,[24,25] CO_2 reduction,[26–29] photoelectrochemical cells[30–32] and so forth.[33–43]

1-1-1 Water Oxidation

Water oxidation is one of the half reactions of water splitting: $2H_2O \rightarrow O_2 + 4H^+ + 4e^-$ (oxidation) and $2H^+ + 2e^- \rightarrow H_2$ (reduction), whose total reaction is $2H_2O \rightarrow 2H_2 + O_2$. In nature, OEC, a metallo-oxo cluster consisting of four manganese and one calcium ions,[44,45] oxidizes water to give molecular oxygen and proton. In the water-oxidation reaction cycle of OEC,[46–48] four electrons are totally brought from water to P680 in PSII. The first well characterized example of a molecular water oxidation catalyst (WOC) was reported by Gersten et al. in 1982[49]: called a ruthenium "blue dimer" whose structure is shown in Scheme 1-2. In the blue dimer, strong electronic coupling between the two ruthenium(II) centers via the oxo group has been known to be the key for water oxidation and rapid oxidation of water can be achieved upon chemical oxidation of the blue dimer: the basis for the catalytic oxidation of water. The mechanisms of water oxidation reported by Meyer et al. in 2007 have revealed that notable features in photosystem II (PSII) are the coupling between proton transfer (PT) and electron–proton transfer (EPT): proton-coupled electron transfer (PCET).[50] These are believed to be the essential elements in water oxidation by the OECs.

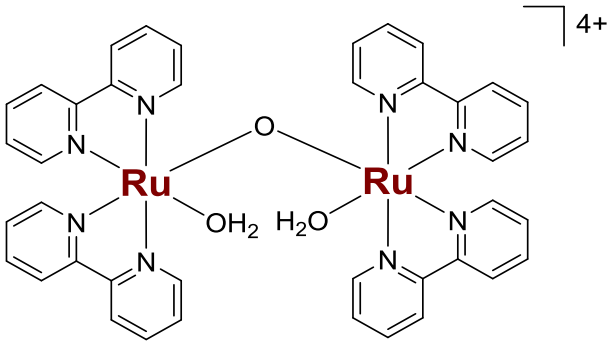

Scheme 1-2 Chemical structure of the ruthenium blue dimer.

After the report on the blue dimer, a large number of WOCs including mononuclear and polynuclear transition metal complexes have been hitherto synthesized.[51–69]

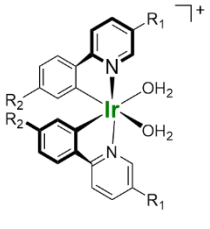

WOC1[51]

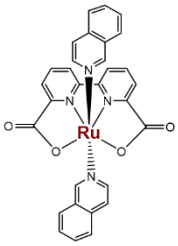

WOC2[52]

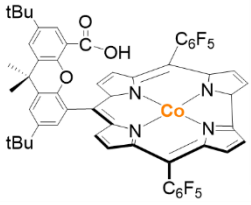

WOC3[53]

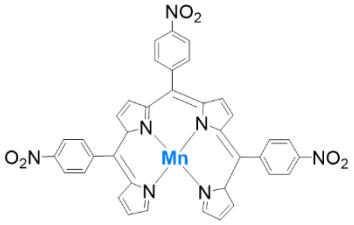

WOC4[54]

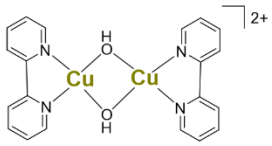

WOC5[55]

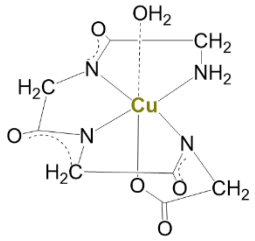

WOC6[56]

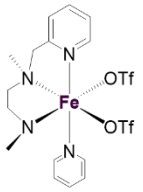

WOC7[57]

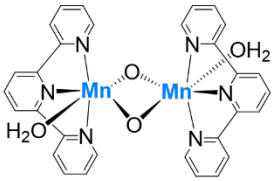

WOC8[58]

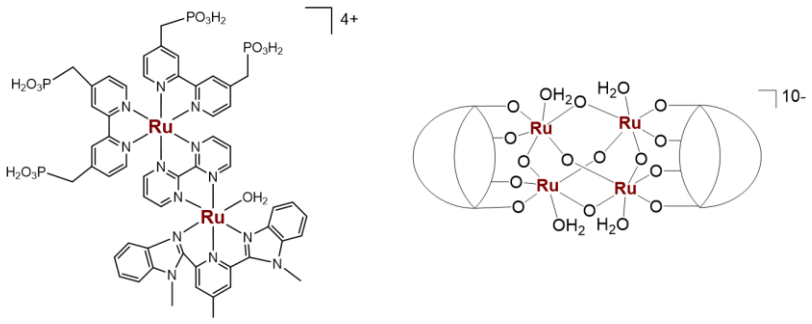

WOC9[59] WOC10[60]

Scheme 1-3 Chemical structures of WOCs based on metal complexes.

It is believed that WOCs with high catalytic abilities and durabilities should possess the following important features: accessibility to higher oxidation states, high thermodynamic energy which associates with the water oxidation process. To complete these features, a class of metal complexes represented by the ruthenium blue dimer and OEC is highly advantageous, since their features are controllable by manipulating the nature of metal centers and/or ligand structures. In practice, a variety of WOCs based on metal complexes shown in Scheme 1-3 have been reported. As a notable example, Duan et al. recently reported that a mononuclear ruthenium catalyst, [Ru(bda)(isoq)$_2$] (WOC2; bda = 2,2'-bipyridine-6,6'-dicarboxulic, isoq = isoquinoline), exhibited a quite good catalytic ability for water oxidation with the turnover frequency (TOF) of 303 s^{-1} in aqueous CF_3SO_3H solutions using a Ce(IV) reagent ($(NH_4)_2[Ce(NO_3)_6]$) as a chemical oxidant.[52] In the catalytic cycle of [Ru(bda)(isoq)$_2$], an initially-formed aquo complex (Ru^{II}–OH_2) is oxidized by the oxidant, followed by twice PCET processes (totally $2e^-$ and $2H^+$ losses) giving the oxo complex (Ru^{V}=O). Then, the peroxo complex (Ru^{IV}–O–O–Ru^{IV}) formed by dimerization of Ru^{V}=O evolves molecular oxygen with recovering Ru^{III}–OH_2.

Light-driven water oxidation was first reported in 1972 by Fujishima and Honda using TiO_2 as described before.[21] After the report, water oxidation has been hitherto extensively studied. As an example, Mallouk et al. have optimized the hybrid system using $IrO_2 \cdot nH_2O$-type nanoparticles as a catalyst and a ruthenium(II) polypyridine complex as a photosensitizer. The rate-determining step of this system is electron transfer between $[Ru(bpy)_3]^{2+}$ (bpy = 2,2'-bipyridine) and surface iridium, which proceeds with the second-order rate constant of 1.3×10^6 $M^{-1}s^{-1}$. In this system, the turnover frequency reaches 160 s^{-1} at a high $[Ru(bpy)_3]^{2+}$ concentration, indicating a possibility to design more efficient systems for photochemical oxygen evolution by using a high local concentration of the sensitizer or increasing the driving force for electron transfer between the sensitizer and the catalyst.[68,69] Following this concept, Puntoriero et al. reported a three-component system composed of WOC10, $[Ru\{(\mu\text{-dpp})Ru(bpy)_2\}_3](PF_6)_8$ (dpp = 2,3-bis(2'-pyridyl)pyrazine) as a photosensitizer and NaS_2O_8 as a sacrificial electron accepter in a buffered (KH_2PO_4) deoxygenated water solution. This system is known to show the highest quantum yield ($\Phi_{O2} = 0.3$) for photochemical oxygen evolution hitherto reported. Furthermore, it has been demonstrated that about 60% of the photons absorbed is used to produce oxygen and 90% of the NaS_2O_8 is consumed, which is also one of the best results so far reported.[60]

1-1-2 Hydrogen Evolution

The reduction of protons into molecular hydrogen is the two-electron process with the reduction potential of $E(H_2O/H_2) = -0.41$ V vs. NHE at pH = 7.[67] While the reaction itself is not necessarily unfavorable thermodynamically, it is disfavored kinetically. Therefore, construction of an efficient hydrogen-evolving system is still an important

research topic. Transition metal complexes have been extensively studied as a possible candidate for a hydrogen evolution catalyst since they can store electrons through multiple redox states.[70–78] The first demonstration of photoinduced hydrogen production was reported in the late 1970s based on $[Ru(bpy)_3]^{2+}$ as a light harvester and platinum colloids as a proton reduction catalyst[79] and, later, Moradpour et al. and Kalyanasundaram et al. reported analogous researches.[80,81] In 1979, Kirch et al. reported that, under visible light irradiation ($\lambda > 400$ nm), the system based on colloidal platinum and $[Ru(bpy)_3]^{2+}$ as a hydrogen evolving catalyst and a photosensitizer, respectively, efficiently produced H_2 in the presence of $[Rh(bpy)_3]^{3+}$ as an electron relay with the TOF of the sensitizer being as high as 10.8 h^{-1}.[82] It was also demonstrated that, even without platinum collides, the analogous system (at pH = 5.2) to that mentioned above also yielded a significant amount of hydrogen with the turnover number (TON) of 6 after irradiation for 3 h. Therefore, it is believed that $[Rh(bpy)_3]^{3+}$ also plays the role as a hydrogen evolving catalyst and the complex is known to be the first molecular photocatalyst for hydrogen evolution. To develop alternative catalysts for generating H_2 with a higher efficiency, other hydrogen evolution systems have been extensively studied as well.[83–91]

Sakai et al. have reported various active photocatalytic hydrogen evolution systems in water using platinum complexes with a nitrogen rich coordination sphere as shown in Scheme 1-5.[92] The best performance has been obtained based on a platinum dinuclear complex shown in Scheme 1-5 and $[Ru(bpy)_3]^{2+}$ as a catalyst and a photosensitizer, respectively, with methyl viologen (MV^{2+}) being used as an electron mediator. The quantum yield of H_2 production of the system has been reported to be as high as 31% with an average TON around 100 under irradiation of visible light.[93]

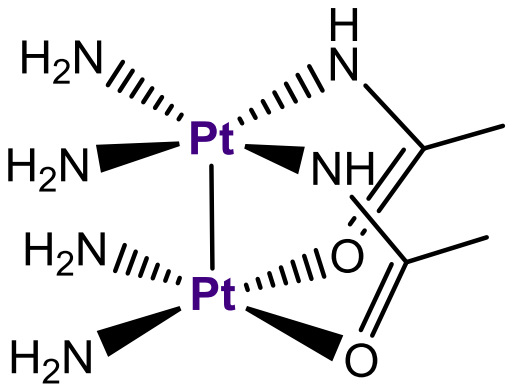

Scheme 1-4 Chemical structure of $[Pt_2(NH_3)_4(\mu\text{-acetamidato})_2]^{2+}$.

In 2014, furthermore, Sakai et al. reported that solar water-reduction processes could be driven by irradiating the metal-to-ligand charge transfer (MLCT) band of $[PtCl_2(bpy)]$ through "Z-scheme" photosynthetic pathways.[24] The photocatalytic H_2 evolution efficiency from water could be improved by the introduction of temporary electron-reservoir sites into the light-harvesting center, which could optimize the "quick recovery of photosensitization capability". These are known to be unique examples of pigment-acceptor–catalyst triads, which provides a new effective artificial photosynthesis system.

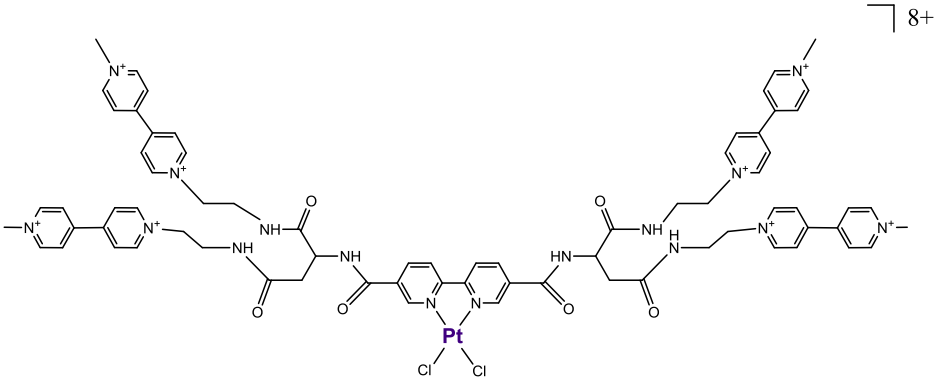

Scheme 1-5 Chemical structure of $[PtCl_2(5,5'\text{-}MV_4)]^{8+}$.

1-1-3 CO_2 Reduction

CO_2 reduction is a quite difficult task since CO_2 is one of the most oxidized carbon compounds. A highly negative potential (E^0 = –1.9 V vs NHE at pH = 7) is required for one-electron reduction of CO_2 to generate active $CO_2^{\bullet-}$ (Eq. (1-1)) due to the rearrangement from the linear to the bent structure, and the products of CO_2 reduction are diverse and depend on experimental conditions: CO, HCOOH, $(COOH)_2$, and so forth.[94,95]

$$CO_2 + e^- \rightarrow CO_2^{\bullet-} \qquad E^0 = -1.9\ V \qquad (1\text{-}1)$$

However, proton-coupled multielectron transfer dramatically decreases the reduction potential and affords stable reduction products: Eqs. (1-2) and (1-3).[96]

$$CO_2 + 2H^+ + 2e^- \rightarrow HCOOH \qquad E^0 = -0.61\ V \qquad (1\text{-}2)$$

$$CO_2 + 2H^+ + 2e^- \rightarrow CO + H_2O \qquad E^0 = -0.53\ V \qquad (1\text{-}3)$$

The research on CO_2 reduction is classified into three major categories: i) photoelectrochemical reduction by semiconductor electrodes, ii) electrochemical reduction by photovoltaic devices, and iii) homogeneous photoreduction by molecular catalysts. Amatore et al. have reported the mechanistic aspects into the selectivity for CO_2 reduction by a semiconductor electrode in water and demonstrated that $HCOO^-$ /HCOOH is the main product of the reaction.[97] Furthermore, it is also reported that CO_2 can be reduced to ethanol and methane on metal electrodes (e.g., Copper), and the selectivity of the product is controllable by the electrode potential.[98,99] After the report, many semiconductor electrodes such as TiO_2, ZnS, CdS, and so on were reported to act as a catalyst for CO_2 reduction.[100–112] For example, Mori et al. studied the CO_2 reduction in H_2O based on several types of titanium oxide and revealed that, under UV-light irradiation, CH_4 was the major product when the reactions were conducted on TiO_2

powders in gaseous CO_2 and H_2O at 275 K, while both CH_3OH and CH_4 were produced by irradiating highly dispersed titanium oxide anchored on a porous glass or ordered porous silica.[113] They also demonstrated that CO_2 reduction in H_2O was governed by the charger transfer excited states of the tetrahedral coordinated Ti-oxide species on the surface as confirmed by *in situ* spectroscopic studies.

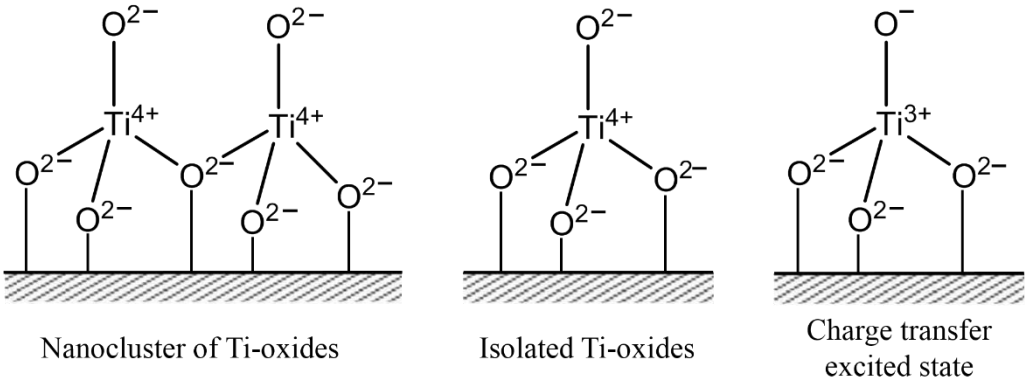

Scheme 1-6 Chemical structures of semiconductor bulk TiO_2 and isolated TiO_2 molecular species.

Furthermore, Habisreutinger et al. have reported CO_2 reduction on TiO_2 and other semiconductors, and pointed out that CO_2 reduction processes proceed only through the adsorbed CO_2 species on TiO_2 or metal co-catalysts due to the negative potential of the one-electron CO_2 reduction.[112] As the result of the negative potential for CO_2 reduction, proton reduction will compete with CO_2 reduction. Moreover, the highly positive potential (+2.94 V, vs. NHE) of the hole in the valence band of TiO_2 will create strong oxidizing species represented by surface trapped holes and $OH^{\bullet}$ radicals. Therefore, sacrificial hole scavengers are in general employed to suppress the re-oxidation reactions. Ishitani et al. also reported for the first time a visible-light-driven

Z-Scheme-type CO_2 photoreduction system composed of a supramolecular metal complex photocatalyst and a semiconductor in the presence of CH_3OH as a sacrificial electron donor.[114] It has been reported that the system produces formic acid and formaldehyde as the main reduction product and the oxidized product of methanol, respectively. In this system, the incident light energy is converted to the chemical energy with the Gibbs free energy of $\Delta G°$ = +83.0 kJ/mol.

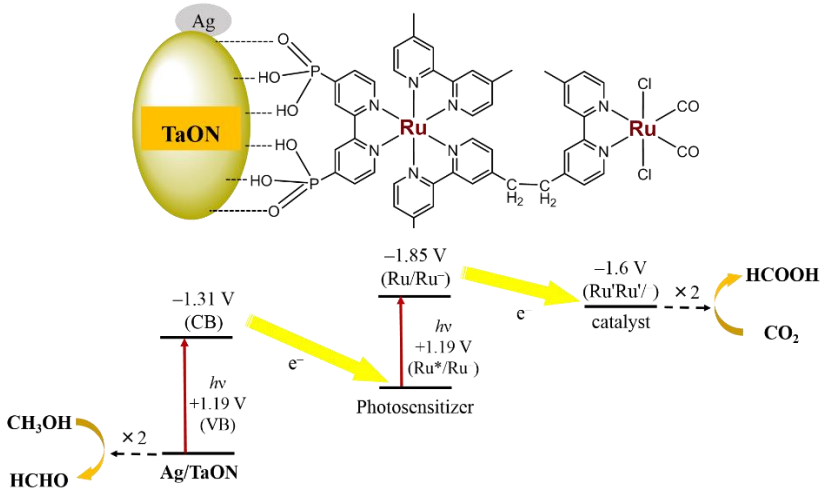

Scheme 1-7 Artificial Z-Scheme-type CO_2 photoreduction system by using a TaON semiconductor.

On the other hand, the most notable electrocatalysts for CO_2 reduction include iron porphyrines,[115] tetraazomacrocyclic complexes,[116] and palladium phosphines as shown in Scheme 1-8.[117] For example, Raebiger et al. reported a new bimetallic palladium complex, $[\{m\text{-(triphos)}_2\}Pd(CH_3CN)_2](BF_4)_4$ (m-(triphos)$_2$ = m-$C_6H_4\{P[CH_2CH_2P(C_6H_{11})_2]_2\}_2$) as a catalyst for electrochemical CO_2 reduction, and demonstrated that the transition state of the complex was composed of one palladium, one CO_2 molecule, and one or two proton as revealed by kinetic studies. As a result, the

two palladium atoms of the complex work independently during the catalytic cycle. Nonetheless, this complex exhibited the highest turnover number among this class of catalysts, due to the steric constraints of the cyclohexyl substituents.

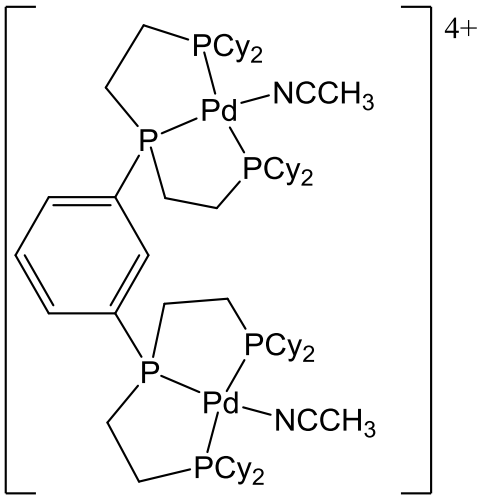

Scheme 1-8 Chemical structure of $[\{m\text{-(triphos)}_2\}Pd(CH_3CN)]_2\}]^{4+}$.

Owing to the low quantum yields and low selectivity of the products in photoelectrochemical and electrochemical CO_2 reduction systems, photochemical CO_2 reduction using transition metal complexes is an attractive alternative. The first photochemical CO_2 reduction was reported by Lehn et al. using $CoCl_2$ and $[Ru(bpy)_3]^{2+}$ as a catalyst and a photosensitizer, respectively.[94] Their system in water with the CO_2 photoreduction quantum yield of 0.012 gave CO and H_2 as the products in the presence of triethanolamine (TEOA) as a sacrificial electron donor. After the report, a lot of photochemical CO_2 reduction systems utilizing transition metal complexes including Ru(II),[118] Re(I), Co(II),[119–121] Mn(I),[122] and Ir(II)[123] have been hitherto reported.

Lehn et al. also reported photochemical reduction of CO_2 to formic acid in a $[Ru(bpy)_3]^{2+}$–TEOA system and demonstrated that the photoreaction generated an

active catalytic Ru(I) intermediate, in which one of the three bpy ligand in $[Ru(bpy)_3]^{2+}$ dissociated upon photoinduced electron transfer with TEOA. The efficiency of formic acid formation in this system is dependent on the presence or absence of both water and an excess ligand. It has been also pointed out that two catalytic cycles are involved in the CO_2 reduction system: a photoredox cycle of $[Ru(bpy)_3]^{2+}$ and a dark dissociation/association cycle of bpy with the ruthenium ion.[124]

For further improvement of the excitation–reaction processes, dyad-type multinuclear complexes, which contains both photosensitizing and catalyzing complexes in a molecule, have been developed.[125–131] As a notable example, Ishitani et al. developed "supramolecular" photocatalysts composed of two kinds of Ru(II) complexes at several Ru(II)-Ru(II)' ratios to conduct photochemical CO_2 reduction, producing formic acid with relatively high selectivity and durability.[132,133] The catalyst and photosensitizer Ru(II) unit ratio has been reported to influence strongly the photocatalytic ability of the system. At a higher photosensitizer unit ratio, the compound **1** ($[\{(dmb)_2Ru(bpyC_2bpy)\}_2Ru(CO)_2]^{6+}$, dmb = 4,4'-dimethyl-2,2'-bipyridine) shown in Scheme 1-9 is known to exhibit the highest photocatalytic activity for formic acid formation: Φ_{HCOOH} = 0.061, TON_{HCOOH} = 671, and TOF_{HCOOH} = 11.6 min^{-1}. The CO_2 photoreduction processes are composed of 1) photoexcitation of the photosensitizer unit, 2) reductive quenching of the excited state of the photosensitizer unit by an electron donor, 3) electron transfer from the one-electron reduced photosensitizer unit to the catalyst unit, and 4) dark reaction of the one-electron reduced catalyst unit with CO_2. The formation of formic acid from CO_2 is the two electron reduction process and, thus, need two one-electron reduced catalyst species, which is the key of the reaction system.

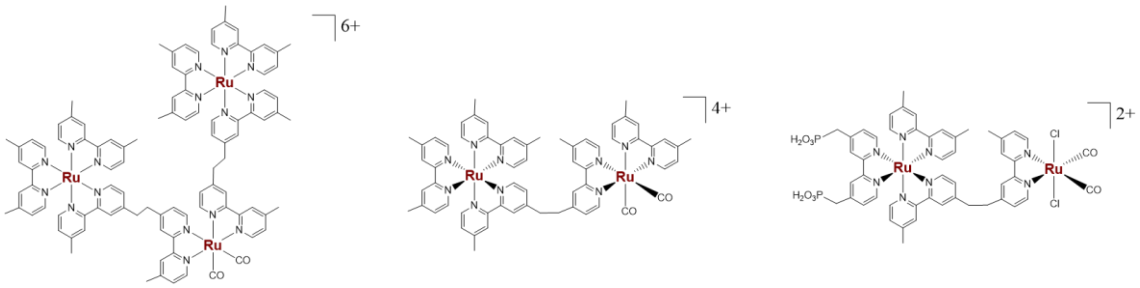

1[132] **2**[132] **3**[133]

Scheme 1-9 Chemical structures of supramolecular photocatalysts.

1-2 Tricarbonyl Rhenium(I) Complexes

Among various transition metal complexes, tricarbonyl rhenium(I) complexes having an aromatic diimine ligand, $[Re(CO)_3LX]$ (L = diimine and X = halogen, imine or trialkylphosphine), have attracted much attention due to the unique spectroscopic, photophysical[134–142] and photoredox properties, including the photocatalytic ability to CO_2 reduction.[130,143–151] As an example, a typical tricarbonyl rhenium complex, $[Re(phen)(CO)_3Cl]$ (phen = 1,10-phenanthroline), is known to be one of the earliest complexes that have been synthesized and reported for its physicochemical properties.[152] Detailed studies on the photophysical and photochemical properties of $[Re(phen)(CO)_3Cl]$ and the related complexes such as $[Re(bpy)(CO)_3X]$ (X = Cl^- or Br^-) have been reported after the paper by Hieber et al. The absorption bands of this kind of complexes in the wavelength region of 350–450 nm have been identified as the metal-to-ligand charge transfer (MLCT) transitions by which the electron in the metal-centered dπ-orbital transfers to the vacant ligand-centered π*-orbital: $d\pi^6 \rightarrow d\pi^5\pi^{*1}$.[153] Furthermore, $[Re(CO)_3LX]$ is known to exhibit typical and excellent excited triplet MLCT (^{3}MLCT) photoluminescence properties, which is used as a triplet emitter

as well.[134,154–158]

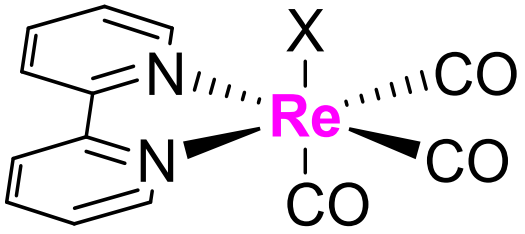

Scheme 1-10 Chemical structure of $[Re(bpy)(CO)_3X]$ (X = Cl or Br).

Photoreduction of CO_2 by a tricarbonyl rhenium(I) complex was first reported for $[Re(bpy)(CO)_3X]$ (Scheme 1-10) by Lehn et al. in 1983 in the presence of a reducing agent, TEOA, in *N*,*N*-dimethylformamide (DMF). The quantum yield of CO formation by using $[Re(bpy)(CO)_3X]$ was determined to be 0.14 (X = Cl), which was the highest efficiency for CO_2 photocatalytic reduction at that time.[118] It is known that tricarbonyl rhenium(I) complexes can act as a photosensitizer as well as a catalyst, and show high efficiency and selectivity for CO production.

After the first report by Lehn et al., the mechanistic studies on CO_2 photoreduction by laser photolysis techniques have been conducted for many years.[151,154–161] These studies demonstrated that the excited triplet (^{3}MLCT) state of a tricarbonyl rhenium(I) complex was reductively quenched by TEOA to form the one-electron reduced species (OERs) of the complex. It takes several seconds for the dissociation of the X ligand from the OERs, producing the so-called "17-electron species". It has been reported by Fijita et al. in 2003 that the coordination unsaturated $[Re(dmb)(CO)_3]$, which is generated by the dissociation of the Cl^- ligand from $[Re(dmb)(CO)_3Cl]$,, can react with CO_2 with an extremely slow rate: $k_{obs} \approx 0.003$ s^{-1} under 0.8 atm of CO_2 in tetrahydrofuran (THF).[162] The reason for the slow CO_2 reaction rate is supposed to be

the localization of the excited electron in the bpy ligand to form $Re^{I}(4,4'\text{-}Me_2bpy^{\bullet-})(CO)_3$, which differs electronically with the electronic state of $[Re^{0}(4,4'\text{-}Me_2bpy)(CO)_3]$. The roles of an anionic ligand (X) in photocatalytic CO_2 reduction by a tricarbonyl rhenium(I) complex were also investigated by Ishitani et al. in 2008.[28] Among three tricarbonyl rhenium(I) complexes, $[Re(bpy)(CO)_3X]$ (X = Cl^-, SCN^- and CN^-), the photocatalytic ability of the complex is quite different with one another, although these complexes show similar photophysical and electrochemical properties. In practice, the complex with an SCN^- ligand shows the highest photocatalytic ability for CO_2 reduction (Φ_{CO} = 0.20 and TON_{CO} = 30), while the CN^- complex cannot act as a photocatalyst. During the investigation on the photochemical production and reactivity of OERs, they found that the OERs produced by photoinduced electron transfer from TEOA to the ^{3}MLCT state of $[Re(bpy)(CO)_3X]$ played two crucial rules: one is the loss of the X ligand to give the precursor of the "17-electron species", which reacts with CO_2 to form a CO_2 adduct with the complex and another is to provide the second electron to the CO_2 adduct of the complex. The different OERs stability between the three complexes and the balance between the two roles mentioned above would explain the different photocatalytic abilities of the three complexes. In practice, the OERs of the CN^- complex is too stable to lose the CN^- ligand, which prevents the following reaction with CO_2, while that of the SCN^- complex is more stable and shows better balance as the reaction intermediate between the precursor of the "17-electron species" and the second electron source compared to that of the Cl^- complex, resulting in the high photocatalytic efficiency for CO_2 reduction.

The mechanisms of CO_2 reduction by $[Re(bpy)(CO)_3X]$ are summarized as follows: see also Scheme 1-11.

1) Photoexcitation of the complex.

2) Reductive quenching of the lowest-energy excited triplet state of the complex by an electron donor (TEOA) to generate OER.

3) Dissociation of the X ligand from the OER to give the "17-electron species", which is a crucial step in the photocatalytic reaction. The proposed structure of the "17-electron species" is $[Re^{I}(bpy^{\bullet -})(CO)_3]$.

4) Coordination of CO_2 to the "17-electron species" to give a CO_2 adduct.

5) Reduction of CO_2 to CO by electron donation from another OER to the CO_2 adduct and simultaneous re-coordination of the X ligand to the Re ion.

According to these backgrounds, it is readily understood that the efficiency of each reaction step should be optimized to realize more efficient photocatalytic systems.

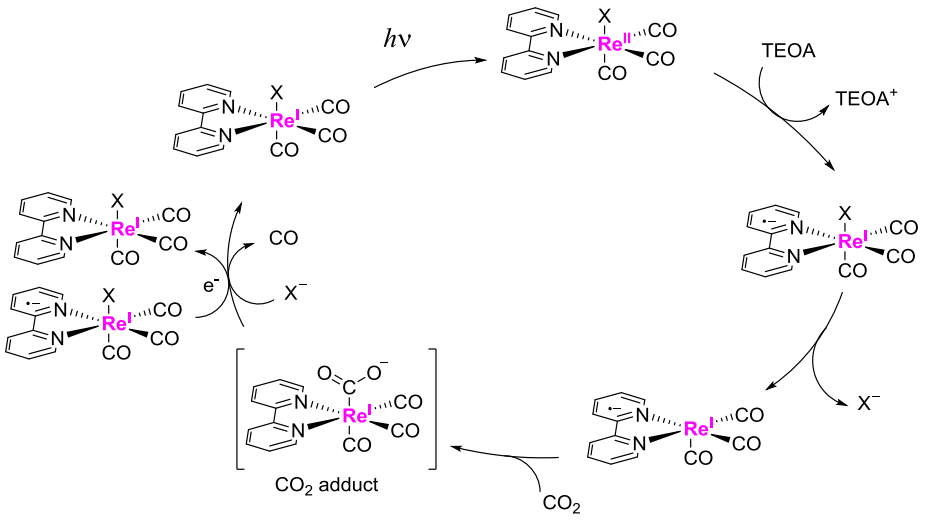

Scheme 1-11 Reaction mechanisms of photocatalytic CO_2 reduction by $[Re(bpy)(CO)_3X]$.

Recently, Sahara et al. reported some efficient photocatalysts for CO_2 reduction.[151] As an example, they developed an efficient photocatalytic system using a ring-shaped

rhenium(I) trinuclear complex (Scheme 1-12) and $[Re(bpy)(CO)_3(MeCN)]^+$ as a redox photosensitizer and a catalyst, respectively. The trinuclear rhenium(I) complex showed characteristic properties such as strong absorption in the visible region, long excited triplet state lifetime and high stability of the OERs, which are all advantageous for the photocatalytic CO_2 reduction. Owing to such properties, the molecular system shows the highest quantum efficiency for CO_2 reduction: Φ_{CO} = 0.82 at λ^{ex} = 436 nm and TON_{CO} = 526.

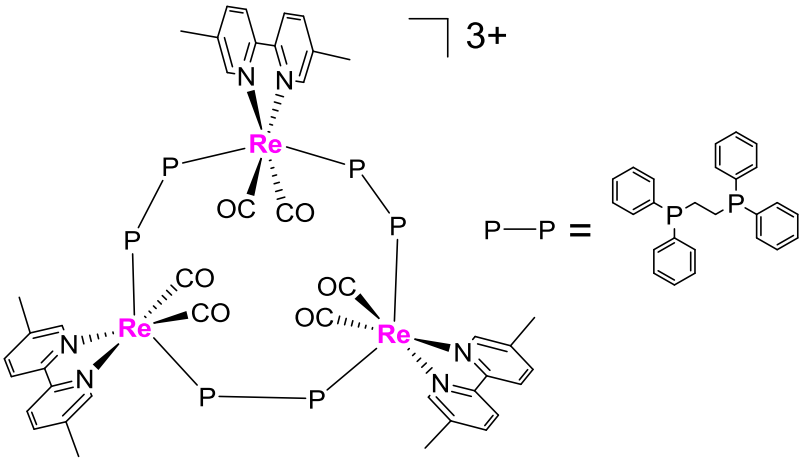

Scheme 1-12 Chemical structure of ring-shaped trinuclear rhenium(I) complex.

The excited-state decay processes of a tricarbonyl rhenium(I) complex are dominated by ligand dissociation in a fluid solution and, ligand and solvent environments also influence the excited-state properties of the complex. Since the MLCT excited-state energy and the redox properties of the complex are very sensitive to a coordinated ligand(s) as well as to a solvent because of the asymmetric structure of the complex, chemical modification and derivatization of the complex are of primary importance for the development of more efficient photocatalytic reaction systems.

On the basis of these backgrounds, transition metal complexes having an arylborane charge transfer unit(s) have been hitherto studied. These complexes are known to show intense light absorption and long-lived excited states, compared to the relevant reference complex without a triarylborane unit. Therefore, the transition metal complexes with an arylborane-appended ligand(s) are worth studying in detail.[28]

1-3 Triarylborane Derivatives

For chemical modifications and functionalization of transition metal complexes, triarylborane groups have received wide interests. Boron is a representative element sit on the left side of carbon in the periodic table. Generally, an organoborane complex is not stable when exposed to air or in solution. However, as a trivalent boron-containing organic compound, boronic acids with an alkyl or aryl substituent (e.g. a C–B bond) and two hydroxyl groups are quite stable against air or solvent.[163] Frankland et al. first reported preparation and isolation of a boronic acid in 1860.[164–166] After the report, arylboronic acid derivatives have been also studied extensively. The X-ray crystal structure of phenylboronic acid was reported by Rettig et al. in 1977.[167] The work has demonstrated that the C-B-O_2 plane of the compound is coplanar with the benzene ring, which is explained by the stabilization of the vacant p-orbital on the boron atom due to the presence of the lone-pair electron on the oxygen atom in the hydroxyl group as well as of the π-orbital of the aryl group.

When a boron atom is connected with relatively large aromatic chromophores, the compound is also known to be quite stable and it is known that boron-containing systems, represented by three-coordinated boron compounds,[168–184] show characteristic absorption and fluorescence owing to the presence of the vacant p-orbital on the boron

atom (p(B)).[185,186] As an example, Ramsey et al. reported the spectroscopic properties of several triarylborane derivatives and demonstrated that the absorption bands of triarylboranes having various π-electron chromophores (aryl = phenyl, tolyl, mesityl or naphthyl group) were shifted to the lower energy, whose spectral shifts correlated linearly with the decreasing order of the ionization potential of the aryl group.[187] The absorption band appeared in the complex can be thus assigned to an intramolecular charge transfer (CT) transition.[187–192]

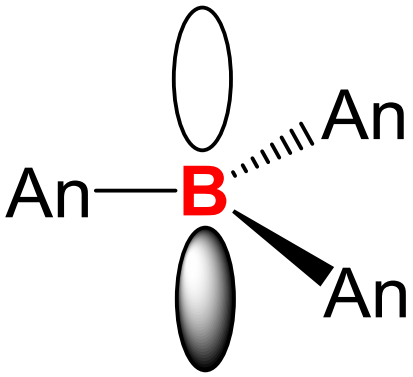

Scheme 1-13 Schematic representation of triarylborane.

After the report by Ramsey et al., synthetic works on organoborane derivatives have been frequently reported, while spectroscopic studies on the compounds have been scarcely reported. In 2000, Yamaguchi et al. have reported the synthesis and preliminary results on the spectroscopic properties of tri-9-anthrylborane (**TAB**, see Figure 1-1),[189,193–196] which shows characteristic spectroscopic and photophysical properties in solution.[189] As seen in Figure 1-1, **TAB** in solution exhibits broad and intense absorption at around 470 nm (Band I) at room temperature in addition to the structured anthracene-like band (Band II) in the wavelength region of 330–380 nm. Moreover, **TAB** shows broad and structureless fluorescence in the wavelength region of 480–650 nm. Anthracene and its derivatives are well known to show structured

absorption and fluorescence spectra at around 330–380 and 380–480 nm, respectively. Therefore, the new absorption band (Band I) and the structureless red-shifted fluorescence for **TAB** are quite interested. According to the theoretical calculations by Yamaguchi et al., band I of **TAB** is ascribed to the electronic charge transfer (CT) transition from the π-orbital of the anthryl group (HOMO) to the vacant p-orbital on the boron atom (LUMO): π(aryl)-p(B) CT.[194] Later, Kitamura et al. demonstrated the spectroscopic and excited-state properties of **TAB** in both solution and solid state in detail.[197–199] The studies have demonstrated that the characteristic absorption (Band I) and fluorescence spectra of **TAB**, which are completely different from those of anthracene, are due to the electronic transition between the ground and CT excited states. The excited state of **TAB** is primarily localized on p(B), which plays an essential role in determining the spectroscopic and excited-state properties of the compound.

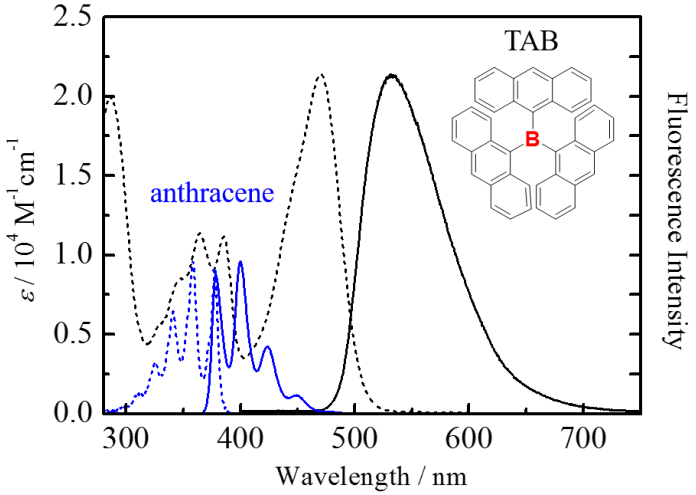

Figure 1-1 Absorption (broken curves) and fluorescence (solid curves) spectra of **TAB** (black; insert structure) and anthracene (blue) in THF.

Other π-conjugated triarylborane derivatives have also attracted much attention. Recently, Ito et al. have reported that the spectroscopic and photophysical properties of triarylborane derivatives can be controlled easily by the nature of both triarylborane core and peripheral electron-donating groups. By a combination of a triarylborane core and an electron-donating group, novel triarylborane derivatives showing π(aryl)-p(B) CT absorption/fluorescence in a wide visible wavelength region have been realized (Scheme 1-14).[200]

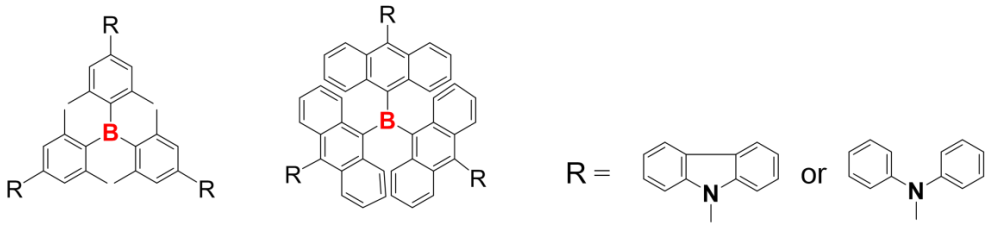

Scheme 1-14 Chemical structure of triarylborane derivatives with electron-donating groups.

On the other hand, Poon et al. have synthesized a series of dithienylethene-containing triarylboranes and reported that the novel triarylborane-containing dithienylethene systems show abundant photochromic and photophysical properties on the basis of the rational design of the molecular structure and the control of the chemical or structural environments around the boron(III) center.[201] Similarly, other triarylborane derivatives have also been reported,[201–207] aiming at anion sensors,[194,208–212] ion/electron-conduction,[213–217] light-emitting,[218–222] optoelectronic[223,224] and nonlinear optical materials.[225–230]

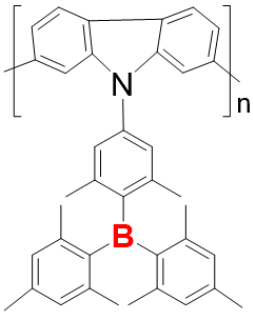

1[204]

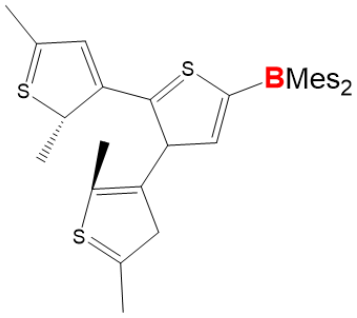

2[206]

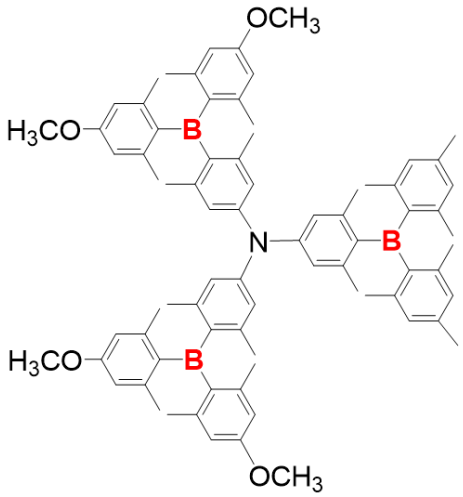

3[185]

Scheme 1-15 Chemical structures of triarylborane derivatives.

1-4 Transition Metal Complexes Having Arylborane Charge Transfer Units

Polypyridine d^6 transition metal complexes have received intense research interests due to their characteristic MLCT absorption and phosphorescence.[231–235] Since the spectroscopic and photophysical properties of transition metal complexes are highly dependent on the electron-donating or accepting ability of the ligand,[153,236–242] synthetic controls of their properties have been explored by an introduction of an arylborane

charge transfer unit(s) in the periphery of the ligand(s). In such a complex, the π(aryl)-p(B) CT characters of the arylborane charge transfer unit are expected to synergistically interact with the MLCT excited state of the transition metal complexes, leading to new and novel spectroscopic/photophysical properties of the complex.

In practice, Sakuda et al. have reported for the first time the introduction of a (dimesityl)phenylborane group to the 4'-position of a 2,2':6',2''-terpyridine (tpy) platinum (II) complex, $[Pt(Btpy)Cl]^+$, which shows unique spectroscopic and photophysical properties. The relatively intense room-temperature emission (Φ^{em} = 0.011) and long lifetime (τ^{em} = 0.6 μs) of $[Pt(Btpy)Cl]^+$ in solution are quite fascinating since the relevant complex without an arylborane group, $[Pt(tpy)Cl]^+$ is non-luminescent at room temperature in solution, revealing the important role of the synergistic interactions between MLCT and π(aryl)-p(B) CT in determining the excited-state properties of the complex. Furthermore, the transition dipole moment of MLCT absorption is also enhanced obviously for $[Pt(Btpy)Cl]^+$ compared to that of the reference complex.[243]

After the first report on $[Pt(Btpy)Cl]^+$, a variety of transition metal complexes bearing an arylborane unit(s) on the ligand have been reported: Pt(II),[244,245] Ir(III),[246–248] Ru(II),[249,250] Re(I)[251,252] and Cu(I)[253,254] and so forth.[255]

Moreover, the ruthenium(II) complex with a (dimesityl)boryldurylethynyl (DBDE) group at the 4-position of a 1,10-phenanthroline (phen) ligand (**4RuB^{2+}**) has been reported to show low-energy (λ^{em} = 681 nm and $\tilde{\nu}^{em}$ = 14700 cm^{-1}) and extremely long-lived emission (τ^{em} = 12 μs in CH_3CN at 298 K). As the characteristics of the complex, **4RuB^{2+}** exhibits temperature-independent emission lifetimes (τ^{em} = 10.7–9.8 μs at 280–330 K), which has been explained by the stabilization of the emissive triplet

MLCT excited state by the synergistic interactions with π(aryl)-p(B) CT and subsequent suppression of excited state decay via thermally-activated paths in the MLCT state.[256]

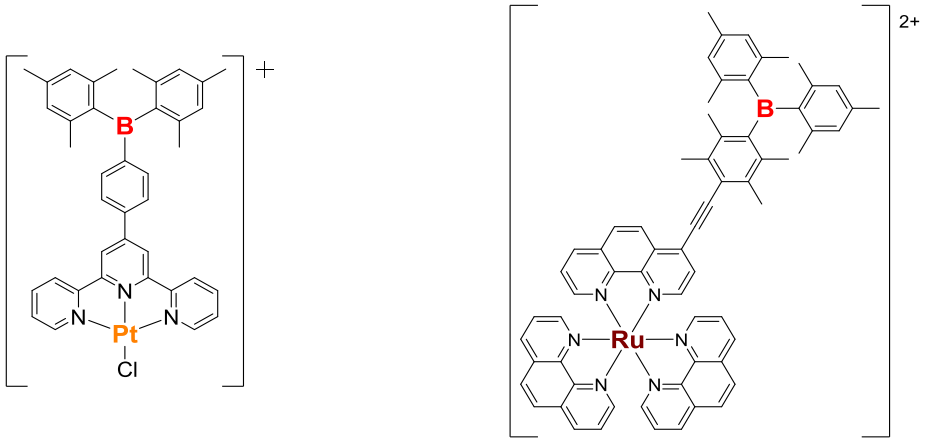

[Pt(Btpy)Cl]$^{+}$ **4RuB^{2+}**

Scheme 1-16 Chemical Structures of **[Pt(Btpy)Cl]$^{+}$** and **4RuB^{2+}**.

These discussions indicate that the spectroscopic, photophysical and photochemical properties of a transition metal complex can be manipulated by an introduction of an arylborane charge transfer unit(s) to the periphery of the ligand. Among various transition metal complexes, nonetheless, the research on the Re(I) complex with an arylborane charge transfer unit(s) is very limited.[142,242,257] In particular, the photochemical properties of the Re(I) complex with an arylborane group(s),[242] including the photocatalytic CO_2 reduction ability of the complex, have not been hitherto studied. To obtain detailed insights into the structure-property relationship of $[Re(CO)_3LX]$ and to discuss the effects of the diimine ligand structure and the presence/absence of an arylborane charge transfer unit(s) on the photophysical and photochemical properties, synthetic and physicochemical studies on a series of

rhenium(I) complexes having an arylborane-appended ligand(s) are absolutely necessary, which is the main target of the present study as described below.

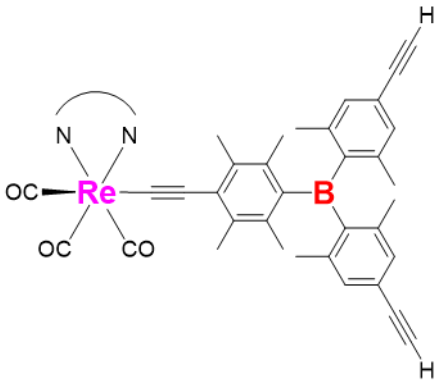

 = 2,9-Me_2phen, phen or 5,6-Br_2phen

Scheme 1-17 Chemical structure of a tricarbonyl rhenium(I)-arylborane complex.[257]

1-5 Purposes and Contents of the Thesis

A tricarbonyl rhenium(I) complex having an aromatic diimine ligand, $[Re(CO)_3LX]$ (L = diimine and X = halogen, phosphine or imine) has been studied extensively since the complex is expected to apply to electroluminescence devices, emissive superamolecules and photocatalysts for CO_2 reduction and so forth. One of the notable features of the complex among its characteristics mentioned above is the ability to photocatalytic reduction of CO_2. It has been known that the photocatalytic CO_2 reduction ability by $[Re(CO)_3LX]$ is controllable by the electronic structures of the complex. Furthermore, the ground- and excited-state properties of $[Re(CO)_3LX]$ are very sensitive to the coordinating ligand(s) (L and/or X) as well as the microenvironments around the complex. Therefore, chemical modifications and derivatizations of $[Re(CO)_3LX]$ are extremely important for further development of an efficient photocatalytic CO_2 reduction system. For synthetic modulation of the

excited-state properties of $[Re(CO)_3LX]$, the electronic structures of triarylborane compounds are very attractive. Triarylborane compounds show characteristic spectroscopic and photophysical properties owing to the intramolecular charge transfer transition between the π-orbital of the aryl group (π(aryl)) and the vacant p-orbital on the boron atom (p(B)) (π(aryl)-p(B) CT) as described above. Furthermore, an introduction of a triarylborane(s) to a transition metal complex leads to characteristic spectroscopic and photophysical properties of the complex by the synergistic MLCT/π(aryl)-p(B) CT interactions as demonstrated by **[Pt(Btpy)Cl]**$^+$ and **4RuB**$^{2+}$: see Scheme 1-16.

In this study, four novel tricarbonyl rhenium(I) complexes having one or two (dimesityl)borylduryletheynyl (DBDE) group(s) in a 1,10-phenanthroline (phen) or 2,2'-bipyridine ligand were designed/synthesized, and the spectroscopic, photophysical, and photoredox properties of the complexes were evaluated in detail. Photoreduction of CO_2 by these complexes was also studied. By introduction of the DBDE group(s), the novel complexes are expected to be the candidates for an efficient photocatalytic CO_2 reduction system.

The thesis consists of five chapters as briefly described below.

In Chapter 1, the research background and purpose of the thesis are described. As the key aspects into the present study, the essence of the chemistry of artificial photosynthesis, tricarbonyl rhenium(I) complexes, triarylborane derivatives and transition metal complexes having an arylborane charge transfer unit(s) are overviewed.

In Chapter 2, systematic studies on triarylborane substitution and diimine ligand structure effects on the spectroscopic and photophysical properties of the two novel

rhenium(I) complexes having one arylborane charge transfer unit, **ReBphen** and **ReBbpy**, are described. On the basis of the spectroscopic and photophysical studies, it is demonstrated that the introduction of the arylborane charge transfer unit to the periphery of the ligand brings about low-energy/intense absorption and low-energy/long-lived emission compared to the absorption/emission characteristics of the reference complexes without a triarylborane group. According to the theoretical calculations, the substitution position of a triarylborane unit in a diimine ligand is shown to play essential roles in governing the photophysical characteristic of $[Re(CO)_3LBr]$.

In Chapter 3, the detailed spectroscopic and photophysical properties of the two novel rhenium(I) complexes having two arylborane charge transfer units, **ReB_2phen** and **ReB_2bpy**, are described and the effects of the number of the arylborane unit in the complex are discussed for a series of **ReB_2phen/ReBphen/Rephen** and **ReB_2bpy/ReBbpy/Rebpy**. It was shown that the introduction of the multiple arylborane units to the complex resulted in further enhancement of the absorption intensity and the molar absorption coefficient of the MLCT band compared to the complex with a single arylborane unit, which was suggested to be favorable for photocatalytic CO_2 reduction.

In Chapter 4, the photocatalytic CO_2 reduction abilities of all of the novel complexes are evaluated. With the increase in the number of the arylborane unit in the complex, the emission quenching rate constants of the complexes by TEOA increased. Nevertheless, unfortunately, the CO_2 photoreduction abilities of **ReB_2phen/ReBphen** and **ReB_2bpy/ReBbpy** were not necessarily high enough compared to those of **Rephen** and **Rebpy**, respectively. The possible reasons for this were discussed.

In Chapter 5, the conclusions and future perspective of the study are summarized.

1-6 References

1. D. Pimentel, G. Rodrigues, T. Wang, R. Abrams, K. Goldberg, H. Staecker, E. Ma, L. Brueckner, L. Trovato, C. Chow, U. Govindarajulu and S. Boerker, *BioScience* **1994**, *44*, 536–547.
2. D. Pimentel, *J. Agr. Environ. Ethic.* **1991**, *4*, 1–13.
3. I. Dinver, *Renew. Sustainable Energy Rev.* **2000**, *4*, 157–175.
4. A. Demirbaş, *Energy Convers. Manage.* **2003**, *44*, 203–213.
5. N. S. Lewis and D. G. Nocera, *Proc. Natl. Acad. Sci. U. S. A.* **2006**, *103*, 15729–15735.
6. R. J. Cogdell, *Trends Plant Sci.* **2006**, *11*, 59–60.
7. A. M. Omer, *Renew. Sustainable Energy Rev.* **2008**, *12*, 2265–2300.
8. D. B. Botkin, E. A. Keller and D. B. Rosenthal, *Environ. Sci. Wiley* **2012**.
9. M. R. Wasielewski, *Chem. Rev.* **1992**, *92*, 435–461.
10. Y. Amao, *ChemCatChem.* **2001**, *3*, 458–474.
11. J. H. Alstrum-Acevedo, M. K. Brennaman and T. J. Meyer, *Inorg. Chem.* **2005**, *44*, 6802–6827.
12. S. Berardi, S. Drouet, L. Francàs, C. Gimbert-Surinach, M. Gutentag, C. Richmond, T. Stoll and A. Llobet, *Chem. Soc. Rev.* **2014**, *43*, 7501–7519.
13. A. Mishra and P. Bäuerle, *Angew. Chem. Int. Ed.* **2012**, *51*, 2020–2067.
14. D. A. Bryant and N. -U. Frigaard, *Trends Microbiol.* **2006**, *14*, 488–496
15. D. Gust and T. A. Moore, *J. Photochem.* **1985**, *29*, 173–184.

16. A. Kay and M. Grätzel, *J. Phys. Chem.* **1993**, *97*, 6272–6277.

17. N. Wakao, N. Yokoi, N. Isoyama, A. Hiraishi, K. Shimada, M. Kobayashi, H. Kise, M. Iwaki, S. Itoh and S. Takaichi, *Plant Cell Physiol.* **1996**, *37*, 889–893.

18. J. Barber, *Biochim. Biophys. Acta Bioenerg.* **1998**, *1365*, 269–277.

19. H. Zhou, X. Li, T. Fan, F. E. Osterloh, J. Ding, E. M. Sabio, D. Zhang and Q. Guo, *Adv. Mater.* **2009**, *22*, 951–956.

20. G. Ciamician, *Science* **1912**, *36*, 385–394.

21. A. Fujishima and K. Honda, *Nature*, **1972**, *238*, 37–38.

22. Q. Yin, J. M. Tan, C. Besson, Y. V. Geletii, D. G. Musaev, A. E. Kuznetsov, A. Luo, K. I. Hardcastle and C. L. Hill, *Science* **2010**, *328*, 342–345.

23. J. L. Fillol, Z. Codolà, I. Garcia-Bosch, L. Gómez, J. J. Pla and M. Costas, *Nature Chem.* **2011**, *3*, 807–813.

24. K. Kitamoto and K. Sakai, *Angew. Chem. Int. Ed.* **2014**, *53*, 4618–4622.

25. H. Ozawa, M. Haga and K. Sakai, *J. Am. Chem. Soc.* **2006**, *128*, 4926–4927.

26. Y. Amao, *ChemCatChem.* **2011**, *3*, 458–474.

27. K. Koike, H. Hori, M. Ishizuka, J. R. Westwell, K. Takeuchi, T. Ibusuki, K. Enjouji, H. Konno, K. Sakamoto and O. Ishitani, *Organometallics* **1997**, *16*, 5724-5729.

28. H. Takeda, K. Koike, H. Inoue and O. Ishitani, *J. Am. Chem. Soc.* **2008**, 130, 2023–2031.

29. H. Hori, F. P. A. Johnson, K. Koike, O. Ishitani and T. Ibusuki, *J. Photochem. Photobiol. A: Chem.* **1996**, *96*, 171–174.

30. W. J. Youngblood, S. A. Lee, Y. Kobayashi, E. A. HernandezPagan, P. G. Hoertz, T. A. Moore, A. L. Moore, D. Gust and T. E. Mallouk, *J. Am. Chem. Soc.* **2009**, *131*, 926–927.

31. L. Li, L. Duan, Y. Xu, M. Gorlov, A. Hagfeldt and L. Sun, *Chem. Commun.* **2010**, *46*, 7307–7309.

32. Y. Gao, X. Ding, J. Liu, L. Wang, Z. Lu, L. Li and L. Sun, *J. Am. Chem. Soc.* **2013**, *135*, 4219–4222.

33. A. Fujishima, K. Kohayakawa and K. Honda, *J. Electrochem. Soc.* **1975**, *122*, 1487–1489.

34. M. D. Ward, J. R. White and A. J. Bard, *J. Am. Chem. Soc.* **1983**, *105*, 27–31.

35. Y. Hori, K. Kikuchi and S. Suzuki, *Chem. Lett.* **1985**, *14*, 1695–1698.

36. D. Gust, T. A. Moore and A. L. Moore, *Acc. Chem. Res.* **1993**, *26*, 198–205.

37. Y. Kobuke and K. Ogawa, *Bull. Chem. Soc. Jpn.* **2003**, *76*, 689–708.

38. M. R. Hoffmann, S. T. Martin, W. Choi and D. W. Bahnemann, *Chem, Rev.* **1995**, *95*, 69–96.

39. A. L. Linsebigler, G. Lu and J. T. Yates, *Chem. Rev.* **1995**, *95*, 735–758.

40. K. Maeda and K. Domen, *J. Phys. Chem. C* **2007**, *111*, 7851–7861.

41. D. Gust, T. A. Moore and A. L. Moore, *Acc. Chem. Res.* **2009**, *42*, 1890–1898.

42. P. D. Frischmann, K. Mahata and F. Würthner, *Chem. Soc. Rev.* **2013**, *42*, 1847–1870.

43. S. N. Habisreutinger, L. Schmidt-Mende and J. K. Stolarczyk, *Angew. Chem. Int. Ed.* **2013**, *52*, 7372–7408.

44. K. Kalyanasundaram and M. Grätzel, *Curr. Opin. Biotechnol.* **2010**, *21*, 298–310.

45. Y. Umena, K. Kawakami, J. R. Shen and N. Kamiya, *Nature* **2011**, *473*, 55–60

46. J. Messinger, *Phys. Chem. Chem. Phys.* **2004**, *6*, 4764–4771.

47. M. Haumann, C. Muller, P. Liebisch, L. Luzzolino, J. Dittmer, M. Grabolle and H. Dau, *Biochem.* **2005**, *44*, 1894–1908.

48. M. W. Kanan and D. G. Nocera, *Science* **2008**, *321*, 1072–1075.

49. S. W. Gersten, G. J. Samuels and T. J. Meyer, *J. Am. Chem. Soc.* **1982**, *104*, 4029–4030.

50. T. J. Meyer, M. H. V. Huynh and H. H. Thorp, *Angew. Chem. Int. Ed.* **2007**, *46*, 5284–5304.

51. N. D. McDaniel, F. J. Coughlin, L. L. Tinker and S. Bernhard, *J. Am. Chem. Soc.* **2008**, *130*, 210–217.

52. L. Duan, F. Bozoglian, S. Mandal, B. Stewart, T. Privalov, A. Llobet and L. Sun, *Nature Chem.* **2012**, *4*, 418–423.

53. D. K. Dogutan, R. McGuireJr. and D. G. Nocera, *J. Am. Chem. Soc.* **2011**, *133*, 9178–9180.

54. Y. Gao, T. Åkermark, J. Liu, L. Sun and B. Åkermark, *J. Am. Chem. Soc.* **2009**, *131*, 8726–8727.

55. S. M. Barnett, K. I. Goldberg and J. M. Meyer, *Nature Chem.* **2012**, *4*, 498–502.

56. M. -T. Zhang, Z. Chen, P. Kang and T. J. Meyer, *J. Am. Chem. Soc.* **2013**, *135*, 2048–2051.

57. J. L. Fillol, Z. Codola, I. GarciaBosch, L. Gomez, J. J. Pla and M. Costas, *Nature Chem.* **2011**, *3*, 807–813.

58. J. Limburg, J. S. Vrettos, L. M. Liable-Sands, A. L. Rheingold, R. H. Crabtree and G. W. Brudvig, *Science* **1999**, *283*, 1524–1527.

59. J. J. Concepcion, J. W. Jurss, P. G. Hoertz and T. J. Meyer, *Angew. Chem. Int. Ed.* **2009**, *48*, 9473-9476.

60. F. Puntoriero, G. L. Ganga, A. Sartorel, M. Carraro, G. Scorrano, M. Bonchio and S. Campagna, *Chem. Commun.* **2010**, *46*, 4725–4727.

61. F. M. Ashmawy, C. A. McAuliffe, R. V. Parish and J. Tames, *J. Chem. Soc., Dalton Trans.* **1985**, 1391–1397.

62. M. Watkinson, A. Whiting and C. A. McAuliffe, *J. Chem. Soc., Chem. Comm.* **1994**, 2141–2142.

63. J. H. Alstrum-Acevedo, M. K. Brennaman and T. J. Meyer, *Inorg. Chem.* **2005**, *44*, 6802–6827.

64. F. Liu, J. J. Concepcion, J. W. Jurss, T. Cardolaccia, J. L. Templeton and T. J. Meyer, *Inorg. Chem.* **2008**, *47*, 1727–1752.

65. J. F. Hull, D. Balcells, J. D. Blakemore, C. D. Incarvito, O. Eisenstein, G. W. Brudvig and R. H. Crabtree, *J. Am. Chem. Soc.* **2009**, *131*, 8730–8731.

66. A. Savini, P. Belanzoni, G. Bellachioma, C. Zuccaccia, D. Zuccaccia and A. Macchioni, *Green Chem.* **2011**, *13*, 3360–3374.

67. S. Berardi, S. Drouet, L. Francas, C. Gimbert-Surinach, M. Guttentag, C. Richmond, T. Stoll and A. Llobet, *Chem. Soc. Rev.* **2014**, *43*, 7501–7519.

68. N. D. Morris, M. Suzuki and T. E. Mallouk, *J. Phys. Chem. A* **2004**, *108*, 9115–9119.

69. P. G. Hoertz, Y. -I. Kim, W. J. Youngblood and T. E. Mallouk, *J. Phys. Chem. B* **2007**, *111*, 6845–6856.

70. M. Kirch, J. M. Lehn and J. P. Sauvage, *Helv. Chim. Acta* **1979**, *62*, 1345–1383.

71. K. Kalyanasundaram and D. Dung, *J. Phys. Chem.* **1980**, *84*, 2551–2556.

72. D. Miller and G. McLendon, *Inorg. Chem.* **1981**, *20*, 950–953.

73. A. J. Bard and M. A. Fox, *Acc. Chem. Res.* **1995**, *28*, 141–145.

74. M. Razavet, V. Artero and M. Fontecave, *Inorg. Chem.* **2005**, *44*, 4786–4795.

75. X. Hu, B. S. Brunschwig and J. C. Peters, *J. Am. Chem. Soc.* **2007**, *129*, 8988–

8998.

76. M. Wang, L. Chen and L. Sun, *Energy Environ. Sci.* **2012**, *5*, 6763–6778.
77. W. T. Eckenhoff and R. Eisenberg. *Dalton Trans.* **2012**, *41*, 13004–13021.
78. V. S. Thoi, Y. Sun, J. R. Long and C. J. Chang, *Chem. Soc. Rev.* **2013**, *42*, 2388–2400.
79. J. M. Lehn and J. P. Sauvage, *Nouv. J. Chim.* **1977**, *1*, 449–451.
80. A. Moradpour, E. Amouyal, P. Keller and H. B. Kagan, *Nouv. J. Chim.* **1978**, *2*, 547–549.
81. K. Kalyanasundaram, K. Kiwi and M. Grätzel, *Helv. Chim. Acta* **1978**, *61*, 2720–2730.
82. M. Kirch, J. M. Lehn and J. P. Sauvage, *Helv. Chim. Acta* **1979**, *62*, 1345–1384.
83. Y. I. Kim, S. J. Atherton, E. S. Brigham and T. E. Mallouk, *J. Phys. Chem.* **1993**, *97*, 11802–11810.
84. T. Yonezawa and N. Toshima, *J. Mol. Catal.* **1993**, *83*, 167–181.
85. B. Hinnemann, P. G. Moses, J. Bonde, K. P. Jørgensen, J. H. Nielsen, S. Horch, I. Chorkendorff and J. K. Nørskov, *J. Am. Chem. Soc.* **2005**, *127*, 5308–5309.
86. J. Greeley, J. K. Nørskov, L. A. Kibler, A. M. El-Aziz and D. M. Kolb, *ChemPhysChem* **2006**, *7*, 1032–1035.
87. J. Greeley, T. F. Jaramillo, J. Bonde, I. B. Chorkendorff and J. K. Nørskov, *Nature Mater.* **2006**, *5*, 909–913.
88. Y. Li, H. Wang, L. Xie, Y. Liang, G. Hong and H. Dai, *J. Am. Chem. Soc.* **2011**, *133*, 7296–7299.
89. D. Merki and X. Hu, *Energy Environ Sci.* **2011**, *4*, 3878–3888.
90. F. Wang, W. G. Wang, H. Y. Wang, G. Si, C. H. Tung and L. Z. Wu, *ACS Catal.*

2012, *2*, 407–416.

91. E. J. Popczun, J. R. McKone, C. G. Read, A. J. Biacchi, A. M. Wiltrout, N. S. Lewis and R. E. Schaak, *J. Am. Chem. Soc.* **2013**, *135*, 9267–9270.
92. K. Sakai and H. Ozawa, *Coord. Chem. Rev*. **2007**, *251*, 2753–2766.
93. K. Sakai, Y. Kizaki, T. Tsubomura and K. Matsumoto, *J. Mol. Catal.* **1993**, *79*, 141–152.
94. J. -M. Lehn and R. Ziessel, *Proc. Natl. Acad. Sci. U. S. A.* **1982**, *79*, 701–704.
95. K. Tanaka and D. Ooyama, *Coord. Chem. Rev.* **2002**, *226*, 211–218.
96. H. Takeda and O. Ishitani, *Coord. Chem. Rev*. **2010**, *254*, 346–354
97. C. Amatore and J. Savéant, *J. Am. Chem. Soc.* **1981**, *103*, 5021–5023.
98. R. Hinogami, Y. Nakamura, S. Yae and Y. Nakato, *J. Phys. Chem. B.* **1998**, *102*, 974–980.
99. Y. Hori, H. Wakebe, T. Tsukamoto and O. Koga, *Electrochim. Acta* **1994**, *39*, 1833–1839.
100. J. F. McCann and A. Khan, *Electrochim. Acta* **1982**, *27*, 89–94.
101. F. R. F. Fan, P. Leempoel and A. J. Bard, *J. Electrochem. Soc.* **1983**, *130*, 1866–1875.
102. A. Henglein, M. Gutiérrez and C. -H. Fischer, *Ber. Bunsenges. Phys. Chem*. **1984**, *88*, 170–175.
103. O. Ishitani, C. Inoue, Y. Suzuki and T. Ibusuki, *J. Photochem. Photobiol. A: Chem*. **1993**, *72*, 269–271.
104. R. Vogel, P. Hoyer and H. Weller, *J. Phys. Chem*. **1994**, *98*, 3183–3188.
105. M. Anpo, H. Yamashita, Y. Ichihashi and S. Ehara, *J. Electroanal. Chem*. **1995**, *396*, 21–26.

106. H. Yoneyama, *Catal. Today* **1997**, *39*, 169–175.

107. K. Ikeue, H. Yamashita, M. Anpo and T. Takewaki, *J. Phys. Chem. B* **2001**, *105*, 8350–8355.

108. H. Yu, X. Quan, S. Chen and H. Zhao, *J. Phys. Chem. C* **2007**, *111*, 12987–12991.

109. C. Wang, R. L. Thompson, P. Ohodnicki, J. Baltrus, C. Matranga, *J. Mater. Chem.* **2011**, *21*, 13452–13457.

110. X. Li, H. Liu, D. Luo, J. Li, Y. Huang, H. Li, Y. Fang, Y. Xu and L. Zhu, *Chem. Eng. J.* **2012**, *180*, 151–158.

111. I. A. Shkrob, N. M. Dimitrijevic, T. W. Marin, H. He and P. Zapol, *J. Phys. Chem. C* **2012**, *116*, 9461–9471.

112. S. N. Habisreutinger, L. Schmidt-Menda and J. K. Stolarczyk, *Angew. Chem. Int. Ed.* **2013**, *52*, 7372–7408.

113. K. Mori, H. Yamashita and M. Anpo, *RSC Adv.* **2012**, *2*, 3165–3172.

114. K. Sekizawa, K. Maeda, K. Domen, K. Koike, and O. Ishitani. *J. Am. Chem. Soc.* **2013**, *135*, 4596–4599.

115. I. Bhugun, D. Lexa and J. -X. Saveant, *J. Am. Chem. Soc.* **1996**, *118*, 1769–1776.

116. B. J. Fisher and R. Eisenberg, *J. Am. Chem. Soc.* **1980**, *102*, 7361–7363.

117. J. W. Raebiger, J. W. Turner, B. C. Noll, C. J. Curtis, A. Miedaner, B. Cox and D. L. Dubois, *Organometallics* **2006**, 25, 3345–3351.

118. J. Hawecker, J. -M. Lehn and R. J. Ziessel, *J. Chem. Soc. Chem. Commun.* **1983**, 536–538.

119. J. Grodkowski, T. Dhanasekaran, P. Neta, P. Hambright, B. S. Brunschwig, K. Shinozaki and E. Fujita, *J. Phys. Chem. A* **2000**, *104*, 11332–11339.

120. T. Ogata, S. Yanagida, B. S. Brunschwig and E. Fujita, *J. Am. Chem. Soc.* **1995**,

117, 6708–6716.

121. D. Behar, T. Dhanasekaran, P. Neta, C. M. Hosten, D. Ejeh, P. Hambright and E. Fujita, *J. Phys .Chem. A* **1998**, *102*, 2870–2877.
122. H. Takeda, H. Koizumi, K. Okamoto and O. Ishitani, *Chem. Commun.* **2014**, *52*, 1491–1493.
123. S. Sato, T. morikawa, T. Kajino and O. Ishitani, *Angew. Chem. Int. Ed.* **2013**, *52*, 988–992.
124. J. -M. Lehn and R. Ziessel, *J. Organomet. Chem.* **1990**, *382*, 157–173.
125. E. Kimura, X. Bu, M. Shionoya, S. Wada and S. Maruyama, *Inorg. Chem.* **1992**, *31*, 4542–4546.
126. E. Kimura, S. Wada, M. Shionoya and Y. Okazaki, *Inorg. Chem.* **1994**, *33*, 770–771.
127. N. Komatsuzaki, Y. Himeda, T. Hirose, H. Sugihara and K. Kasuga, *Bull. Chem. Soc. Jpn.* **1999**, *72*, 725–731.
128. D. S. Laitar, P. Muller and J. P. Sadighi, *J. Am. Chem. Soc.* **2005**, *49*, 17196–17197.
129. M. Elvington and K. J. Brewer, *Inorg. Chem.* **2006**, 5242–5244.
130. J. Agarwal, R. P. Johnson and G. Li, *J. Phys. Chem. A* **2011**, *115*, 2877–2881.
131. B. Kumar, M. Llorente, J. Froehlich, T. Dang, A. Sathrum and C. P. Kubiak, *Annu. Rev. Phys. Chem.* **2012**, *63*, 541–569.
132. Y. Tamaki, T. Morimoto, K. Koike and O. Ishitani, *Proc. Natl. Acad. Sci.* **2012**, *109*, 15673–15678.
133. K. Sekizawa, K. Maeda, K. Domen, K. Koike and O. Ishitani, *J. Am. Chem. Soc.* **2013**, *135*, 4596–4599.

134. L. Sacksteder, A. P. Zipp, E. A. Brown, J. Streich, J. N. Demas and B. A. DeGraff, *Inorg. Chem.* **1990**, *29*, 4335–4340.

135. L. Wallace and D. P. Rillema, *Inorg. Chem.* **1993**, *32*, 3836–3843.

136. G. Ferraudi, M. Feliz, E. Wolcan, I. Hsu, S. A. Moya and J. Guerrero, *J. Phys. Chem.* **1995**, *99*, 4929–4934.

137. M. K. Itokazu, A. S. Polo, D. L. A. de Faria, C. A. Bignozzi and N. Y. M. Iha, *Inorg. Chim. Acta* **2001**, *313*, 149–155.

138. P. Thanasekaran, R. -T. Liao, Y. -H. Liu, T. Rajendran, S. Rajagopal and K. -L. Lu, *Coord. Chem. Rev.* **2005**, *249*, 1085–1110.

139. A. Coleman, C. Brennan, J. G. Vos and M. T. Pryce, *Coord. Chem. Rev.* **2008**, *252*, 2585–2595.

140. A. O. T. Patrocinio, M. K. Brennaman, T. J. Meyer and N. Y. Murakami Iha, *J. Phys. Chem. A* **2010**, *114*, 12129–12143.

141. B. Machura, M. Wolff, M. Jaworska, P. Lodowski, E. Benoist, C. Carrayon, N. Saffon, R. Kruszynski and Z. Mazurak, *J. Organomet. Chem.* **2011**, *696*, 3068–3075.

142. Y. Kang, A. Ito, E. Sakuda and N. Kitamura, *J. Photochem. Photobiol. A: Chem.* **2015**, *313*, 107–116.

143. J. Hawecker, J. -M. Lehn and R. Ziessel, *Helv. Chim. Acta* **1986**, *69*, 1990–2012.

144. R. Ziessel, J. Hawecker and J. -M. Lehn, *Helv. Chim. Acta* **1986**, *69*, 1065–1084.

145. H. Hori, F. P. A. Johnson, K. Koike, O. Ishitani and T. Ibusuki, *J. Photochem. Photobiol. A: Chem* **1996**, *96*, 171–174.

146. H. Hori, K. Koike, M. Ishizuka, K. Takeuchi, T. Ibusuki and O. Ishitani, *J. Organomet. Chem.* **1997**, *530*, 169–176.

147. B. Gholamkhass, H. Mametsuka, K. Koike, T. Tanabe, M. Furue and O. Ishitani, *Inorg. Chem.* **2005**, *44*, 2326–2336.

148. C. Riplinger, M. D. Sampson and A. M. Ritzmann, *J. Am. Chem. Soc.* **2014**, *136*, 16285–16298.

149. K. Koike, S. Naito, S. Sato, Y. Tamaki and O. Ishitani, *J. Photochem. Photobiol. A: Chem.* **2009**, *207*, 109–114.

150. H. Takeda and O. Ishitani, *Coord. Chem. Rev.* **2010**, *254*, 346–354.

151. G. Sahara and O. Ishitani, *Inorg. Chem.* **2015**, *54*, 5096–5104.

152. W. Hieber and H. Fuchs, *Z. Anorg. Allg. Chem.* **1941**, *248*, 269–275.

153. P. Kurz, B. Probst, B. Spingler and R. Alberto, *Eur. J. Inorg. Chem.* **2006**, 2966–2974.

154. J. N. Demas and B. A. DeGraff, *Anal. Chem.* **1991**, *63*, 829A–837A.

155. D. A. Bardwell, F. Barigelletti, R. L. Cleary, L. Flamigni, M. Guardigli, J. C. Jeffery and M. D. Ward, *Inorg. Chem.* **1995**, *34*, 2438–2446.

156. V. W. W. Yam, B. Li, Y. Yang, B. W. K. Chu, K. M. C. Wong and K. K. Cheung, *Eur. J. Inorg. Chem.* **2003**, *22*, 4035–4042.

157. O. S. Wenger, L. M. Henling, M. W. Day, J. R. Winkler and H. B. Gray, *Inorg. Chem.* **2004**, *43*, 2043–2048.

158. Z. Si, J. Li, B. Li, F. Zhao, S. Liu and W. Li, *Inorg. Chem.* **2007**, *46*, 6155–6163.

159. C. Kutal, M. A. Weber, G. Ferraudi and D. Geiger, *Organometallics* **1985**, *4*, 2161−2166.

160. K. Kalyanasundaram, *J. Chem. Soc., Faraday Trans. 2* **1986**, *82*, 2401−2415.

161. C. Kutal, J. A. Corbin and G. Ferraudi, *Organometallics* **1987**, *6*, 553−557.

162. Y. Hayashi, S. Kita, B. S. Brunschwig and E. Fujita, *J. Am. Chem. Soc.* **2003**, *125*,

11976–11987.

163. D. G. Hall ed. *Boronic Acids*, Wiley-VCH: Weinheim, **2005**.

164. E. Frankland and B. F. Duppa, *Justus Liebigs Ann. Chem*. **1860**, *115*, 319–322.

165. E. Frankland and B. F. Duppa, *Proc. Royal Soc. (London)* **1860**, *10*, 568.

166. E. Frankland, *J. Chem. Soc.* **1862**, *152*, 167–183.

167. S. J. Rettig and J. Trotter, *Can. J. Chem*. **1977**, 55, 3071-3075.

168. C. Lamber, S. Stadler, G. Bourhill and C. Brauchle, *Angew. Chem. Int. Ed.* **1996**, *35*, 644–646.

169. K. C. Ching, M. Lequan, R. M. Lequan, A. Grisard and D. Markovitsi, *J. Chem. Soc., Faraday Trans.* **1991**, *87*, 2225–2228.

170. M. J. G. Lesley, A. Woodward, N. J. Taylor, T. B. Marder, I. Cazenobe, I. Ledoux, J. Zyss, A. Thornton, D. W. Bruce and A. Kakkar, *Chem. Mater.* **1998**, *10*, 1355–1365.

171. Z. M. Su, X. J. Wang, Z. H. Huang, R. S. Wang, J. K. Feng and J. Z. Sun, *Synth. Met*. **2001**, *119*, 583–584.

172. S. Kroeker and F. S. Jonathan, *Inorg. Chem*. **2001**, *40*, 6239–6246.

173. Q. Zhao, F. Li and C. Huang, *Chem. Soc. Rev.* **2010**, *8*, 3007–3030.

174. Q. Wu, M. Esteghamation, N. -X. Hu, Z. Popovic, G. Enwright, Y. Tao, M. DIorio and S. Wang, *Chem. Mater.* **2000**, *12*, 79–83.

175. X. T. Tao, H. Suzuki, T. Wada, S. Miyata and H. Sasabe, *J. Am. Chem. Soc.* **1999**, *121*, 9447–9448.

176. X. T. Tao, H. Suzuki, T. Wada, H. Sasabe and S. Miyata, *Appl. Phys. Lett*. **1999**, *75*, 1655.

177. A. Hassan and S. Wang, *Chem. Commun*. **1998**, 211–212.

178. M. Esteghamation, N. X. Hu, Z. Popovic, G. Enright, S. R. Breeze and S. Wang, *Angew. Chem. Int. Ed.* **1999**, *38*, 985–988.

179. S. Wang, *Coord. Chem. Rev.* **2001**, *215*, 79–88.

180. H. Imahori, H. Norieda, H. Yamada, Y. Nishimura, I. Yamazaki, Y. Sakata and S. Fukuzumi, *J. Am. Chem. Soc.* **2001**, *123*, 100–110.

181. F. Li, S. I. Yang, Y. Ciringh, J. Seth, C. H. Martin, D. L. Singh, D. KimR, R. Birge, D. F. Bocian, D. Holten and J. S. Lindsey, *J. Am. Chem. Soc.* **1998**, *120*, 10001–10017.

182. T. Gareis, C. Huber, O. S. Wolfbeis and J. Daub, *Chem. Commun.* **1997**, 1717–1718.

183. K. Rurack, M. Kollmannsberger and J. Daub, *New. J. Chem.* **2001**, *25*, 289–292.

184. G. Beer, K. Rurack and J. Daub, *Chem. Commun.* **2001**, 1138–1139.

185. C. D. Entwistle and T. B. Marder, *Angew. Chem. Int. Ed.* **2002**, *41*, 2927–2931.

186. C. D. Entwistle and T. B. Marder, *Chem. Marter.* **2004**, *16*, 4574–4585.

187. B. G. Ramsey, *J. Phys. Chem.* **1966**, *70*, 611–618.

188. C. Cornelissen-Gude and W. Tetting, *J. Phys. Chem. A* **1998**, *102*, 7754–7760.

189. S. Yamaguchi, S. Akiyama and K. Tamao, *J. Am. Chem. Soc.* **2000**, *122* 6335–6336.

190. R. Stahl, C. Lambert, C. Kaiser, R. Wortmann and R. Jakober, *Chem. Eur. J.* **2006**, *12*, 2358–2370.

191. G. Zhou, M. Baumgarten and K. Müllen, *J. Am. Chem. Soc.* **2008**, *130*, 12477–12484.

192. Z. Zhou, A. Wakamiya, T. Kushida and S. Yamaguchi, *J. Am. Chem. Soc.* **2012**, *134*, 4529–4532.

193. S. Yamaguchi, S. Akiyama and K. Tamao, *Org. Lett*. **2000**, *2*, 4129–4132.

194. S. Yamaguchi, S. Akiyama and K. Tamao, *J. Am. Chem. Soc.* **2001**, *123*, 11372–11375.

195. S. Yamaguchi, S. Akiyama and K. Tamao, *J. Orgnomet. Chem*. **2002**, *652*, 3–9.

196. S. Yamaguchi, S. Shirasaka, S. Akiyama and K. Tamao, *J. Am. Chem. Soc.* **2002**, *124*, 8816–8817.

197. N. Kitamura and E. Sakuda, *J. Phys. Chem. A* **2005**, *109*, 7429–7434.

198. N. Kitamura, E. Sakuda, T. Yoshizawa, T. Iimori and N. Ohta, *J. Phys. Chem. A* **2005**, *109*, 7435–7441.

199. E. Sakuda, K. Tsuge, Y. Sasaki and N. Kitamura, *J. Phys. Chem. B* **2005**, *109*, 22326–22331.

200. A. Ito, K. Kawanishi, E. Sakuda and N. Kitamura, *Chem. Eur. J.* **2014**, *20*, 3940–3953.

201. C. -T. Poon, W. H. Lam, H. -L. Wong and V. W. Yam, *Chem. Eur. J.* **2015**, *21*, 2182–2192.

202. A. G. Bonn and O. S. Wenger, *J. Org. Chem*. **2015**, *80*, 4097–4107.

203. J. Kwak, N. V. Nghia, J. Lee, H. Kim, M. H. Park and M. H. Lee, *Dalton Trans.* **2015**, *44*, 4765–4722.

204. S. Zhang, Z. Qu, P. Tao, B. Brooks, Y. Shao, X. Chen and C. Liu, *J. Phys. Chem. C* **2012**, *116*, 12434–12442.

205. S. Dahmen and M. Lormann, *Org. Lett*. **2005**, 7, 4597–4600.

206. D. D. C. Bradley, *Curr. Opin. Solid State Mater. Sci.* **1996**, *1*, 789–797.

207. A. B. Holmes, D. D. C. Bradley, A. R. Brown, P. L. Burn, J. H. Burroughes, R. H. Friend, N. C. Greenham, R. W. Gymer, D. A. Halliday, R. W. Jackson, A. Kraft, J.

H. F. Martens, K. Pilcher and I. D. W. Samuel, *Synth. Met.* **1993**, *55–57*, 4031–4040.

208. Y. Kubo, M. Yamamoto, M. Ikeda, M. Takeuchi, S. Shinkai, S. Yamaguchi and K. Tamao, *Angew. Chem. Int. Ed.* **2003**, *42*, 2036–2040.

209. M. Melaimi and F. P. Gabbai, *J. Am. Chem. Soc.* **2005**, *127*, 9680–9681.

210. K. Parab, K. Venkatasubbaiah and F. Jäkle, *J. Am. Chem. Soc.* **2006**, *128*, 12879–12885.

211. Y. Sun, N. Ross, S.-B. Zhao, K. Huszarik, W. -L. Jia, R. -Y. Wang, D. Macartney and S. Wang, *J. Am. Chem. Soc.* **2007**, *129*, 7510–7511.

212.C. R. Wade, A. E. J. Broomsgrove, S. Aldridge and F. P. Gabbai, *Chem. Rev.* **2010**, *110*, 3958–3984.

213. N. Matsumi, K. Sugai and H. Ohno, *Macromolecules* **2002**, *35*, 5731–5733.

214. N. Matsumi, K. Sugai and H. Ohno, *Macromolecules* **2003**, *36*, 2321–2326.

215. N. Matsumi, T. Mizumo and H. Ohno, *Polym. Bull.* **2004**, *51*, 389–394.

216. N. Matsumi, K. Sugai, M. Miyake and H. Ohno, *Macromolecules* **2006**, *39*, 6924–6927.

217. A. K. C. Mengel, B. He and O. S. Wenger, *J. Org. Chem.* **2012**, *77*, 6545–6552.

218. N. Matsumi, K. Naka and Y. Chujo, *J. Am. Chem. Soc.* **1998**, *120*, 10776–10777.

219. W. -L. Jia, D. Song and S. Wang, *J. Org. Chem.* **2003**, *68*, 701–705.

220. Y. Qin, I. Kiburu, S. Shah and F. Jäkle, *Macromolecules* **2006**, *39*, 9041–9048.

221. Y. Nagata and Y. Chujo, *Macromolecules* **2008**, *41*, 2809–2813.

222. Y. Nagata and Y. Chujo, *Macromolecules* **2008**, *41*, 3488–3492.

223. A. Hayek, J. -F. Nicoud, F. Bolze, C. Bourgogne and P. L. Baldeck, *Angew. Chem. Int. Ed.* **2006**, *118*, 6616–6619.

224. L. Zhao, G. Yang, Z. Su and L. Yan, *J. Mol. Struct. (THEOCHEM)* **2008**, *855*, 69–76.

225. Z. Yuan, N. J. Taylor, T. B. Marder, I. D. Williams, S. K. Kurtz and L. -T. Cheng, *J. Chem. Soc., Chem. Commun.* **1990**, 1489–1492.

226. Z. Yuan, N. J. Taylor, Y. Sun, T. B. Marder, I. D. Williams and L. -T. Cheng, *J. Organomet. Chem.* **1993**, *449*, 27–37.

227. C. Branger, M. Lequan, R. M. Lequan, M. Large and F. Kajzar, *Chem. Phys. Lett.* **1997**, *272*, 265–270.

228. Z. Yuan, J. C. Collings, N. J. Taylor, T. B. Marder, C. Jardin and J. -F. Halet. *J. Solid State Chem.* **2000**, *154*, 5–12.

229. C. D. Entwistle and T. B. Marder, *Chem. Mater.* **2004**, *16*, 4574–4585.

230. J. Frieder, *Chem. Rev.* **2010**, *110*, 3985–4022.

231. K. Kalyanasundaram, Coord. *Chem. Rev.* **1982**, *46*, 159–244.

232. J. V. Caspar and T. J. Meyer, *J. Am. Chem. Soc.* **1983**, *105*, 5583–5590.

234. Y. Kawanishi, N. Kitamura and S. Tazuke, *Inorg. Chem.* **1989**, *28*, 2968–2975.

235.C. N. Fleming, K. A. Maxwell, J. M. Desimone, T. J. Meyer and J. M. Papanikolas, *J. Am. Chem. Soc.* **2001**, *123*, 10336–10347.

236. J. V. Caspar and T. J. Meyer, *J. Phys. Chem.* **1983**, *87*, 952–957.

237. L. Sacksteder, A. P. Zipp, E. A. Brown, J. Streich, J. N. Demas and B. A. Degraff, *Inorg. Chem.* **1990**, *29*, 4335–4340.

238. P. Y. Chen, R. Duesing, D. K. Graff and T. J. Meyer, *J. Phys. Chem.* **1991**, *95*, 5850–5858.

239. L. Wallace and D. P. Rillema, *Inorg. Chem.* **1993**, *32*, 3836–3843.

240. R. J. Shaver, M. W. Perkovic, D. P. Rillema and C. Woods, *Inorg. Chem.* **1995**, *34*,

5446–5454.

241. K. Koike, N. Okoshi, H. Hori, K. Takeuchi, O. Ishitani, H. Tsubaki, I. P. Clark, M. W. George, F. P. A. Johnson and J. J. Turner, *J. Am. Chem. Soc.* **2002**, *124*, 11448–11455.
242. A. Ito, Y. Kang, S. Saito, E. Sakuda and N. Kitamura, *Inorg. Chem.* **2012**, *51*, 7722–7732.
243. E. Sakuda, A. Funahashi and N. Kitamura, *Inorg. Chem.* **2006**, *45*, 10670–10677.
244. N. Kitamura, E. Sakuda and Y. Ando, *Chem. Lett.* **2009**, *38*, 938–943.
245. Z. M. Hudson, C. Sun, K. J. Harris, B. E. Lucier, R. W. Schurko and S. Wang, *Inorg. Chem.* **2011**, *50*, 3447–3457.
246. A. Ito, T. Hirokawa, E. Sakuda and N. Kitamura, *Chem. Lett.* **2011**, *40*, 34–36.
247. Y. You and S. Y. Park, *Adv. Mater.* **2008**, *20*, 3820–3826.
248. R. S. Vadavi, K. M. Lee, T. Kim, J. Lee and M. H. Lee, *Organometallics* **2011**, *31*, 31–34.
249. C. R. Wade and F. P. Gabbai, *Inorg. Chem.* **2010**, *49*, 714–720.
250. Y. Sun, X. M. Hudson, Y. Rao and S. Wang, *Inorg. Chem.* **2011**, *50*, 3373–3378.
251. J. Wang, F. -Q. Bai, B. -H. Xia, J. Chen and H. -X. Zhang, *J. Organomet. Chem.* **2011**, *696*, 2943–2948.
252. S. T. Lam, N. Zhu and V. W. -W. Yam, *Inorg. Chem.* **2009**, *48*, 9664–9670.
253. S. -B. Zhao, T. McCormick and S. Wang, *Inorg. Chem.* **2007**, *46*, 10965–10967.
254. Y. Sun, N. Ross, S. -B. Zhao, K. Huszarik, W. -L. Jia and R. -Y. Wang, *J. Am. Chem. Soc.* **2007**, *129*, 7510–7511.
255. Z. M. Hudson and S. Wang, *Dalton Trans.* **2011**, *40*, 7805–7816.
256. E. Sakuda, Y. Ando, A. Ito and N. Kitamura, *Inorg. Chem.* **2011**, *50*, 1603–1613.

257. S. T. Lam, N. Zhu and V. W. -W. Yam, *Inorg. Chem*. **2009**, *48*, 9664–9670.

Chapter 2. Spectroscopic and Photophysical Properties of Tricarbonyl Rhenium(I) Complexes Having an Arylborane Charge Transfer Unit

2-1 Introduction

Polypyridine d^6 transition metal complexes have attracted wide interests due to the metal-to-ligand charge transfer (MLCT) absorption/phosphorescence.[1–3] Among various transition metal complexes, a tricarbonyl rhenium(I) complex having an aromatic diimine ligand, *fac*-[$Re(CO)_3LX$] (L = diimine and X = halogen, imine or trialkylphosphine), has been paid much attention due to the unique spectroscopic, photophysical and photoredox properties,[4–6] including the photocatalytic ability to CO_2 reduction.[7–11] It is well known that the photocatalytic CO_2 reduction efficiency by *fac*-[$Re(CO)_3LX$] is controllable by its electronic structures and, the ground- and excited-state properties of *fac*-[$Re(CO)_3LX$] are very sensitive to the coordinating ligand(s) (L and/or X) as well as the microenvironments around the complex.[12,13] Therefore, chemical modifications and derivatizations of *fac*-[$Re(CO)_3LX$] are extremely important for further development of an efficient photocatalytic CO_2 reduction system.

This thesis focuses the study on synthetic modulation of the spectroscopic and photophysical properties of transition metal complexes by an arylborane group introduced to the periphery of the π-chromophoric ligand of a complex. A triarylborane derivative possesses the sp^2-hybridized structure of the boron–carbon bonds and the vacant p-orbital on the boron atom in the electronic ground state. Owing to such characteristics, a triarylborane compound shows characteristic spectroscopic and photophysical properties ascribed to synergistic MLCT/π(aryl)-p(B) CT interactions as

described in Chapter 1.

It should be emphasized that, although there are some reports on transition metal complexes bearing an arylborane charge transfer unit, the report on the tricarbonyl rhenium(I) complex with an arylborane charge transfer unit(s) is still few.

In this chapter, the synthesis, electrochemical, spectroscopic and photophysical properties of the two novel tricarbonyl rhenium(I) complexes having a mono-arylborane charge transfer unit at the 4-position of 1,10-phenanthroline (*fac*-[Re(CO)$_3$(4-DBDE-phen)Br] = **ReBphen**) or 2,2'-bipyridine (*fac*-[Re(CO)$_3$(4-DBDE-phen)Br] = **ReBbpy**) are described: DBDE = (dimesitylboryl)durylethynyl group. The diimine ligand structure and arylborane substituent effects on the spectroscopic and photophysical properties of the complexes are also described. The complexes having the arylborane charge transfer unit, **ReBphen** and **ReBbpy**, showed low-energy/intense absorption and low-energy/long-lived emission compared to the corresponding reference complexes without an arylborane charge transfer unit: **Rephen** (*fac*-[Re(CO)$_3$(phen)Br]) and **Rebpy** (*fac*-[Re(CO)$_3$(bpy)Br]), respectively. Furthermore, **ReBphen** showed the larger DBDE effects on the spectroscopic and photophysical properties compared to **ReBbpy**, and the origin of such results was discussed in detailed. The conclusion described above indicates that the substituted position of a triarylborane unit in a diimine ligand plays essential roles in governing the photophysical characteristics of [Re(CO)$_3$LBr].

2-2 Experimental

2-2-1 Chemicals and Measurements

All of the chemicals used for the synthesis of **ReBphen** and **ReBbpy** were

purchased from Wako Pure Chemical Ind., Ltd., Kanto Chemical Co., Inc., Tokyo Chemical Ind. Co., Ltd. or Sigma-Aldrich Co., LLC, and used as supplied. Column chromatography was carried out by using GE healthcare Sephadex LH-20 or Recycling Preparative HPLC (Japan Analytical Industry Company, LC-9201) with a JAIGEL-1H gel-permeation chromatography (GPC) column equipped with UV-3740 UV/Vis and RI-50s RI detectors. *N*,*N*-Dimethylformamide (DMF) and propylene carbonate (PC) for spectroscopic/photophysical measurements were distilled prior to use. Spectroscopic grade tetrahydrofuran (THF), toluene and acetonitrile (CH_3CN) were used as supplied for solvent dependence studies. Cica-Reagent DMF for nonaqueous titrimetry (Kanto Chemical Co., Inc.) was used for electrochemical measurements as supplied.

^1H NMR spectra were recorded on a JEOL JME-EX270 FT-NMR system (270 MHz). The chemical shifts of the spectra determined in $CDCl_3$ are given in ppm with tetramethylsilane being an internal standard (0.00 ppm). Electrospray ionization (ESI) mass spectra were recorded on a Waters micromassZQ spectrometer. Elemental analysis was conducted in the Instrumental Analysis Division, Equipment Management Center, Creative Research Institution, Hokkaido University.

2-2-2 Synthesis

ReBphen or **ReBbpy** was synthesized by the Sonogashira–Hagihara cross-coupling reaction between (ethynylduryl)dimesitylborane **(**EDDB) and *fac*-[$Re(CO)_3$(4-Br-phen)Br] (4-Br-phen = 4-bromo-1,10-phenanthroline) or *fac*-[$Re(CO)_3$(4-Br-bpy)Br] (4-Br-bpy = 4-bromo-2,2'-bipyridine), respectively. Scheme 2-1 shows the synthetic routes for EDDB and, Schemes 2-2 and 2-3 show the synthetic routes for **ReBphen** and **ReBbpy**, respectively. EDDB[14] and 4-Br-bpy[15,16] were synthesized according to the literatures with some modifications. **Rephen** and **Rebpy** as

the reference complexes for **ReBphen** and **ReBbpy**, respectively, were also synthesized according to the literature procedures.[17]

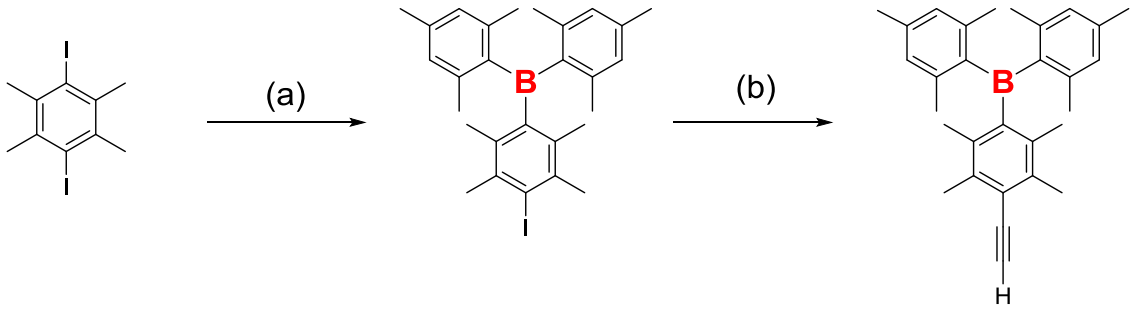

Scheme 2-1 Synthetic routes for EDDB: (a) 1. *n*-BuLi, dry Et_2O, –78 ℃, 2. $B(mes)_2F$, –78 ℃ then r.t. overnight, (b) 1. $Me_3Si{-}{\equiv}{-}H$, $Pd(PPh_3)_2Cl_2$, CuI, $HNEt_2$, THF, reflux 18 h, 2. KOH, methanol/THF, r.t. overnight.

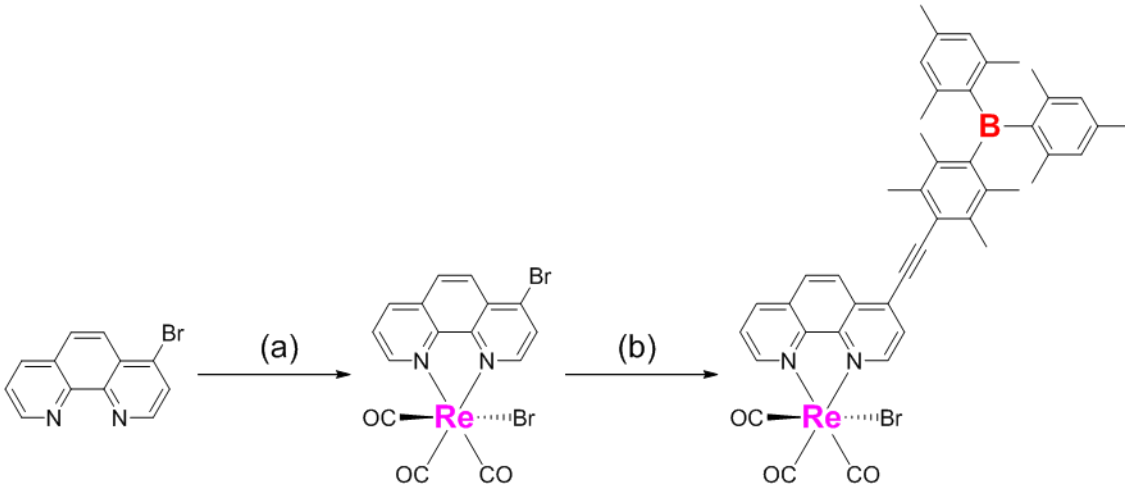

Scheme 2-2 Synthetic routes for **ReBphen**: (a) $[Re(CO)_5Br]$, toluene, reflux 2 h, (b) EDDB, $Pd(PPh_3)_2Cl_2$, CuI, THF/Et_3N, 50 ℃ 2 h.

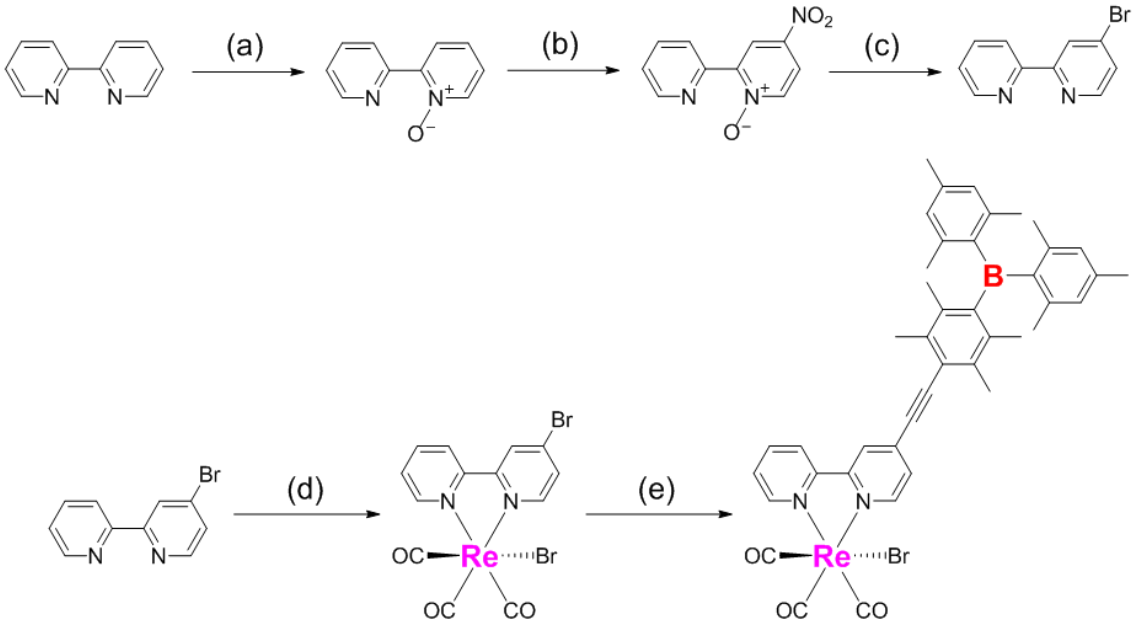

Scheme 2-3 Synthetic routes for **ReBbpy**: (a) H_2O_2, glacial acetic acid, 85 ℃ 3 h, (b) concentrated sulfuric acid, fuming sulfuric acid, fuming nitric acid, 90 ℃ 10 h, (c) acetyl bromide, phosphorus tribromide, glacial acetic acid, 85 ℃ 1 h, (d) $[Re(CO)_5Br]$, toluene, reflux 2 h, (e) $Pd(PPh_3)_2Cl_2$, CuI, THF/Et_3N, 50 ℃ 3 h.

Synthesis of (Ethnylduryl)dimesitylborane (EDDB)

An oven-dried Schlenk tube was evacuated and filled with an Ar gas and, then, 1,4-diiododurene (2.6 g, 6.7 mmol) and dry diethyl ether (50 mL) were added. After cooling the mixture at –78 ℃ in an acetone/dry ice bath for 30 min, *n*-butyllithium (1.62 M in *n*-hexane, 4.5 mL, 7.3 mmol) was added dropwise to the mixture and kept at –78 ℃ for another 1 h. After quick addition of dimesitylboron fluoride (3.8 g, 14 mmol) at –78 ℃, the reaction mixture was allowed to warm to room temperature and stirred overnight. Water (50 mL) was added to the mixture and extracted with diethyl ether (50 mL × 2). The organic phase was washed with an aqueous HCl solution (1 M, 50 mL) and brine (50 mL), dried over anhydrous $MgSO_4$, and evaporated to dryness under reduced pressure. Purification of the crude product by column chromatography (SiO_2, chloroform/*n*-hexane = 1/1) afforded (iododuryl)dimesitylborane (IDDB) as colorless solids. (2.0 g, 59%). R_f = 0.91 (SiO_2, chloroform/*n*-hexane = 1/1). ^{1}H NMR (270 MHz, $CDCl_3$): δ/ppm 1.94 (s, 12H, *ortho*-CH_3 of mesityl), 2.09 (s, 6H, *ortho*-CH_3 of duryl), 2.26 (s, 6H, *para*-CH_3 of mesityl), 2.43 (s, 6H, *meta*-CH_3 of duryl), 6.73 (s, 4H, Ar-H of mesityl).

An oven-dried Schlenk tube was evacuated and filled with an Ar gas. After adding IDDB (0.67 g, 1.3 mmol), CuI (42 mg, 0.22 mmol) and $Pd(PPh_3)_2Cl_2$ (62 mg, 0.088 mmol), the reaction vessel was additionally evacuated and filled with an Ar gas. An Ar-gas-purged triethylamine/THF mixture (10 mL/5 mL) was added and, then, stirred at room temperature for 20 min. A solution of trimethylsilylacetylene (0.23 mL, 1.6 mmol) in triethylamine (2.1 mL) was added dropwise to the mixture at 0 ℃. After refluxing at 68 ℃ for 12 h, trimethylsilylacetylene (0.1 mL, 0.70 mmol) was added further to the mixture, which was heated at reflux temperature for another 6 h. After the reaction was

completed, water (13 mL) was poured into the mixture and the mixture was extracted with diethyl ether (30 mL × 3). The organic phase was washed with an aqueous HCl solution (1 M, 33 mL) and brine (50 mL), dried over anhydrous $MgSO_4$, and evaporated to dryness under reduced pressure. The resulting oily products were purified by column chromatography (SiO_2, *n*-hexane) to afford (trimethylsilylethynylduryl)dimesitylborane (0.37 g, 59%). R_f = 0.30 (SiO_2, *n*-hexane).

(Trimethylsilylethynylduryl)dimesitylborane in methanol/THF (20 mL/17 mL) was stirred in the presence of KOH (0.4 g) for 12 h at room temperature. After concentration of the solution under reduced pressure followed by an addition of water (35 mL), the mixture was extracted with diethyl ether (70 mL). The organic phase separated was washed with water (35 mL), dried over anhydrous $MgSO_4$ and evaporated to dryness under reduced pressure. Recrystallization of the crude product from *n*-hexane afforded pure EDDB as colorless crystals (0.12 g, 36%). R_f = 0.40 (SiO_2, chloroform/*n*-hexane = 1/9). ^{1}H NMR (270 MHz, $CDCl_3$): δ/ppm 1.95 (s, 12H, *ortho*-CH_3 of mesityl), 1.98 (s, 6H, *ortho*-CH_3 of duryl), 2.24 (s, 6H, *para*-CH_3 of mesityl), 2.33 (s, 6H, *meta*-CH_3 of duryl), 3.51 (s, 1H, CCH), 6.73 (s, 4H, Ar-H of mesityl).

Synthesis of *fac*-Bromotricarbonyl(4-bromo-1,10-phenanthroline)rhenium(I) ([Re(CO)$_3$(4-Br-phen)Br]).

Bromopentacarbonylrhenium(I) ([$Re(CO)_5Br$], 0.50 g, 1.22 mmol) in toluene (50 mL) was refluxed in the presence of 4-bromo-1,10-phenanthroline[18,19] (4-Br-phen, 0.31 g, 1.20 mmol) under Ar-gas atmosphere after all of the reactants were dissolved in the solution. After refluxing for 2 h, the reaction mixture was cooled to room temperature and the solvent was evaporated under reduced pressure. The *facial* isomer of [$Re(CO)_3$(4-Br-phen)Br] was obtained as an orange powder after purification by column

chromatography (Al_2O_3, chloroform) (0.69 g, 84%). The purity of the complex was determined to be more than 90%, which was thought to be pure enough to employ in the following reactions. R_f = 0.42 (Al_2O_3, chloroform). ^{1}H NMR (270 MHz, $CDCl_3$): δ 7.92 (ddd, 1H, J = 0.43, 5.2, 8.3 Hz, 8-Ar-H), 8.14 (d, 1H, J = 4.8 Hz, 3-Ar-H), 8.13 (d, 1H, J = 5.5 Hz, 6-Ar-H), 8.38 (dd, 1H, J = 4.2, 4.7 Hz, 5-Ar-H), 8.60 (dd, 1H, J = 0.84, 8.3 Hz, 7-Ar-H), 9.18 (d, 1H, J = 5.6 Hz, 2-Ar-H), 9.46 (dd, 1H, J = 0.92, 5.2 Hz, 9-Ar-H). ESI-MS m/z 529 ($[M-Br]^+$).

Synthesis of *fac*-Bromotricarbonyl[4-(dimesitylboryl)durylethynyl-1,10-phenanthroline]rhenium(I) (ReBphen).

After an oven-dried Schlenk tube was evacuated and filled with an Ar gas, $[Re(CO)_3(4\text{-Br-phen})Br]$ (464 mg, 0.76 mmol), CuI (17.9 mg, 0.094 mmol), and $Pd(PPh_3)_2Cl_2$ (32 mg, 0.046 mmol) were added. The tube was evacuated and filled with Ar gas one more time, and an Ar-gas-purged tetrahydrofuran (THF)/triethylamine (22 mL/10 mL) mixture was added to the tube and stirred for 15 min at room temperature. A THF (16 mL) solution of EDDB (410 mg, 1.0 mmol) was added dropwise to the reaction mixture. The mixture was stirred at 50 ℃ for 2 h under N_2-gas atmosphere and, then, allowed to cool to room temperature. The insoluble solids were removed by filtration through Celite® and washed with toluene. The crude product was purified successively by column chromatography (LH-20, ethanol/chloroform = 1/2, v/v), recrystallization from toluene and binary phase diffusion by adding the concentrated toluene solution of the crude product to cyclohexane. The *facial* isomer of **ReBphen** was obtained as a dark orange powder (0.11 g, 15 %). R_f = 0.42 (Al_2O_3, chloroform). ^{1}H NMR (270 MHz, $CDCl_3$): δ 1.99 (s, 12H, *ortho*-CH_3 of mesityl), 2.08 (s, 6H, *ortho*-CH_3 of duryl), 2.28 (s, 6H, *para*-CH_3 of mesityl), 2.54 (s, 6H, *meta*-CH_3 of duryl), 6.77 (s,

4H, Ar-H of mesityl), 7.89 (dd, 1H, J = 5.0, 8.2 Hz, 8-Ar-H of phen), 7.92 (d, 1H, J = 5.5 Hz, 3-Ar-H of phen), 8.08 (d, 1H, J = 9.0 Hz, 6-Ar-H of phen), 8.56 (dd, 1H, J = 1.8, 8.4 Hz, 7-Ar-H of phen), 8.56 (d, 1H, J = 8.9 Hz, 5-Ar-H of phen), 9.33 (d, 1H, J = 5.5 Hz, 2-Ar-H of phen), 9.43 (dd, 1H, J = 1.4, 5.2 Hz, 9-Ar-H of phen). ESI-MS *m/z* 856 ($[M–Br]^+$). Analysis: $C_{45}H_{41}BBrN_2O_3Re$ 0.1$CHCl_3$. Calc.: C, 57.04; H, 4.68; N, 2.95; Br, 9.53. Found: C, 56.95; H, 4.42; N, 3.09; Br, 9.28.

Synthesis of *fac*-Bromotricarbonyl(1,10-phenanthroline)rhenium(I) (Rephen).

$[Re(CO)_5Br]$ (0.25 g, 0.60 mmol) and 1,10-phenanthroline (0.12 g, 0.60 mmol) were stirred in toluene (25 mL) until the reactants were completely dissolved. After refluxing the mixture for 2 h under Ar-gas atmosphere, the solvent was removed by evaporation under reduced pressure. The crude product was washed with a large amount of *n*-hexane, affording the *facial* isomer of **Rephen** as a yellow powder (0.28 g, 92%). R_f = 0.39 (Al_2O_3, chloroform). ^{1}H NMR (270 MHz, $CDCl_3$): δ 7.91 (dd, 1H, J = 5.1, 8.3 Hz, 3-Ar-H), 8.06 (s, 1H, 5-Ar-H), 8.58 (dd, 1H, J = 1.4, 8.3 Hz, 4-Ar-H) 9.45 (dd, 1H, J = 1.4, 5.0 Hz, 2-Ar-H). ESI-MS *m/z* 451 ($[M–Br]^+$). Analysis: $C_{15}H_8BrN_2O_3Re$. Calc.: C, 33.97; H, 1.52; N, 5.28; Br, 15.07. Found: C, 33.95; H, 1.69; N, 5.33; Br, 15.08.

Synthesis of 4-Bromo-2,2'-bipyridine (4-Br-bpy)

A suspended solution of 2,2'-bipyridine (6.01 g, 38.6 mmol) in glacial acetic acid (20 mL) and a 30wt% hydrogen peroxide solution (8 mL) was stirred until bpy was dissolved completely. After stirring at 70 ℃ for 1.5 h, an aqueous NaOH solution (1.3 M, 60 mL) was added, and the mixture was extracted with chloroform (75 mL × 2). Evaporation of the organic phase to dryness under reduced pressure gave 2,2'-bipyridyl-*N*-oxide as a light yellow powder (2.48 g, 38%). R_f = 0.36 (SiO_2, chloroform/methanol). ^{1}H NMR (270 MHz, $CDCl_3$): δ/ppm 7.28–7.41 (3H, m, 3-, 4-

and 5'-Ar-H), 7.84 (1H, dt, *J* = 1.8, 7.8 Hz, 4'-Ar-H) 8.18 (1H, dd, *J* = 2.1, 8.0 Hz, 5-Ar-H), 8.32 (1H, td, *J* = 0.69, 6.3 Hz, 6-Ar-H), 8.74 (1H, ddd, *J* = 0.91, 1.8, 4.8 Hz, 3'-Ar-H), 8.90 (1H, td, *J* = 0.97, 8.2 Hz, 6'-Ar-H).

A concentrated sulfuric acid solution (10.8 mL) of 2,2'-bipyridyl-*N*-oxide (2.69 g, 15.6 mmol) was stirred at room temperature. After cooling to –10 ℃, fuming sulfuric acid (15%, 10.8 mL) and fuming nitric acid (100%, 6.5 mL) were added. The mixture was refluxed for 10 h and, then, poured into 200 g of ice, followed by neutralization with an aqueous NaOH solution (10 M). The insoluble solids were collected by filtration and washed with a large amount of water. The crude product was purified by recrystallizations from ethanol for 3 times, affording pure 4-nitro-2,2'-bipyridyl-*N*-oxide as a colorless powder (1.2 g, 35%). ^{1}H NMR (270 MHz, $CDCl_3$): δ/ppm 7.44 (1H, ddd, *J* = 0.98, 4.8, 7.6 Hz, 5'-Ar-H), 7.88 (1H, dt, *J* = 1.9, 7.9 Hz, 4'-Ar-H), 8.07 (1H, dd, *J* = 3.3, 7.2 Hz, 5-Ar-H), 8.36 (1H, d, *J* = 7.2 Hz, 6-Ar-H), 8.79 (1H, ddd, *J* = 0.88, 1.7, 4.7 Hz, 3'-Ar-H), 8.89 (1H, td, *J* = 1.0, 8.1 Hz, 6'-Ar-H), 9.17 (1H, d, *J* = 3.3 Hz, 3-Ar-H). ESI-MS m/z 219 ($[M+H]^+$).

4-Nitro-2,2'-bipyridyl-*N*-oxide (1.10 g, 5.1 mmol) in glacial acetic acid (22 mL) was stirred until the reactant was dissolved completely. Addition of acetyl bromide (5.5 mL) to the mixture gave yellow precipitates and, then, phosphorus tribromide (5.5 mL) was added to the mixture. Upon slow heating of the mixture, the precipitates were dissolved completely at 40 ℃. After refluxing for 1 h, a concentrated NaOH solution (10 M) was added to the reaction mixture to allow pH of the solution to be ~ 9 and, then, the mixture was extracted with chloroform (75 mL × 3). The combined organic phase was evaporated under reduced pressure. Sublimation of the crude product in vacuo afforded pure 4-Br-bpy as a colorless powder (0.61 g, 51%). ^{1}H NMR (270 MHz, $CDCl_3$): δ/ppm

7.34 (1H, ddd, *J* = 1.1, 4.8, 7.5 Hz, 5'-Ar-H), 7.48 (1H, dd, *J* = 1.9, 5.3 Hz, 5-Ar-H), 7.84 (1H, dt, *J* = 1.6, 7.8 Hz, 4'-Ar-H), 8.39 (1H, td, *J* = 1.0, 8.0 Hz, 6'-Ar-H), 8.49 (1H, dd, *J* = 0.51, 5.3 Hz, 6-Ar-H), 8.63 (1H, dd, *J* = 0.55, 2.0 Hz, 3-Ar-H), 8.69 (1H, ddd, *J* = 0.88, 1.7, 4.8 Hz, 3'-Ar-H). ESI-MS m/z 257 ($[M+Na]^+$).

Synthesis of *fac*-Bromotricarbonyl(4-bromo-2,2'-bipyridine)rhenium(I) ($[Re(CO)_3(4\text{-}Br\text{-}bpy)Br]$)

Bromopentacarbonylrhenium(I) (1.92 g, 4.73 mmol) and 4-Br-bpy (1.08 g, 4.59 mmol) were heated at reflux temperature in toluene (177 mL) for 2 h under Ar-gas atmosphere. Evaporation of the mixture to dryness under reduced pressure afforded the *facial* isomer of $[Re(CO)_3(4\text{-}Br\text{-}bpy)Br]$ as a dark yellow powder with a high purity (>90%) for the following reaction (2.38 g, 86%). ^{1}H NMR (270 MHz, $CDCl_3$): δ/ppm 7.59 (1H, ddd, *J* = 1.4, 5.5, 7.5 Hz, 5'-Ar-H), 7.68 (1H, dd, *J* = 1.9, 6.0 Hz, 5-Ar-H), 8.09 (1H, dt, *J* = 1.6, 7.9 Hz, 4'-Ar-H), 8.21 (1H, td, *J* = 1.1, 8.1 Hz, 6'-Ar-H), 8.33 (1H, d, *J* = 1.9 Hz, 3-Ar-H), 8.86 (1H, d, *J* = 5.9 Hz, 6-Ar-H), 9.10 (1H, ddd, *J* = 0.70, 1.5, 5.5 Hz, 3'-Ar-H). ESI-MS m/z 609 ($[M+Na]^+$).

Synthesis of *fac*-Bromotricarbonyl[4-(dimesitylboryl)durylethynyl-2,2'-bipyridine]rhenium(I) (ReBbpy)

An oven-dried Schlenk tube was evacuated and filled with an Ar gas. After adding $[Re(CO)_3(4\text{-}Br\text{-}bpy)Br]$ (331 mg, 0.57 mmol), CuI (21.5 mg, 0.11 mmol) and $Pd(PPh_3)_2Cl_2$ (32 mg, 0.046 mmol), the reaction vessel was additionally evacuated and filled with an argon gas. An Ar-gas-purged tetrahydrofuran (THF)/triethylamine (17.5 mL/8.75 mL) mixture was added and, then, the mixture was stirred at room temperature for 15 min. A THF (12 mL) solution of EDDB (293 mg, 0.72 mmol) was added dropwise to the mixture. After stirring at 50 ℃ for 3 h, the reaction mixture was allowed

to cool to room temperature. The insoluble solids were removed by filtration through Celite® and washed with toluene. The crude product obtained by evaporation of the solution was purified by washing with *n*-hexane, column chromatography (LH-20, $CHCl_3$/ethanol = 2/1, v/v) and GPC, followed by binary phase diffusion of the toluene solution of the product to *n*-hexane. The *facial* isomer of **ReBbpy** was obtained as yellow needles (0.11 g, 21 %). ^{1}H NMR (270 MHz, CD_3CN): δ/ppm 2.00 (6H, s, *ortho*-CH_3 of duryl), 2.11 (12H, s, *ortho*-CH_3 of mesityl), 2.26 (6H, s, *para*-CH_3 of mesityl), 2.47 (6H, s, *meta*-CH_3 of duryl), 6.81 (4H, s, Ar-H of mesityl), 7.62–7.69 (2H, m, 5- and 5'-Ar-H), 8.21 (1H, dt, J = 1.5, 7.9 Hz, 4'-Ar-H), 8.49–8.52 (2H, m, 3- and 6'-Ar-H), 8.97–9.07 (2H, m, 6- and 3'-Ar-H). Analysis: $C_{43}H_{41}BBrN_2O_3Re$. Calc.: C, 56.71; H, 4.54; N, 3.08; Br, 8.77. Found: C, 56.78; H, 4.49; N, 3.05; Br, 8.34. ESI-MS m/z 933 ($[M+Na]^+$).

Synthesis of *fac*-Bromotricarbonyl(2,2'-bipyridine)rhenium(I) (Rebpy)

$[Re(CO)_5Br]$ (1.13 g, 2.76 mmol) and 2,2'-bipyridine (0.42 g, 2.73 mmol) were stirred in toluene (115 mL) until the reactants were completely dissolved. After refluxing the mixture for 2 h under Ar-gas atmosphere, the solvent was removed by evaporation. The crude product was washed with a large amount of *n*-hexane, affording the *facial* isomer of **Rebpy** as a yellow powder with a high purity (1.31 g, 95%). ^{1}H NMR (270 MHz, $CDCl_3$): δ/ppm 7.56 (2H, ddd, J = 1.4, 5.6, 7.5 Hz, 5,5'-Ar-H), 8.08 (2H, dt, J= 1.5, 7.9 Hz,4,4'-Ar-H), 8.17 (2H, td, J= 1.0, 8.2 Hz, 6,6'-Ar-H), 9.10 (2H, ddd, J= 0.72, 1.5, 5.5 Hz, 3,3'-Ar-H). Elemental Analysis Calcd. for $C_{13}H_8BrN_2O_3Re$: C, 30.84; H, 1.59; N, 5.53; Br, 15.78. Found: C, 30.96; H, 1.74; N, 5.56; Br, 15.82.

2-2-3 Electrochemical and Spectroscopic Measurements

Cyclic and differential pulse voltammograms were recorded on an electrochemical

analyzer (BAS, ALS-701A) with a three-electrode system by using Pt working, Pt auxiliary, and SCE (saturated calomel electrode) reference electrodes in DMF. The concentrations of the complexes were set at ~1 × 10^{-3} M (= mol/dm^3), and 0.1 M of tetra-*n*-butylammonium hexafluorophosphate ($TBAPF_6$) was used as a supporting electrolyte. Prior to measurements, sample solutions were deaerated by purging an Ar-gas stream for 15 min. The sweep rate in cyclic voltammetry was 100 mVs^{-1} and differential pulse voltammetry was conducted with 50 mV height pulses (0.05 s duration) being stepped by 0.5 mV intervals (2.0 s interval between the two pulses).

Absorption and corrected emission spectra of the complexes were measured by using a Hitachi U-3300 or U-3900H spectrophotometer and a Hamamatsu multichannel photodetector (PMA-11, excitation wavelength = 355 nm), respectively. The absolute emission quantum yields of the complexes were measured by a Hamamatsu C9920-02 system equipped with an integrating sphere and a red-sensitive multichannel photodetector (PMA-12, excitation wavelength = 400 nm). Emission decay measurements were conducted by using a Hamamatsu C4334 streak camera as a photodetector with 355-nm (LOTIS TII Ltd., LS-2137 Nd^{3+}:YAG laser, full-width at half maximum (fwhm): 16–18 ns, repetition rate: 10 Hz) or 405-nm (Hamamatsu PLP-040 diode laser, fwhm: 70 ps, repetition rate: 100 MHz) laser pulse excitation. The absorbance of the sample solution for the emission measurements was set < 0.05 at the excitation wavelength, and the sample solutions were deaerated by purging an Ar-gas stream for 20 min prior to the measurements. For temperature-controlled experiments, a liquid N_2 cryostat (Oxford Instruments, DN 1704) was used to control a sample temperature.

2-2-4 Theoretical Calculations

Theoretical calculations for the complexes were conducted on the Gaussian 09W programs.[20] Optimizations of the ground-state geometries of the complexes were performed by using the B3LYP density functional theory (DFT). The LanL2DZ[21–23] and 6-31G(d,p)[24,25] basis sets were used to treat the geometrical structures of the rhenium and all other atoms, respectively. Time-dependent (TD)-DFT calculations were then performed to estimate the energies and oscillator strengths of the 15 lowest-energy singlet absorption transitions. All of the calculations were carried out as in DMF by using a Polarizable Continuum Model (PCM).[26] Molecular-orbital contours of the complexes were plotted using GaussView 5.0.[27]

2-2-5 Franck–Condon Analysis of the Emission Spectra at Room Temperature.

Franck–Condon analysis of an emission spectrum is a spectral fitting analysis which provides information about the electronic and vibrational structures of an excited-state molecule, and the fundamental equation is given in Eq. (2-1).[28–31]

$$I(\tilde{\nu}) = \sum_{v_M=0}^{\infty}\sum_{v_L=0}^{\infty}\left(\frac{E_0 - v_M\hbar\omega_M - v_L\hbar\omega_L}{E_0}\right)^4\left(\frac{{S_M}^{v_M}}{v_M!}\right)\left(\frac{{S_L}^{v_L}}{v_L!}\right)\exp\left[-4\ln 2\left(\frac{\tilde{\nu} - E_0 + v_M\hbar\omega_M + v_L\hbar\omega_M}{\tilde{\nu}_{1/2}}\right)^2\right] \quad (2\text{-}1)$$

In Eq. (2-1), $I(\tilde{\nu})$ is the emission intensity at the energy in wavenumber (cm^{-1}) relative to that of the 0→0 transition. E_0 is the energy gap between the zeroth vibrational levels in the ground and excited states. $\hbar\omega_M$ and $\hbar\omega_L$ are the quantum spacings for averaged medium- and low-frequency vibrational modes governing nonradiative decay of a molecule, respectively. S_M and S_L are the Huang–Rhys factors[32] reflecting nuclear distortions along the coordinates of the medium- and low-frequency quantum modes, respectively. $\tilde{\nu}_{1/2}$ is the full width at half-maximum (fwhm) for an individual vibronic line. The photon numbers of the emission spectrum were corrected in a wavenumber scale by using the equation $I(\tilde{\nu}) = I(\lambda)$ x λ^2,[33,34] and the parameters E_0, S_M, S_L, $\hbar\omega_M$, $\hbar\omega_L$

and $\tilde{\nu}_{1/2}$ were optimized with a least-squares minimization routine using a Generalized Reduced Gradient (GRG2) algorithm.[35] The summation was carried out over 11 vibrational levels for both ν_M and ν_L: $0 \rightarrow 10$.

2-3 Results and Discussion

2-3-1 Cyclic and Differential Pulse Voltammograms

The DBDE groups on the phen and bpy ligands in **ReBphen** and **ReBbpy**, respectively, would influence the redox potentials of the complexes due to the electron-accepting abilities of the vacant p-orbitals on the boron atoms. Figure 2-1 shows the cyclic and differential pulse voltammograms of **ReBphen** and **ReBbpy** in DMF, together with those of corresponding reference complexes, **Rephen** and **Rebpy**, and the redox potentials of the complexes are summarized in Table 2-1. As seen in Figure 2-1, the metal oxidation potential of **ReBphen** ($E_{1/2}(Re^{II/I})$ = +1.45 V vs. SCE) was almost comparable with that of **Rephen** ($E_{1/2}(Re^{II/I})$ = +1.42 V), indicating similar energy of the highest-energy occupied molecular orbital (HOMO) with one another. On the other hand, **ReBphen** exhibited the first ($E_{1/2}(Re^{I/0})$, reduction of phen) and second ($E_{1/2}(Re^{0/-I})$, dissociation of the bromine ligand) reduction potentials at –0.98 and –1.38 V, respectively, which were both shifted to the positive direction by 250 mV compared to the relevant values of the reference complex, **Rephen**: see Table 2-1. These results can be explained by the increase in the electron-accepting ability of the complex by the presence of p(B) in the DBDE group as well as by mixing of the π*-orbital of phen with p(B). In addition to the positive potential shifts of $E_{1/2}(Re^{I/0})$ and $E_{1/2}(Re^{0/-I})$ observed for **ReBphen**, **ReBphen** shows the third reduction wave at –1.61 V, which can be

ascribed to the reduction of the boron atom in the DBDE group. This would play important roles in the excited-state characteristics for **ReBphen**, which will not be expected for **Rephen**.

Similar behaviors with those of **ReBphen** and **Rephen** were also observed for **ReBbpy** and **Rebpy**. First, all of the four complexes showed comparable oxidation potential at around $E_{1/2}(Re^{II/I})$ = +1.41 ~ +1.45 V. The similar oxidation potentials for the complexes reveal the similar HOMO energies between the complexes, demonstrating that the introduction of the DBDE group to the 4-position of phen or bpy does not influence largely the effective nuclear charge of the Re(I) ion. On the other hand, the first and second reduction potentials of **ReBbpy** were observed at –1.13 V and –1.45 V, respectively, which were shifted to the positive direction by 130 and 250 mV, respectively, compared to those of the reference complex, **Rebpy** (Table 2-1). The smaller arylborane substituent effects on $E_{1/2}(Re^{0/-I})$ observed for **ReBbpy** relative to those for **ReBphen** might indicate the weaker electronic coupling between the π*-orbital of phen and p(B). **ReBbpy** also showed the third reduction wave at –1.80 V, similar to that of **ReBphen**, which was also ascribed to the reduction of the boron atom in the DBDE group. Such electrochemical characteristics of **ReBphen** and **ReBbpy** should reflect on the excited-state characteristics of the complexes as described in the following sections.

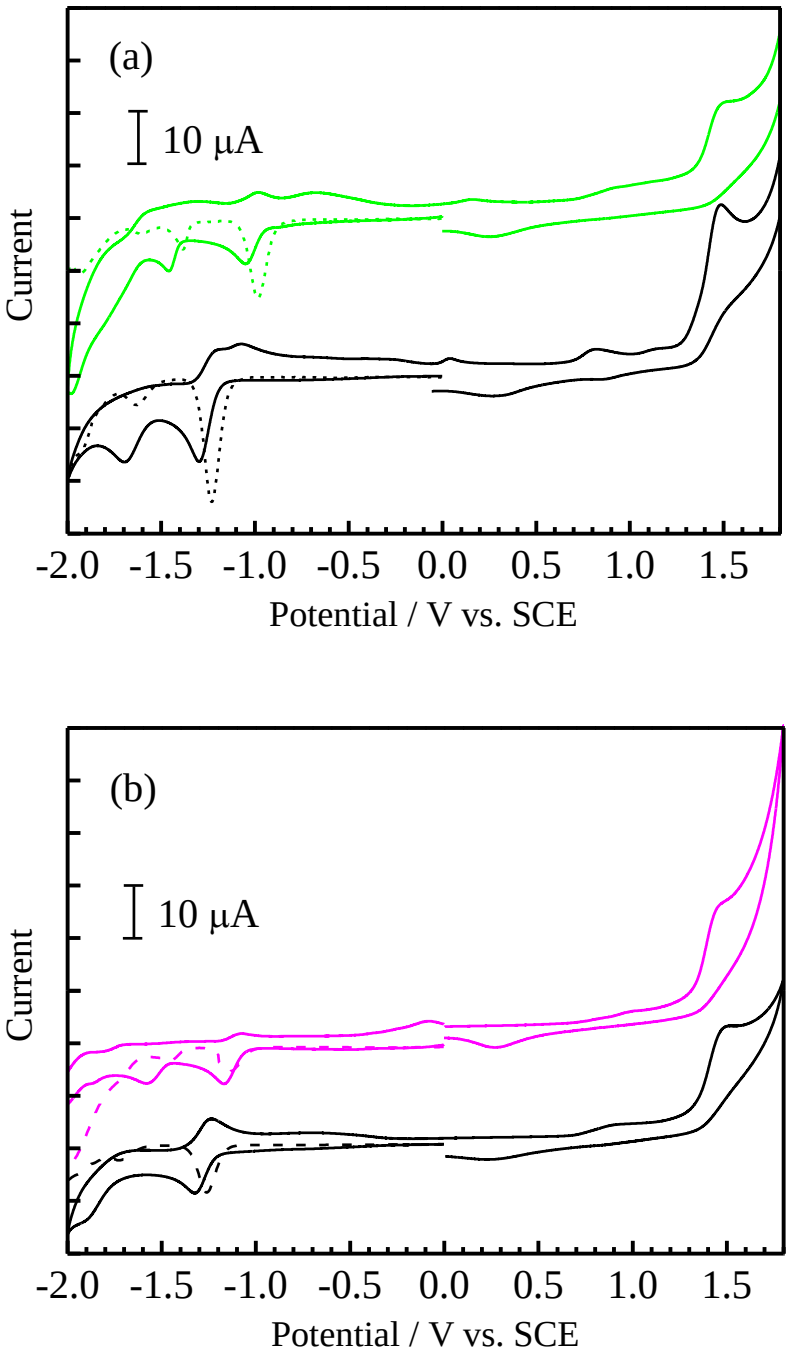

Figure 2-1 Cyclic (solid curves) and differential pulse voltammograms (broken curves) of (a) **ReBphen** (green) and **Rephen** (black), and those of (b) **ReBbpy** (pink) and **Rebpy** (black) in DMF containing ~0.1 M $TBAPF_6$.

Table 2-1 Redox potentials of the complexes in DMF containing 0.1 M $TBAPF_6$.

complex[a]	$E_{1/2}$ / V vs. SCE			
	$Re^{-I/-II}$	$Re^{0/-I}$	$Re^{I/0}$	$Re^{II/I}$
ReBphen	–1.61	–1.38	–0.98	+1.45
Rephen		–1.63	–1.23	+1.42
ReBbpy	–1.80	–1.45	–1.13	+1.42
Rebpy		–1.70	–1.26	+1.41

a) [**ReBphen**] = 1.03×10^{-3} M, [**Rebpy**] = 0.99×10^{-3} M, [**ReBbpy**] = 1.00×10^{-3} M, [**Rebpy**] = 1.00×10^{-3} M.

2-3-2 Absorption Spectra

Figure 2-2 shows the absorption spectra of **ReBphen** and **ReBbpy** in DMF at 298 K. The absorption maximum wavelengths (λ^{abs}) and the relevant molar absorption coefficients (ε) of the complexes are summarized in Table 2-2, together with those of corresponding reference complexes. As seen in the figure, the absorption band at around 290 nm and 320–390 nm (λ^{abs} = 378 nm, ε_{378} = 2.93 × 10^4 $M^{-1}cm^{-1}$) observed for **ReBphen** could be ascribed to the $^1\pi\pi^*$ transition in the phen ring and the ligand-centered (LC) transitions, respectively, where the latter is composed of the $^1\pi\pi^*$ transition in the durylethynyl-phen unit and the π(aryl)-p(B) CT transition. Both $^1\pi\pi^*$ and ^{1}MLCT absorption bands of **ReBphen** were shifted to the lower energy compared to those of **Rephen** as seen in Figure 2-2 and Table 2-2, and these characteristics were in good accordance with the negative shift of the first reduction potential of **ReBphen** relative to that of **Rephen**. The band observed for **ReBphen** at 438 nm is assigned to the ^{1}MLCT transition which shows a bathochromic shift and an increase in the ε value compared to the ^{1}MLCT band of **Rephen** due to the electron-accepting ability of the DBDE group in **ReBphen**.

ReBbpy also showed broad and intense absorption bands in 270–500 nm. The $^1\pi\pi^*$ transition in the bpy ring and the ligand-centered (LC) transitions were observed at 294 nm and 320 – 390 nm (λ^{abs} = 361 nm, ε_{361} = 3.39 × 10^4 $M^{-1}cm^{-1}$), respectively, which were shifted to the lower-energy compared to those of **Rebpy** as seen in Figure 2-2 and Table 2-2. These shifts were also in accordance with the negative shift of the first reduction potential of **ReBbpy**. Furthermore, the band at 392 nm observed for **ReBbpy** can be assigned to the ^{1}MLCT transition due to the similarity with that of **ReBphen**.

As the diimine ligand structure effects, an introduction of the arylborane unit to the

bpy ligand resulted in the larger ^{1}MLCT absorption band shift (**ReBphen** ~4050 cm^{-1}) relative to that of **ReBbpy** (~1160 cm^{-1}). This will be explained by the larger HOMO – LUMO energy gap difference between **ReBphen** and **Rephen** as estimated by the ($E_{1/2}(Re^{II/I}) - E_{1/2}(Re^{I/0})$) value between the two complexes (1800 cm^{-1}) compared to that between **ReBbpy** and **Rebpy**: 970 cm^{-1}: see Table 2-1.

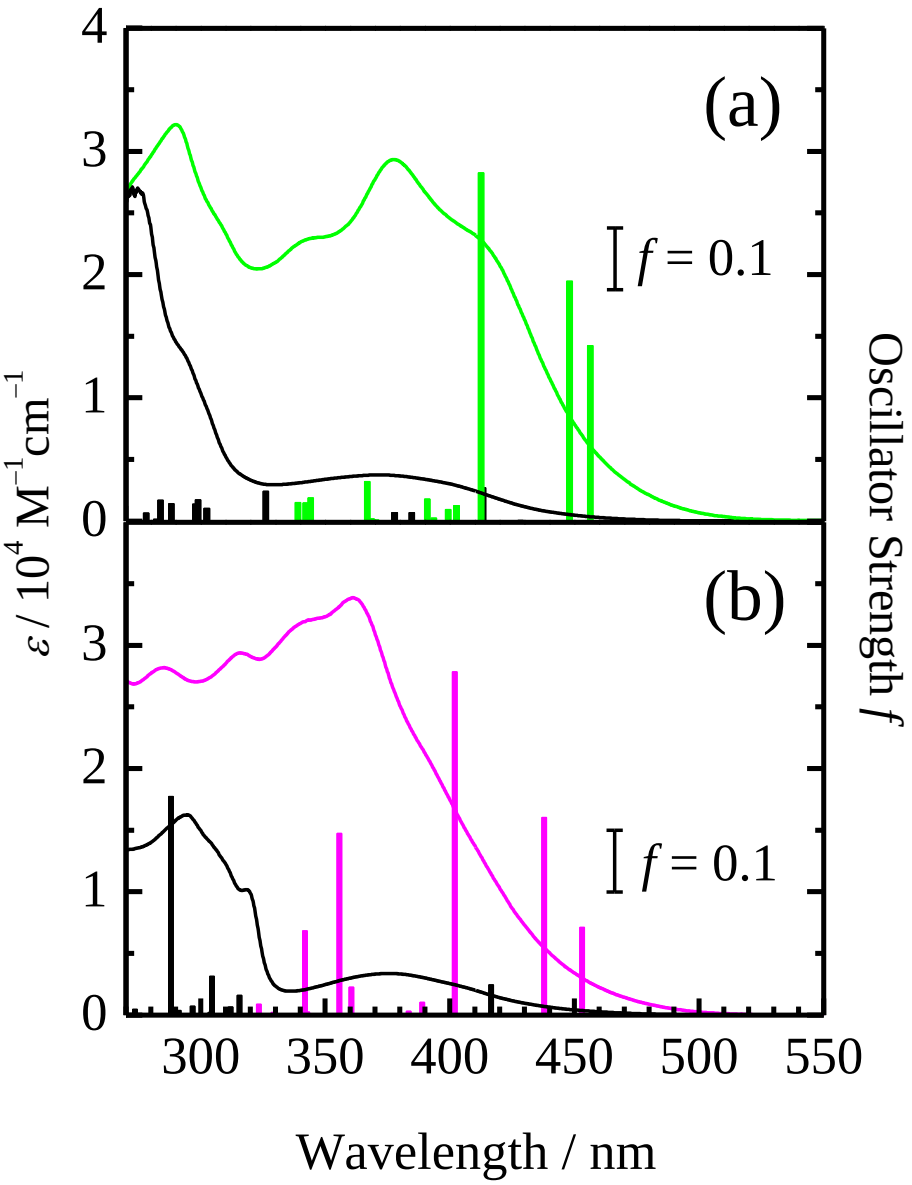

Figure 2-2 Absorption spectra of (a) **ReBphen** and **Rephen**, (b) **ReBbpy** and **Rebpy** in DMF at 298 K. The perpendicular bars represent the oscillator strengths of the absorption transitions calculated by TD-DFT. The colors in the figure correspond to **ReBphen** (green), **Rephen** (black), **ReBbpy** (pink), and **Rebpy** (black).

Table 2-2 Absorption maxima (λ^{abs}) and corresponding molar absorption coefficients (ε) of the complexes in DMF at 298 K.

complex	λ^{abs}/ nm (ε / 10^4 $M^{-1}cm^{-1}$)		
	ππ*	π(aryl)-p(B) CT	MLCT
ReBphen	290 (3.22)	378 (2.93)	438 (2.27)
Rephen	272 (2.71)		372 (0.37)
ReBbpy	316 (2.94)	361 (3.39)	392 (2.05)
Rebpy	294 (1.62)		375 (0.34)

2-3-3 Time-Dependent Density Functional Theory (TD-DFT) Calculations

Since the intense and featureless absorption bands in the UV–visible region observed for **ReBphen** and **ReBbpy** are fascinating to utilize the complexes as photosensitizers or photocatalysts, the detailed absorption characteristics of the complexes have been studied based on TD-DFT calculations. The lowest-energy excited states of the complexes calculated by TD-DFT are summarized in Table 2-3. The data demonstrate that the lowest-energy absorption transition of **ReBbpy** is the mixed HOMO–3 (15%)/HOMO–1 (39%)/HOMO (46%) → LUMO transitions, while those of other complexes are shown to be the HOMO → LUMO transitions. On the basis of the contours of the frontier molecular orbitals (i.e., HOMO and LUMO) shown in Figure 2-3 and the contribution of each atom in the relevant MO in Tables 2-4 and 2-5, it is predicted that the electron of **ReBphen** or **ReBbpy** in HOMO distributes to the d-orbital of the rhenium(I) center and, partly, to the π-orbital of each durylethynyl-diimine ligand. Contrarily, the LUMO of **ReBphen** is best characterized by the contributions of the π*-orbital of phen and p(B). Therefore, the lowest-energy excited singlet state of **ReBphen** is assigned to the synergistic MLCT/π(aryl)-p(B) CT state, while that of **Rephen** possesses almost pure MLCT characters. **ReBbpy** and **Rebpy** also show the similar behaviors to those of **ReBphen** and **Rephen**: the lowest-energy excited singlet state of **ReBbpy** is ascribed to the synergistic MLCT/π(aryl)-p(B) CT state, while **Rebpy** possesses almost pure MLCT characters. Since the MO population of **ReBbpy** in HOMO–1 is analogous to that of **Rebpy** or **Rephen** in HOMO, the contribution of the π(aryl)-p(B) type HOMO–1 → LUMO transition (i.e., 39%) to the lowest-energy absorption transition in **ReBphen** will be more important compared to that in **ReBbpy**.

The results agree very well with those by the electrochemical and absorption data as described before.

The TD-DFT calculations provide further significant insights into the excited state characteristics of the complexes. The absorption transition energies to the lowest-energy excited singlet states of **ReBphen** and **ReBbpy** (2.7103 and 2.7310 eV, respectively) are lower than the corresponding values of **Rephen** and **Rebpy** (2.9016 and 2.8611 eV, respectively). Furthermore, the oscillator strengths of the lowest-energy absorption transitions of **ReBphen** or **ReBbpy** (shown in Table 2-3) are much enhanced compared to those of the relevant reference complexes. Such results are in good agreement with the experimentally observed absorption data on the complexes in Figure 2-2 and Table 2-2. In the case of **ReBphen**, the increase in the absorption transition dipole moment upon photoexcitation could be due to the π^*(phen)–p(B) interaction in the 4-DBDE-phen ligand (i.e., p–π interactions observed in common triarylboranes[36]) and the MLCT interaction in the complex: the synergistic MLCT and π(aryl)-p(B) CT interactions. Analogous triarylborane substitution effects to those of the phen-type complexes are also observed for **ReBbpy**.

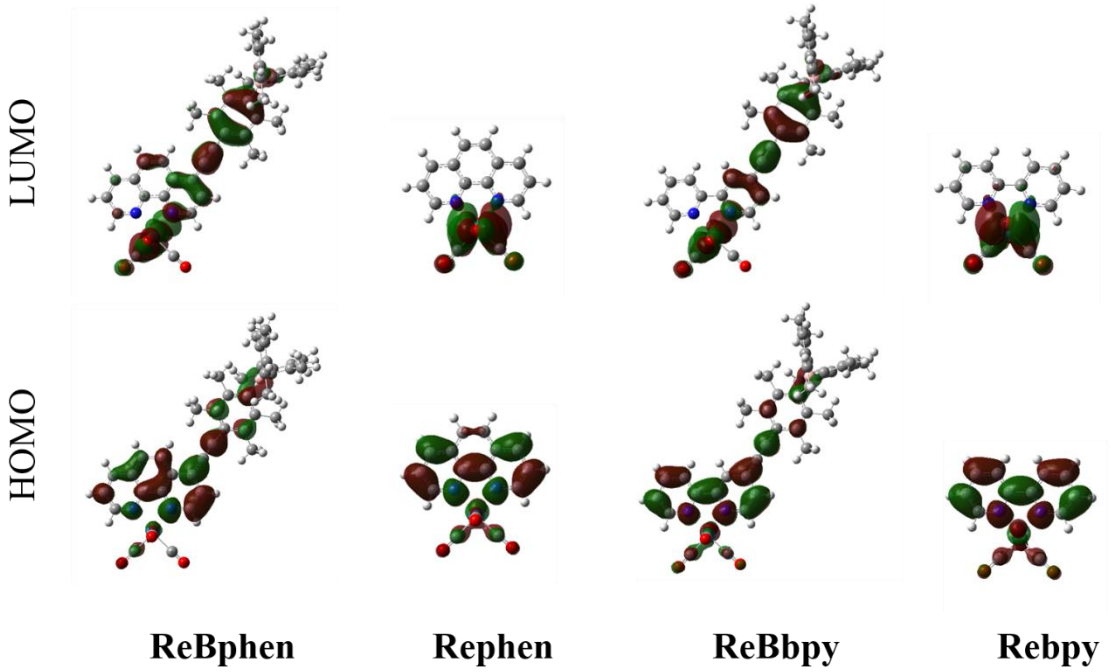

Figure 2-3 Frontier molecular orbitals (contour = 0.03 eÅ^{-3}) of the complexes.

Table 2-3 Calculated excited states of the complexes in DMF.

ReBphen			**ReBbpy**		
Excited State	Transition	Energy[a] (Wavelength) / Oscillator Strength[a]	Excited State	Transition	Energy[a] (Wavelength) / Oscillator Strength[a]
1	HOMO → LUMO	2.7103 eV (457.46 nm) / 0.2848	1	HOMO–3 → LUMO (15 %) HOMO–1 → LUMO (39 %) HOMO → LUMO (46 %)	2.7310 eV (453.98 nm) / 0.1423
2	HOMO–1 → LUMO (58 %) HOMO → LUMO (42 %)	2.7603 eV (449.16 nm) / 0.3892	2	HOMO–1 → LUMO	2.8249 eV (438.89 nm) / 0.3204
3	HOMO–3 → LUMO (72 %) HOMO → LUMO (28 %)	2.9971 eV (413.68 nm) / 0.5653	3	HOMO–3 → LUMO	3.0767 eV (402.97 nm) / 0.5572
4	HOMO–3 → LUMO (41 %) HOMO → LUMO+1 (59 %)	3.0705 eV (403.80 nm) / 0.0248	4	HOMO–4 → LUMO (33 %) HOMO–2 → LUMO (67 %)	3.1800 eV (389.89 nm) / 0.0208
5	HOMO–4 → LUMO (32 %) HOMO–2 → LUMO (68 %)	3.0961 eV (400.45 nm) / 0.0187	5	HOMO–4 → LUMO	3.2252 eV (384.42 nm) / 0.0057
Rephen			**Rebpy**		
Excited State	Transition	Energy (Wavelength) / Oscillator Strength	Excited State	Transition	Energy (Wavelength) / Oscillator Strength
1	HOMO → LUMO	2.9016 eV (427.29 nm) / 0.0011	1	HOMO → LUMO	2.8611 eV (433.34 nm) / 0.0017
2	HOMO–1 → LUMO	3.0076 eV (412.24 nm) / 0.0538	2	HOMO–1 → LUMO	2.9831 eV (415.62 nm) / 0.0490
3	HOMO → LUMO+1	3.2315 eV (383.68 nm) / 0.0136	3	HOMO–2 → LUMO	3.4154 eV (363.02 nm) / 0.0003
4	HOMO–1 → LUMO+1	3.2910 eV (376.74 nm) / 0.0135	4	HOMO → LUMO+1	3.8985 eV (318.03 nm) / 0.0000
5	HOMO–2 → LUMO	3.4638 eV (357.94 nm) / 0.0003	5	HOMO–4 → LUMO (80 %) HOMO → LUMO+1 (20 %)	3.9368 eV (314.94 nm) / 0.0008

[a] The complete calculated transitions are summarized in the appendix.

Table 2-4 Molecular-orbital contributions of **ReBphen** and **Rephen** in DMF.

ReBphen

Molecular Orbital	Eigenvalues / Hartrees	Contribution / %							
		rhenium	phen	ethynyl	duryl	boron	mesityl	CO	bromide
LUMO+3	–0.04097	1.48	77.42	4.46	7.11	1.18	5.53	1.87	0.95
LUMO+2	–0.06491	0.08	7.89	1.16	16.76	28.24	45.72	0.09	0.06
LUMO+1	–0.08488	1.60	92.85	0.72	1.26	0.20	0.26	1.97	1.14
LUMO	–0.09928	3.04	70.30	9.22	9.76	1.14	1.61	2.97	1.96
HOMO	–0.21825	20.96	15.05	11.38	25.08	0.44	4.62	10.21	12.26
HOMO–1	–0.22376	37.51	4.35	0.27	0.61	0.01	0.16	17.82	39.27
HOMO–2	–0.22608	0.01	0.01	0.05	11.19	1.07	87.66	0.00	0.01
HOMO–3	–0.22855	20.05	5.46	4.48	15.56	0.38	9.01	8.69	36.37

Rephen

Molecular Orbital	Eigenvalues / Hartrees	Contribution / %							
		rhenium	phen	ethynyl	duryl	boron	mesityl	CO	bromide
LUMO+3	–0.03248	22.40	24.65	--	--	--	--	51.14	1.81
LUMO+2	–0.03758	6.24	79.36	--	--	--	--	9.76	4.64
LUMO+1	–0.08133	0.11	99.22	--	--	--	--	0.66	0.01
LUMO	–0.08956	4.52	87.84	--	--	--	--	4.41	3.23
HOMO	–0.22362	38.65	3.18	--	--	--	--	18.70	39.47
HOMO–1	–0.22520	36.55	6.46	--	--	--	--	16.03	40.96
HOMO–2	–0.24623	67.64	2.73	--	--	--	--	29.34	0.29
HOMO–3	–0.25417	3.88	59.11	--	--	--	--	4.01	33.00

Table 2-5 Molecular-orbital contributions of **ReBbpy** and **Rebpy** in DMF.

ReBbpy

Molecular Orbital	Eigenvalues / Hartrees	Contribution / %							
		rhenium	bpy	ethynyl	duryl	boron	mesityl	CO	bromide
LUMO+3	–0.05250	1.79	31.59	0.47	0.54	0.44	1.13	2.70	1.02
LUMO+2	–0.05979	0.33	52.92	2.56	8.53	19.37	37.09	0.42	0.11
LUMO+1	–0.07181	0.40	73.80	5.91	14.74	10.44	14.60	0.75	0.24
LUMO	–0.09685	4.21	9.76	6.35	6.58	0.90	1.26	4.06	2.84
HOMO	–0.21898	22.22	3.68	11.81	26.90	0.46	5.27	10.70	12.88
HOMO–1	–0.22420	36.77	0.00	0.76	1.92	0.03	0.55	17.27	39.02
HOMO–2	–0.22596	0.00	5.10	0.05	12.35	1.06	86.54	0.00	0.00
HOMO–3	–0.22841	20.80		4.28	14.98	0.37	8.68	9.05	36.74

Rebpy

Molecular Orbital	Eigenvalues / Hartrees	Contribution / %							
		rhenium	bpy	ethynyl	duryl	boron	mesityl	CO	bromide
LUMO+3	–0.03219	23.00	22.06	--	--	--	--	53.10	1.84
LUMO+2	–0.04868	0.41	96.99	--	--	--	--	2.57	0.03
LUMO+1	–0.05455	2.42	93.97	--	--	--	--	2.23	1.38
LUMO	–0.09078	4.46	87.88	--	--	--	--	4.42	3.24
HOMO	–0.22364	38.95	3.23	--	--	--	--	18.78	39.04
HOMO–1	–0.22585	36.76	4.60	--	--	--	--	15.98	42.66
HOMO–2	–0.24588	67.28	3.03	--	--	--	--	29.36	0.33
HOMO–3	–0.26187	21.35	11.72	--	--	--	--	11.03	55.90

2-3-4 Emission Spectra and Photophysical Properties

Figures 2-4 and 2-5 display the corrected emission spectra and emission decay profiles of **ReBphen** and **ReBbpy** in DMF at 298 K, respectively, together with those of the corresponding reference complexes. The intensities of the emission spectra are normalized to those at the maximum wavelength (λ^{em}) in Figure 2-4, and the photophysical parameters are summarized in Table 2-6. All of the complexes showed broad and structureless emission from the excited triplet states with the MLCT-type characters. The emission spectrum of **ReBphen** (λ^{em} = 679 nm) was red-shifted compared to that of **Rephen** (λ^{em} = 609 nm), which could be explained by the synergistic MLCT/π(aryl)-p(B) CT interactions, as predicted by the redox potentials, the absorption spectrum, and the TD-DFT calculations of the complex as described before. Similar emission properties to those of **ReBphen** have been also confirmed for **ReBbpy** as seen in Table 2-6, Figures 2-4 and 2-5. The emission spectrum of **ReBbpy** (λ^{em} = 645 nm) was also red-shifted compared to that of **Rebpy** (λ^{em} = 622 nm). It is worth noting that the difference in the emission maximum energy ($\Delta\tilde{\nu}^{em}$) between the complexes with and without the arylborane group is 1700 or 540 cm^{-1} for the phen-type (**ReBphen** vs. **Rephen**) or bpy-type complexes (**ReBbpy** vs. **Rebpy**), respectively. The larger $\Delta\tilde{\nu}^{em}$ value observed for **ReBphen** relative to that for **ReBbpy** can be also explained by the redox potentials of the complexes as discussed in the previous section.

The emission decay profile of **ReBphen** in DMF at 298 K was analyzed by a single exponential function and the emission lifetime (τ^{em} = 610 ns) was determined to be 2.2 times longer than that of **Rephen** (τ^{em} = 270 ns). Analogous triarylborane substitution effects to those of the phen-type complexes have been observed for the bpy-type complexes: τ^{em} = 100 and 50 ns for **ReBbpy** and **Rebpy**, respectively. In

contrast, the emission quantum yield of **ReBphen** was smaller (0.011) than that of **Rephen** (0.037) while the Φ^{em} value of **ReBbpy** was almost the same with that of **Rebpy** (Φ^{em} = 0.010). On the basis of the Φ^{em} and τ^{em} values, the radiative (k_r) and nonradiative decay rate constants (k_{nr}) of the complexes were evaluated by the relations: $\Phi^{em} = k_r / (k_r + k_{nr})$ and $\tau^{em} = 1 / (k_r + k_{nr})$. The results on **ReBphen** and **Rephen** are included in Table 2-6, together with those on **ReBbpy** and **Rebpy** for comparison. The data demonstrate that the k_{nr} value of **ReBphen** or **ReBbpy** is almost half of that of **Rephen** or **Rebpy**, respectively, indicating the important role of the DBDE group in determining the nonradiative decay path from the emitting excited state. Generally, the k_{nr} value of the ^{3}MLCT excited state of a transition metal complex increases with a decrease in the emission energy ($\tilde{\nu}^{em}$), as predicted by the energy gap dependence of k_{nr}: $\ln k_{nr} = \alpha \times \tilde{\nu}^{em}$ + constant ($\alpha < 0$).[28,37–38] However, **ReBphen** and **ReBbpy** shows an opposite trend to the prediction by the energy gap law, displaying smaller k_{nr} for the lower-energy emission compared to the k_{nr} and $\tilde{\nu}^{em}$ values of **Rephen** and **Rebpy**. Therefore, the emission properties of **ReBphen** and **ReBbpy** are unusual. Nonetheless, this is typical characteristics of the emission from the transition metal complex with a triarylborane-appended ligand(s) as reported in the previous publications on the analogous Ru(II) complexes.[19] It has been known that another factor governing k_{nr} of a transition metal complex is thermal activation from the emissive MLCT excited state to the non-emitting dd (ligand-field)/higher-energy lying (fourth) MLCT excited states and subsequent fast nonradiative decay to the ground state.[39] If such thermal processes participate in excited state decay, the emission lifetime of the complex should depend strongly on temperature (T), which is worth studying in some more detail as described in the following section.

In contrast to k_{nr}, one can find significant differences in the DBDE effects on k_r between the bpy- and phen-type complexes, where the k_r value of **ReBphen** or **ReBbpy** is one-tenth or almost half, respectively, compared to the relevant values of the complexes without the DBDE group. This could be explained by the difference in the degree of the electronic overlap between the excited and ground states of the complex: **ReBphen** vs. **ReBbpy**. The degree of the electronic overlap between the excited and ground states will be larger for **ReBphen** owing to the relatively large contribution of π(aryl)-p(B) CT to the electronic absorption transition compared to that in **ReBbpy**, as confirmed by the TD-DFT calculations. These results are also in good accordance with the differences in the redox potential ($E_{1/2}(Re^{I/0})$–$E_{1/2}(Re^{0/-I})$) and the ε value between the two complexes.

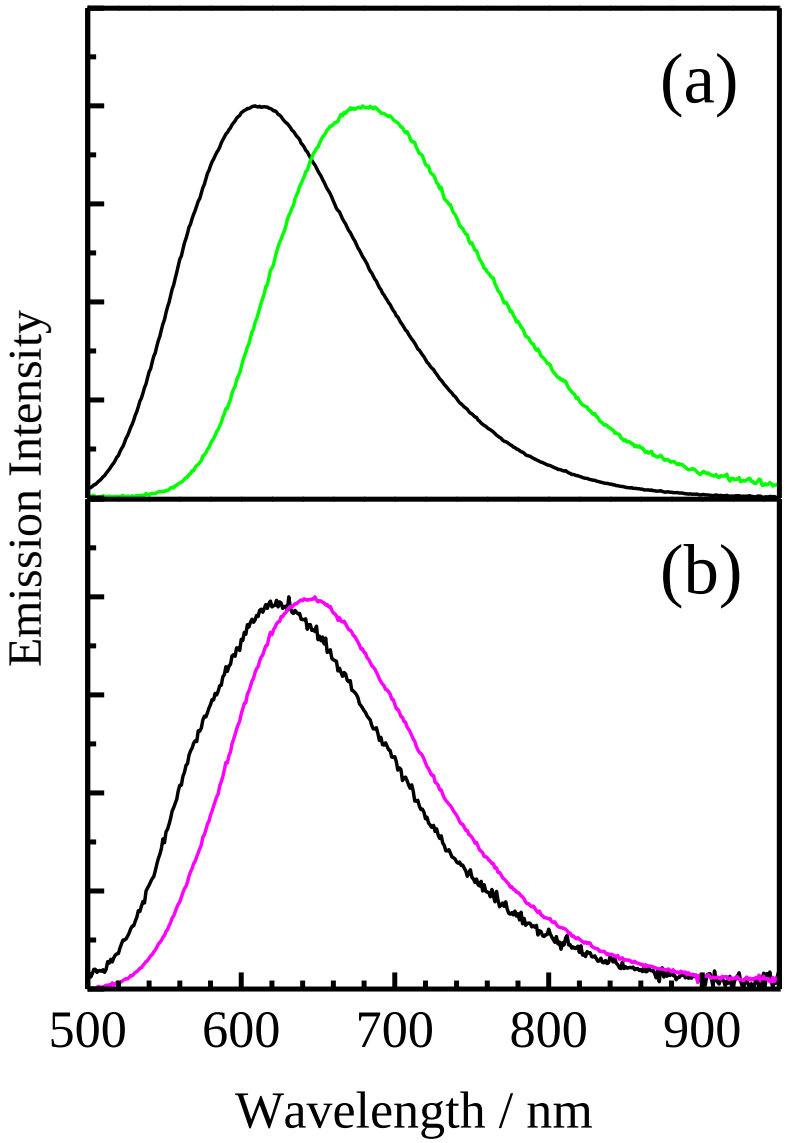

Figure 2-4 Corrected emission spectra of (a) **ReBphen** (green) and **Rephen** (black), (b) **ReBbpy** (pink) and **Rebpy** (black) in DMF at 298 K.

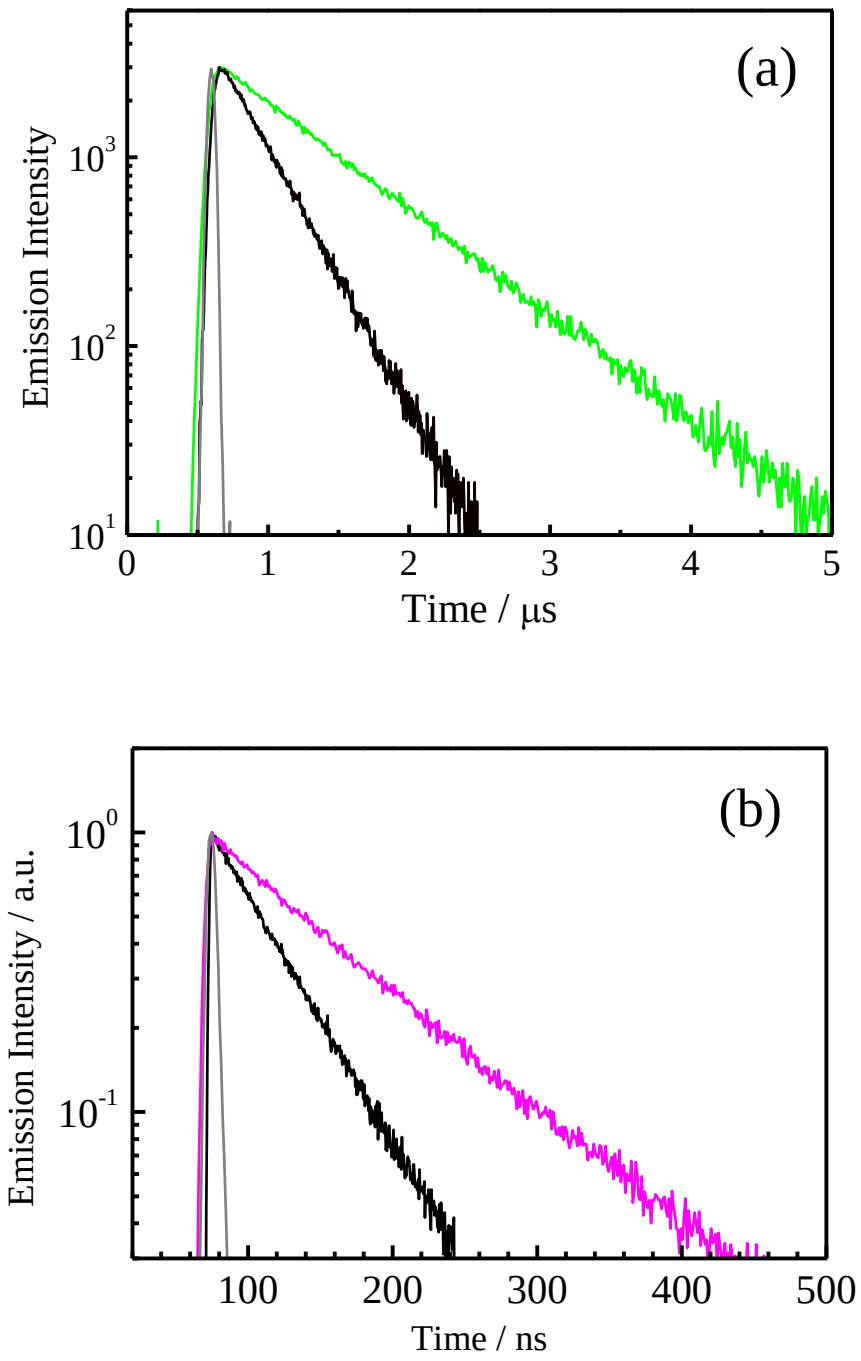

Figure 2-5 Emission decay profiles of (a) **ReBphen** (green) and **Rephen** (black), (b) **ReBbpy** (pink) and **Rebpy** (black) in DMF at 298 K. Gray curves represent those of the instrumental response function (IRF).

Table 2-6 Spectroscopic and photophysical properties of the complexes in DMF at 298 K.

complex	λ^{em} / nm	Φ^{em}	τ^{em} / μs	k_r / 10^5 s^{-1}	k_{nr} / 10^5 s^{-1}
ReBphen	679	0.011	610	0.18	16
Rephen	609	0.037	270	1.4	36
ReBbpy	645	0.010	100	1.0	99
Rebpy	622	0.010	50	2.0	200

2-3-5 Solvent Dependences of the Spectroscopic and Photophysical Properties of ***ReBphen*** *and* ***Rephen***.

The absorption and emission spectra of **ReBphen** and **Rephen** were measured in toluene, THF, and CH_3CN to evaluate their solvent dependences. Figure 2-6 (a) shows the absorption spectra of **ReBphen** in a series of solvents, together with those of **Rephen** as a reference. **ReBphen** exhibited the absorption bands at λ^{abs} (wavelength) ~ 290 nm and 320–390 nm irrespective of the solvent which were ascribed to the $^1\pi\pi^*$ transition in the phen ring and the LC transitions, respectively, and the band at around 430 nm could be assigned to the ^{1}MLCT absorption due to the similarity with that in DMF. Also, both $^1\pi\pi^*$ and ^{1}MLCT absorption bands of **ReBphen** were shifted to the lower-energy compared to those of **Rephen**, irrespective of the solvent. Furthermore, a hypsochromic shift of the MLCT absorption band with an increase in the solvent polarity was observed for **ReBphen**. It can be explained by the stabilization of the ground state in energy by the solvent.

Figure 2-6 (b) shows the emission spectra of **ReBphen** and **Rephen** in different solvent, where the emission intensities were normalized to those at the maximum wavelengths. The emission spectrum of **ReBphen** (λ^{em} = 669, 681, and 676 nm in toluene, THF, and CH_3CN, respectively) is red-shifted and slightly broadened compared to the corresponding data for **Rephen** (λ^{em} = 605, 613, and 611 nm in the relevant solvent), irrespective of the solvent due to the stabilization of the excited state in energy and strong excited-state solvation by the presence of the DBDE group in the phen ligand of **ReBphen**, similar to those in DMF. The emission spectra of both complexes are red shifted with an increase in the solvent polarity due to the stabilization of the excited states by the solvent.

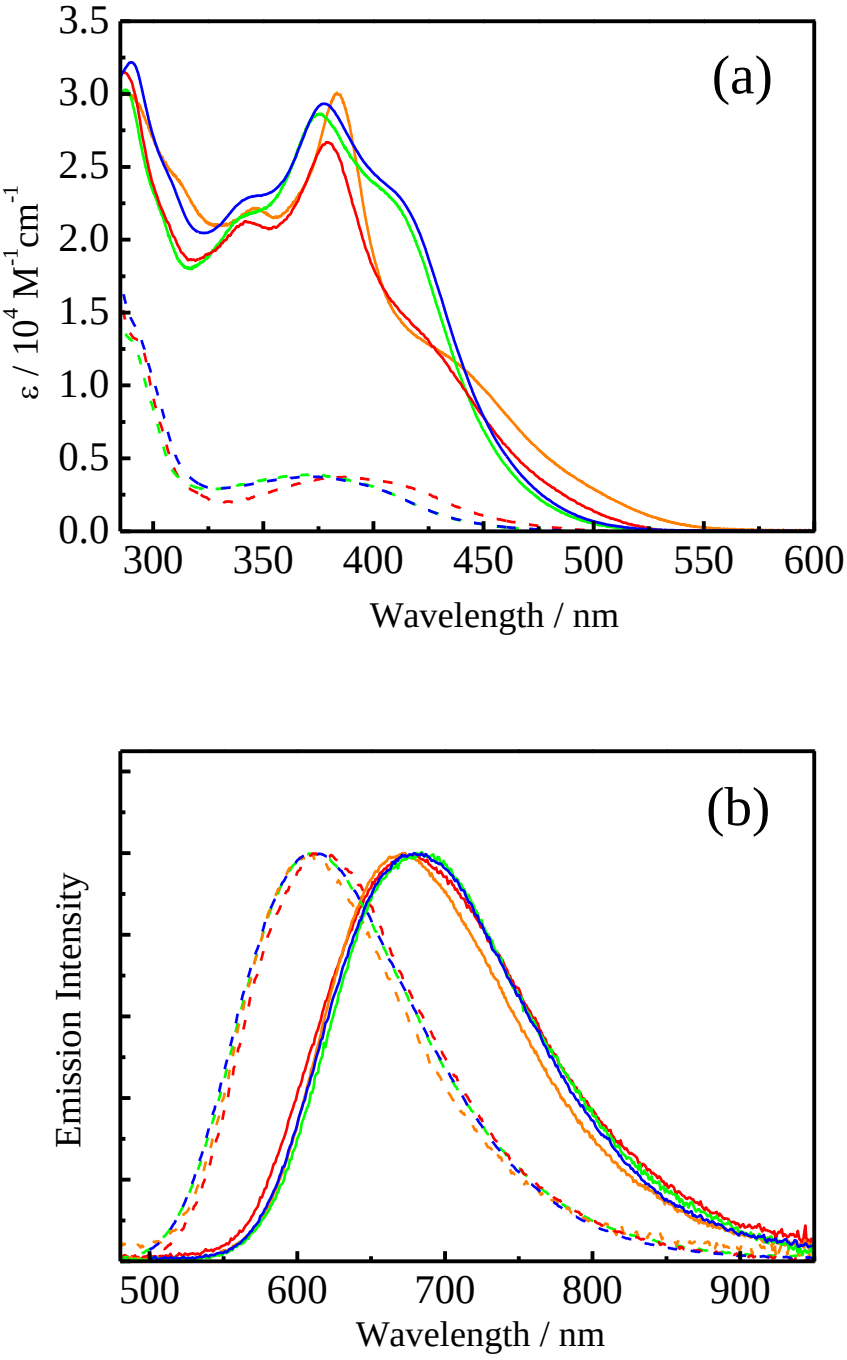

Figure 2-6 Absorption (a) and emission spectra (b) of **ReBphen** (solid curves) and **Rephen** (broken curves) in toluene (orange), THF (red), CH_3CN (green) and DMF (blue).

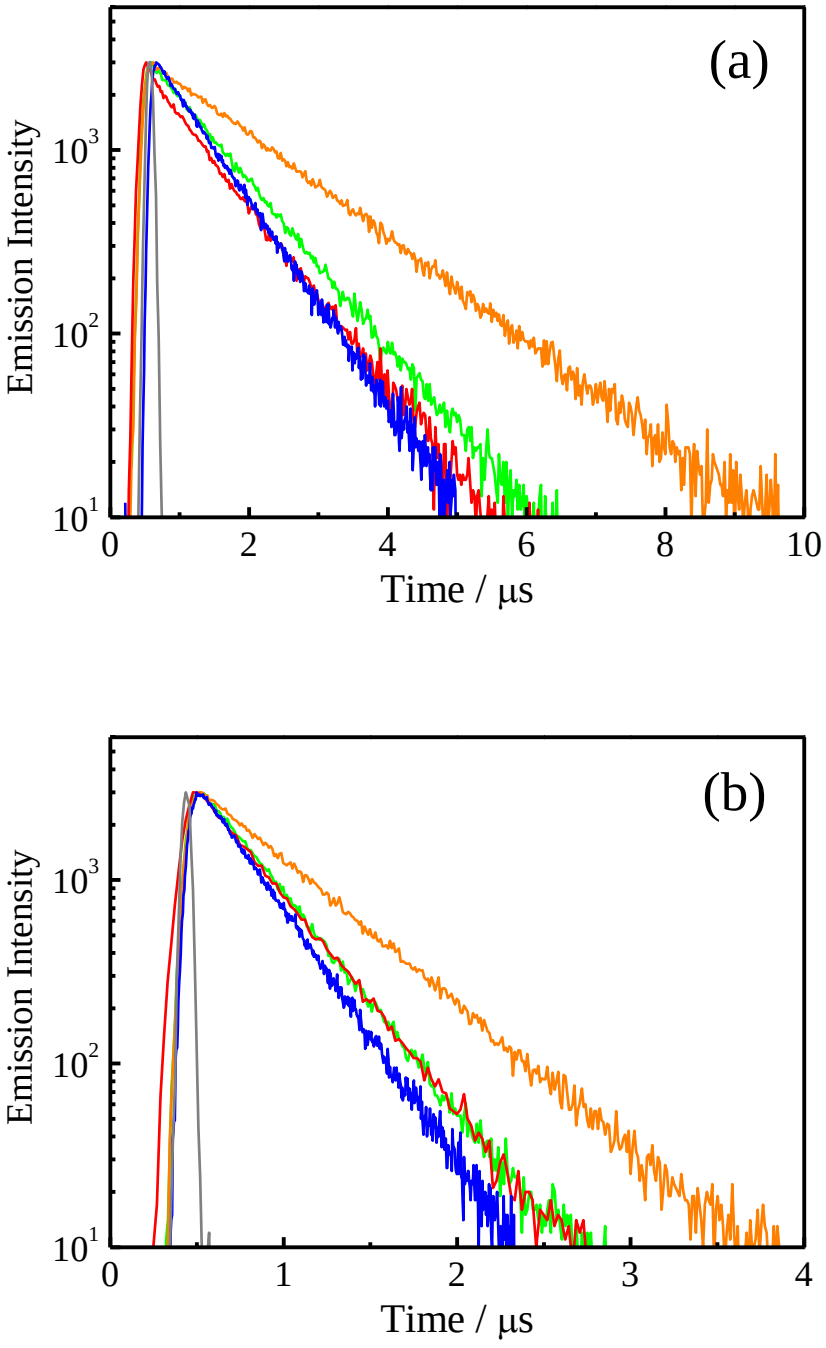

Figure 2-7 Emission decay profiles of (a) **ReBphen** and (b) **Rephen** in toluene (orange), THF (red), CH_3CN (green) and DMF (blue). Gray curves represent those of the instrumental response function (IRF).

Table 2-7 Solvent dependences of the spectroscopic and photophysical properties of **ReBphen** and **Rephen**.

Complex	Solvent	λ^{abs} / nm (ε / 10^4 M^{-1} cm^{-1})			λ^{em} / nm	Φ^{em}	τ^{em} / ns	k_r / 10^5 s^{-1}	k_{nr} / 10^5 s^{-1}
	toluene	288 (3.00)	384 (3.00)	438 (sh, 1.15)	669	0.033	1570	0.21	6.1
ReBphen	THE	287 (3.15)	380 (2.67)	420 (sh, 1.39)	681	0.017	900	0.19	11
	CH_3CN	287 (3.02)	375 (2.86)	411 (sh, 2.23)	676	0.015	960	0.16	10
	toluene	n. d. (n.		392 (n. d.)[a]	605	0.070	560	1.3	17
Rephen	THE	269 (3.07)		385 (0.37)	613	0.044	390	1.1	24
	CH_3CN	267 (2.78)		370 (0.39)	611	0.043	370	1.2	26

[a]Not determined due to overlap with absorption of the solvent.

2-3-6 Temperature Dependence of the Emission Lifetime

To clarify the nature of the small k_{nr} values observed for **ReBphen** and **ReBbpy**, temperature (T) dependences of the emission lifetimes of the complexes in propylene carbonate (PC) in T = 220–330 K were studied, together with those of the reference complexes. As shown in Figure 2-8, the emission decay profiles of the complexes were analyzed by single exponential functions irrespective of T (= 220–330 K) and the emission lifetimes of the complexes decreased with an increase in T. The T dependence of τ^{em} ($\tau^{em}(T)$) observed for [Re(CO)$_3$LX] is known to be analyzed by an Arrhenius-type equation in Eq. (2-2).[40]

$$[\tau^{em}(T)]^{-1} = \frac{k_0 + k_1 \exp(-\Delta E/RT)}{1 + \exp(-\Delta E/RT)} \quad (2\text{-}2)$$

In Eq. (2-1), k_0 is the sum of T-independent radiative (k_r^0) and nonradiative decay rate constants (k_{nr}^0), and k_1 is the frequency factor for thermal activation from the emitting excited state to the higher-energy nonemitting excited state with the energy barrier between the two states being ΔE: see Scheme 2-4.

As shown in Figure 2-9, the T dependences of τ^{em} were adequately analyzed by Eq. (2-2) using the parameters summarized in Table 2-8. The ΔE value of **ReBphen** (960 cm^{-1}) was almost 1.7-times larger than that of **Rebpy** (560 cm^{-1}), and the similar trends observed for these complexes were also confirmed for $\tau^{em}(T)$ of **ReBbpy** (1000 cm^{-1}) and **Rebpy** (560 cm^{-1}) as the data were included in Table 2-8. The larger ΔE value gives rise to the smaller contribution of the nonemitting state to excited-state decay and, thus, the τ^{em} values of **ReBphen** and **ReBbpy** are less sensitive to T compared to those of **Rephen** and **Rebpy**, respectively.

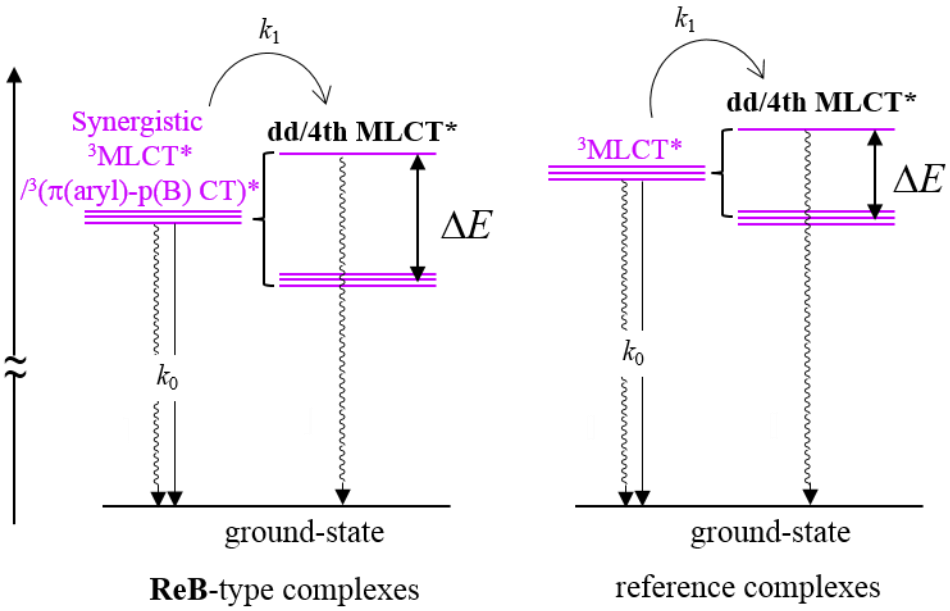

Scheme 2-4 Energy diagrams for the temperature-dependent emission lifetimes of the complexes.

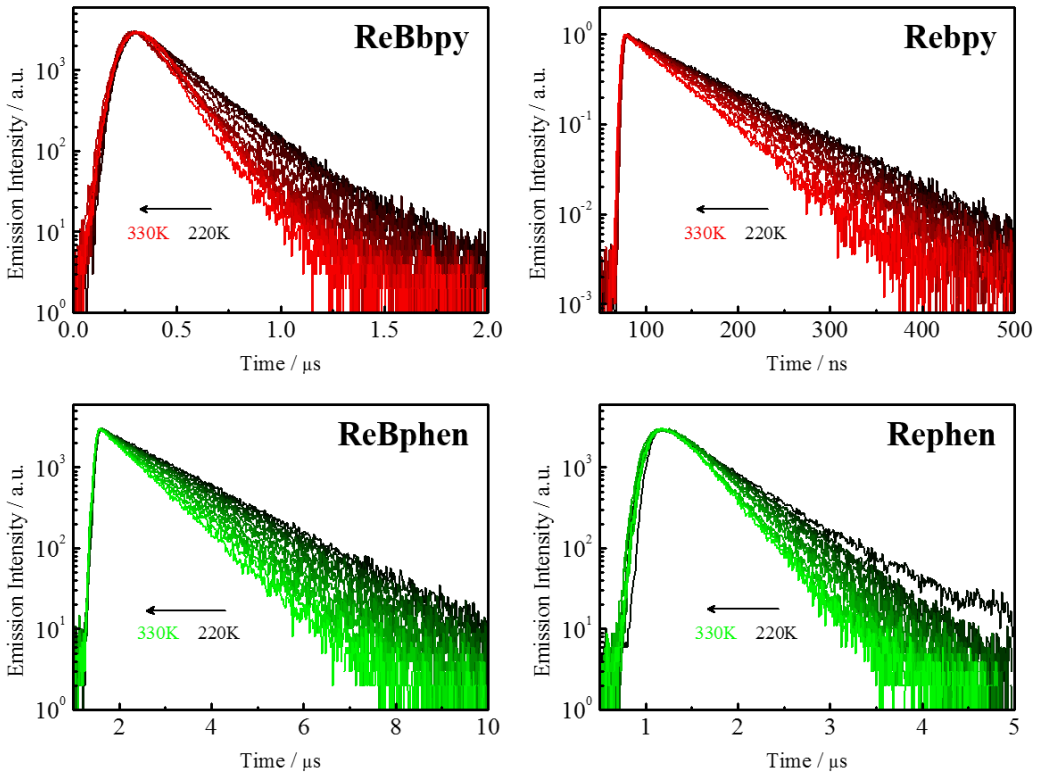

Figure 2-8 Temperature (T = 220–330 K) dependent emission decay profiles of the complexes in propylene carbonate.

Table 2-8 Temperature dependent emission parameters of the complexes in propylene carbonate.

complex	ΔE / cm^{-1}	k_0 / 10^6 s^{-1}	k_1 / 10^8 s^{-1}
ReBphen	960	0.61	0.43
Rephen	560	0.94	0.30
ReBbpy	1000	3.7	4.1
Rebpy	560	19	2.6

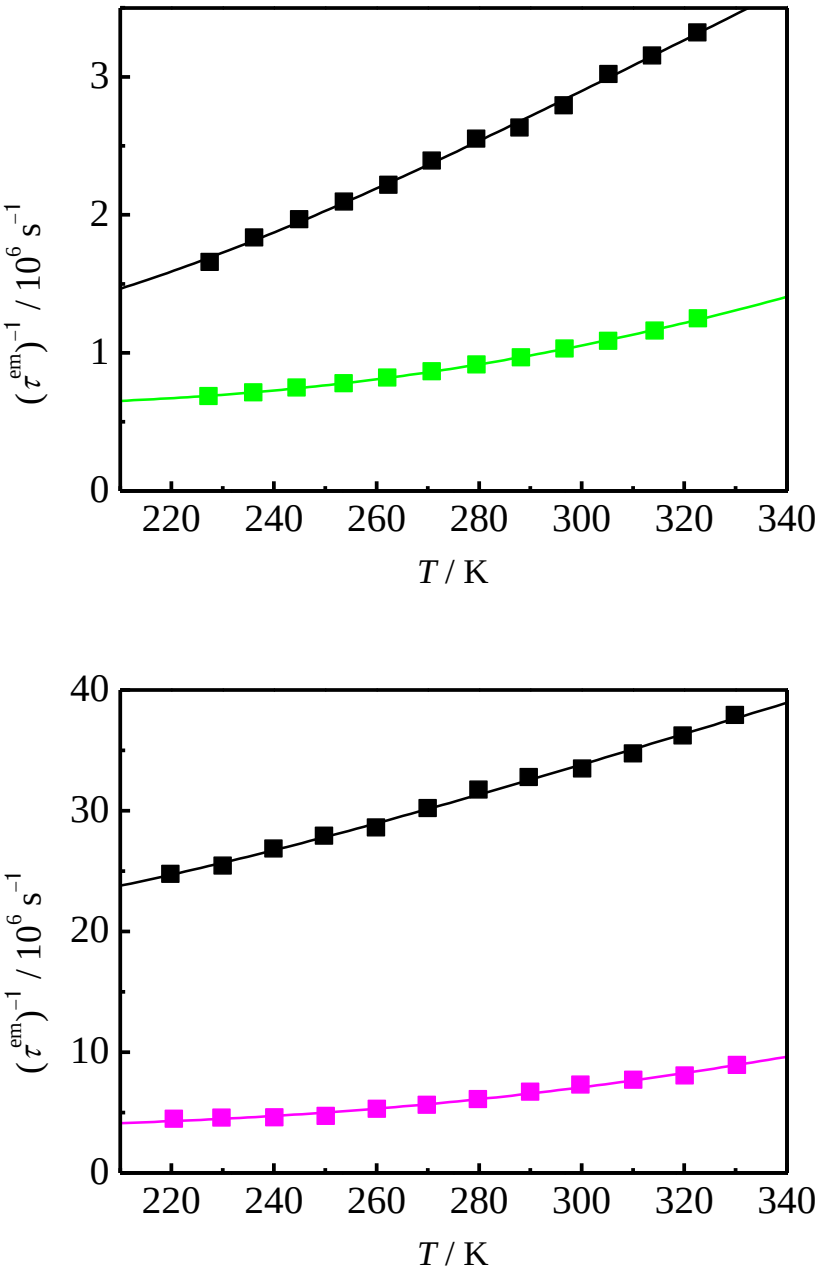

Fig 2-9 Temperature dependences of the emission lifetimes of the complexes in propylene carbonate. The curves represent the theoretical fits by Eq. (2-2). The colors in the figure correspond to **ReBphen** (green), **Rephen** (black), **ReBbpy** (pink), and **Rebpy** (black).

2-3-7 Franck–Condon Analysis of the Emission Spectrum at Room Temperature

Frank–Condon analysis of the emission spectra was conducted by Eq. (2-1) to discuss further the effects of the DBDE group on nonradiative decay of **ReBphen** and **Rephen**. Figure 2-10 shows the corrected and simulated emission spectra of **ReBphen** and **Rephen** in DMF at room temperature, and Table 2-9 summarizes the optimized spectral fitting parameters. The emission spectra of both **ReBphen** and **Rephen** were reproduced very well with the correlation coefficients more than 0.998. The smaller E_0 value of **ReBphen** (15,800 cm^{-1}) compared to that of **Rephen** (18,000 cm^{-1}) is in good accordance with the experimental results. The correlation coefficients of the emission spectral fittings by Franck-Condon analysis for **ReBbpy** and **Rebpy** were also more than 0.999, and the smaller E_0 value of **ReBbpy** (17,200 cm^{-1}) compared to that of **Rephen** (17,900 cm^{-1}) also agreed very well with the experimental results. Furthermore, the $\hbar\omega_M$ (1450 cm^{-1}) and $\hbar\omega_L$ (500 cm^{-1}) values observed for **Rephen** and **Rebpy** also agreed very well with the reported values.[29]

As it is known, the medium-frequency vibrational mode can be ascribed to the ring-breathing vibration in a diimine ligand, while the low-frequency vibrational mode is characterized by the stretching vibration between a metal ion and a ligating nitrogen atom. The results imply that the excited state accepting frequencies of the complex does not correspond to the vibrational properties of the DBDE group in **ReBphen** or **ReBbpy**. However, the smaller Huang–Rhys factors of **ReBphen** and **ReBbpy** (S_M = 0.71 and S_L = 2.42 for **ReBphen** and S_M = 0.58 and S_L = 4.04 for **ReBbpy**) indicate that the vibrational displacements between the emitting ^{3}MLCT excited and ground states of the complexes along the medium- and low-frequency mode coordinates are smaller than those of **Rephen** and **Rebpy**. The results suggest another possibility for the smaller k_r

and k_{nr} values of **ReBphen** and **ReBbpy**. Furthermore, the larger $\tilde{\nu}_{1/2}$ value of **ReBphen** (2580 cm^{-1}) compared to that of **Rephen** (2410 cm^{-1}) is induced clearly by the presence of the DBDE group in **ReBphen**.

The results obtained from the Frank–Condon analysis indicate the increase in the solvent interactions in the ^{3}MLCT excited states of **ReBphen** and **ReBbpy** through the synergistic MLCT and π(aryl)-p(B) CT interactions.

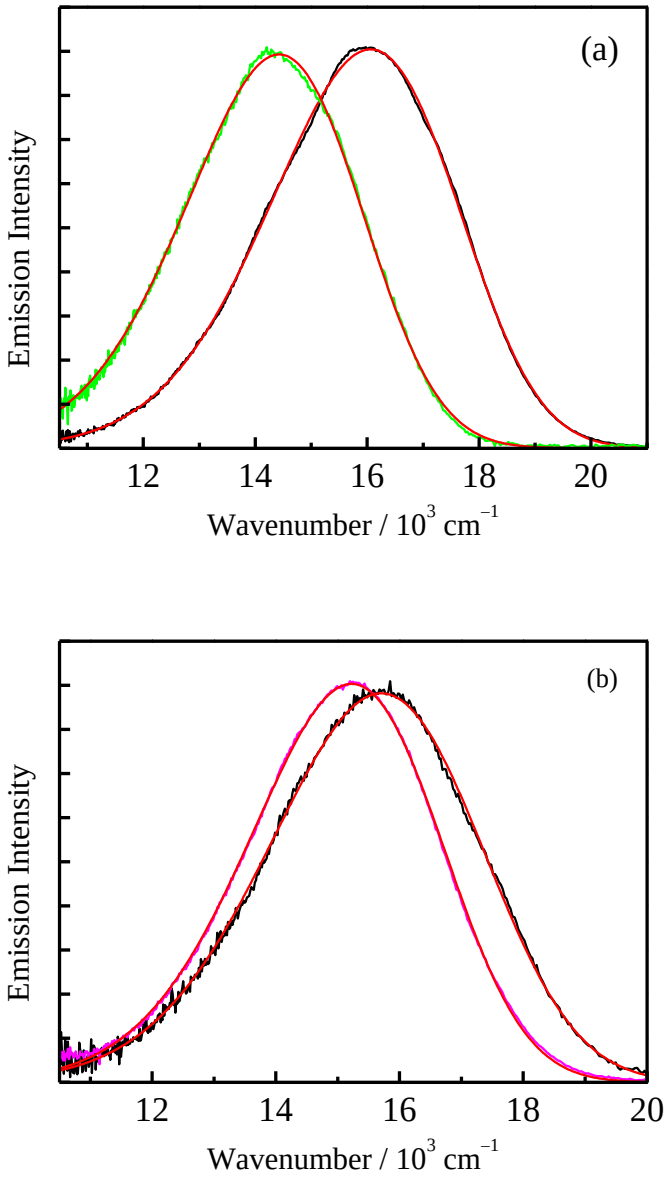

Figure 2-10 Corrected emission spectra at 298 K and the calculated emission fits (red) of **ReBphen** (green), **Rephen** (black) (a) and **ReBbpy** (pink), **Rebpy** (black) (b) in DMF.

Table 2-9 Spectral fitting parameters for the complexes in DMF at 298 K.

Complex	E_0 / cm^{-1}	$\tilde{\nu}_{1/2}$ / cm^{-1}	$\hbar\omega_M$ / cm^{-1}	$\hbar\omega_L$ / cm^{-1}	S_M	S_L	r [a]
ReBphen	15800	2580	1450	500	0.71	2.42	0.99942
Rephen	18000	2410	1450	500	0.85	3.69	0.99875
ReBbpy	17200	2580	1450	500	0.58	4.04	0.99963
Rebpy	17900	2688	1450	500	0.65	4.22	0.99979

[a] correlation coefficient.

2-3-8 Diimine Ligand Structure and Triarylborane Substitution Effects

The present studies on **ReBphen**/**Rephen** and **ReBbpy**/**Rebpy** demonstrate explicitly that an introduction of the DBDE group to the periphery of the diimine ligand in $[Re(CO)_3LX]$ can commonly modulate both spectroscopic and photophysical properties of the complex. However, the effects of the DBDE group on the properties of the complex are somewhat different between the bpy- and phen-type complexes. To design and synthesis of new and novel $[Re(CO)_3LX]$, the diimine ligand structure and DBDE substitution effects on the spectroscopic and photophysical properties of the complexes are worth discussing in detail.

The structure of phen is more rigid than that of bpy owing to the presence of the carbon atoms at the 5- and 6-positions in phen. Such structural rigidity of phen will impede more or less nonradiative decay from the excited state of the complex. In practice, both k_0 and k_1 values of **Rephen** are significantly smaller than those of **Rebpy** and, therefore, the excited state of **Rephen** is considerably longer-lived than **Rebpy**: see Table 2-6. The photophysical behaviors analogous to those of **Rephen**/**Rebpy** can be also seen for $[RuL_3]^{2+}$ complexes. As an example, the k_0 and k_1 values of $[Ru(bpy)_3]^{2+}$ are larger than those of $[Ru(phen)_3]^{2+}$, while the emission lifetime of $[Ru(phen)_3]^{2+}$ is shorter than that of $[Ru(bpy)_3]^{2+}$ due to the smaller energy barrier (ΔE) to the higher-energy lying nonemitting excited state.[41] Even in the presence of the DBDE group in L, similar characteristics to the photophysical properties of **Rephen**/**Rebpy** or $[Ru(phen)_3]^{2+}$/$[Ru(bpy)_3]^{2+}$ can be seen for **ReBphen** and **ReBbpy** (Tables 2-2 and 2-6).

Beside the structural rigidity of L, its electronic structures will be also the important factor controlling the excited-state characteristics of $[Re(CO)_3LX]$. It is worth pointing out that phen possesses the expanded π-electron system compared to bpy. As

seen in Tables 2-4 and 2-5, more than 87% of MO in LUMO of **Rephen** or **Rebpy** is populated in the respective diimine ligand and the MO contours of the two complexes are quite similar with each other. To compare the differences in the electronic structures between **Rephen** and **Rebpy**, the MO population at each carbon atom in L of **Rephen** or **Rebpy** at the LUMO level was evaluated as the results were shown in Figure 2-11, where those of the symmetric carbon atoms at the 4- and 7-positions of phen were averaged and indicated as the percentage in the whole molecule. As seen in the figure, MO of **Rephen** is relatively localized at the 4-position (10.15%) of phen, while that of **Rebpy** at the 4-position of bpy is 7.38%. The larger MO population at the 4-position of phen or bpy presumably enhances the electronic interaction between the ligand and the arylborane unit in **ReBphen** or **ReBbpy**, respectively. This will be one of the important diimine ligand structure and triarylborane substitution effects on the excited-state properties of the complexes.

The above discussion suggests that the substitution position of the DBDE group in bpy or phen would be another key controlling the photophysical properties of the complex. Therefore, DFT calculations for the isomeric 3- and 5-DBDE ReBphen complexes (**3-ReBphen**/**5-ReBphen**) and ReBbpy (**3-ReBbpy**/**5-ReBbpy**) as well as those for ethynylduryl(dimesityl)borane (EDDB) as an arylborane unit were conducted. The ground-state geometries of the complexes and EDDB were optimized as in DMF. The chemical structures of EDDB and isomeric complexes are shown in Figure 2-12, together with their frontier molecular orbitals, and the HOMO/LUMO energies of the compounds are shown in Figure 2-13. The HOMO–LUMO energy gap of the complex decreases by introducing the DBDE group to L irrespective of the substituted position, while the most pronounced substituent effects are found for the 4-substituted complexes

(i.e., **ReBphen** and **ReBbpy**). Furthermore, one can find significant differences in the MO contours between the substitution positions of the DBDE group in bpy or phen. It is worth emphasizing that the HOMOs of **3-ReBphen/3-ReBbpy** and **5-ReBphen/5-ReBbpy** are best characterized by the π-orbitals of the durylethynyl-diimine moiety, and their LUMOs are localized primarily on the π*-orbitals of the ethynyl-diimine moiety. Assuming the lowest-energy excited states of the complexes are originated from their HOMO–LUMO transitions, the excited states of **3-ReBphen/3-ReBbpy** and **5-ReBphen/5-ReBbpy** can be ascribed to LC/intraligand charge transfer (ILCT) characters with a small or almost no contribution of MLCT and π(aryl)-p(B) CT characters. It is important to note that the synergistic MLCT/π(aryl)-p(B) CT excited states are predicted for **ReBphen** and **ReBbpy** alone among the isomeric complexes as seen in Figure 2-12. Although further sophisticated theoretical calculations are absolutely necessary, the data in Figure 2-11 demonstrate clearly that the linear arrangement of Re(I) center–coordinating nitrogen–substituted carbon for the durylethynyl group boron atom in bpy or phen results in the most efficient MLCT/π(aryl)-p(B) CT interactions and, thus, the unique spectroscopic and photophysical properties of such a type of complexes.

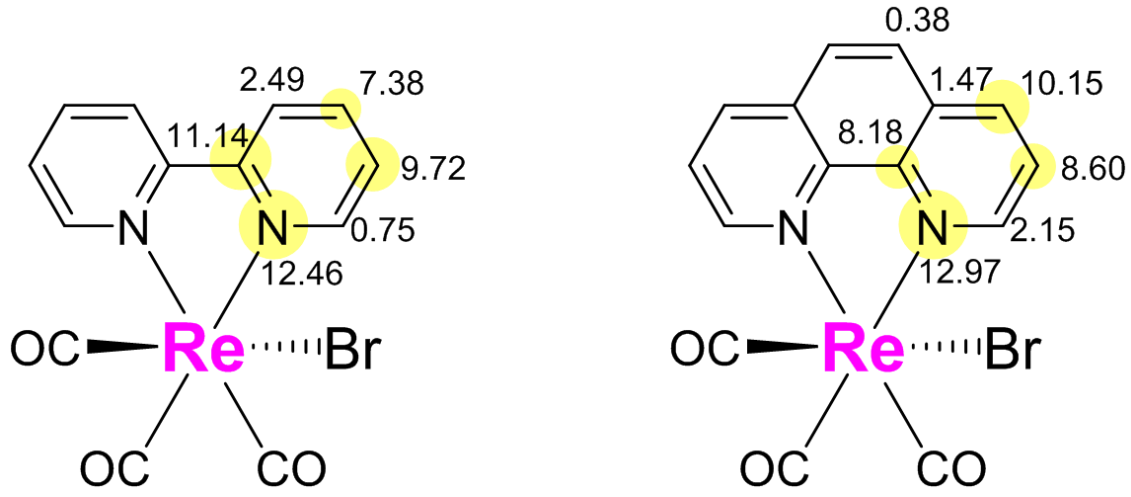

Figure 2-11 Molecular-orbital populations for the carbon atoms in the diimine ligands of **Rephen** and **Rebpy** at the LUMO levels.

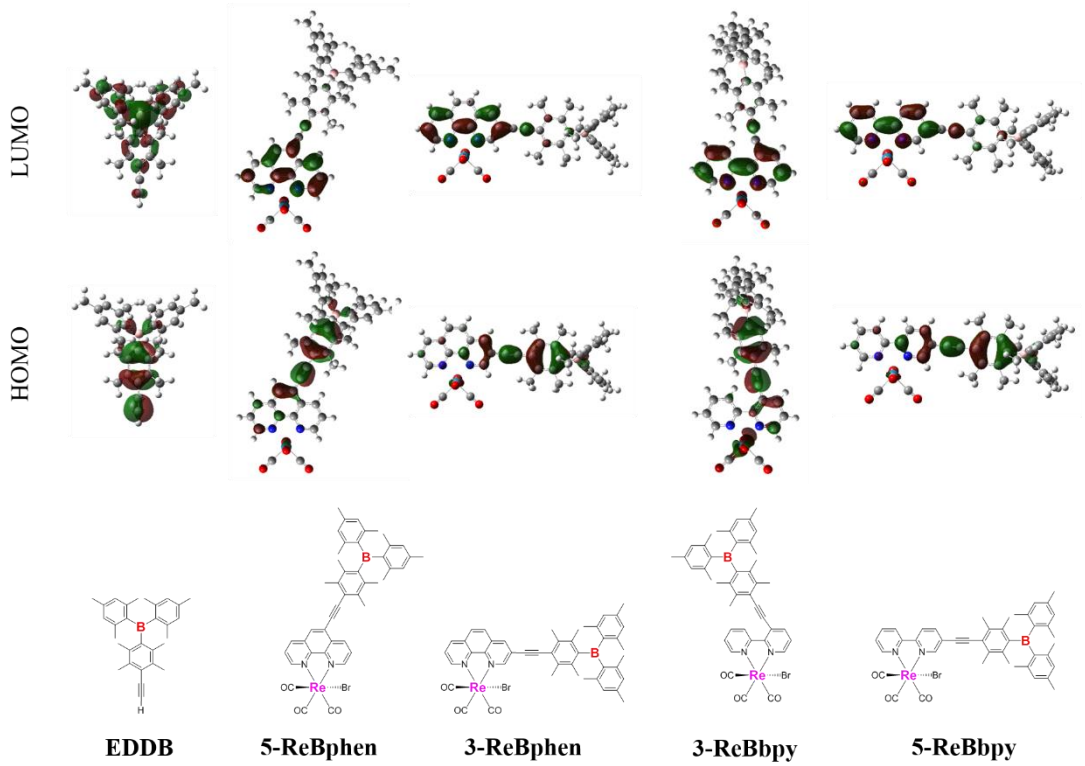

Figure 2-12 Chemical structures and frontier molecular orbitals (contours = 0.03 eÅ^{-3}) of EDDB and the isomeric complexes of **ReBphen** and **ReBbpy**.

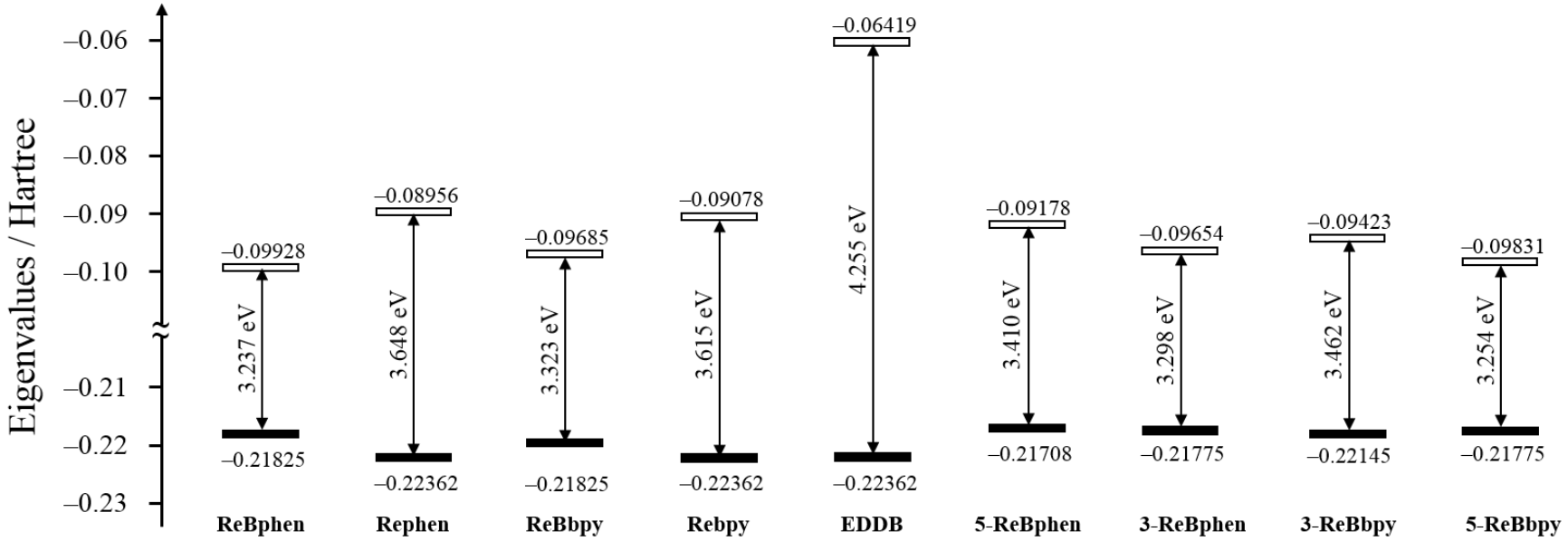

Figure 2-13 HOMO and LUMO energy gaps of the complexes.

2-4 Conclusions

In this work, the diimine ligand structure (L = phen vs. bpy) and arylborane substituent (DBDE group) effects on the redox, spectroscopic, and photophysical properties of $[Re(CO)_3LBr]$ were studied in detail. The complexes having the DBDE units, **ReBphen** and **ReBbpy**, showed low-energy/intense absorption and low-energy/long-lived emission compared to the corresponding reference complexes, **Rephen** and **Rebpy**. While the spectroscopic and photophysical properties of **ReBphen** and **ReBbpy** are explained reasonably by the synergistic interactions between MLCT and π(aryl)-p(B) CT, **ReBphen** shows more efficient MLCT/π(aryl)-p(B) CT interactions compared to **ReBbpy**. The differences in the properties between the bpy- and phen-type complexes were discussed in detail on the basis of the experimental and theoretical data. Theoretical calculations for the HOMO–LUMO electronic structures of the isomeric complexes of **ReBphen** and **ReBbpy**, **3-/5-ReBphen** and **3-/5-ReBbpy**, were also conducted toward future molecular design of related complexes. The results indicated that the substituted position of a triarylborane unit in a diimine ligand played essential roles in governing the photophysical characteristics of $[Re(CO)_3LBr]$.

2-5 References

1. B. Durham, J. V. Caspar, J. K. Nagle and T. J. Meyer, *J. Am. Chem. Soc.* **1982**, *104*, 4803–4810.
2. C. N. Fleming, K. A. Maxwell, J. M. DeSimone, T. J. Meyer and J. M. Papanikolas, *J. Am. Chem. Soc.* **2001**, *123*, 10336–10347.
3. J. Andersson, F. Puntoriero, S. Serroni, A. Yartsev, T. Pascher, T. Polivka, S. Campagna and V. Sundstrom, *Chem. Phys. Lett.* **2004**, *386*, 336–341.

4. M. Wrighton and D. L. Morse, *J. Am. Chem. Soc.* **1974**, *96*, 998–1003.

5. L. Sacksteder, A. P. Zipp, E. A. Brown, J. Streich, J. N. Demas and B. A. DeGraff, *Inorg. Chem.* **1990**, *29*, 4335–4340.

6. K. Koike, N. Okoshi, H. Hori, K. Takeuchi, O. Ishitani, H. Tsubaki, I. P. Clark, M. W. George, F. P. A. Johnson and J. J. Turner, *J. Am. Chem. Soc.* **2002**, *124*, 11448–11455.

7. K. Koike, H. Hori, M. Ishizuka, J. R. Westwell, K. Takeuchi, T. Ibusuki, K. Enjouji, H. Konno, K. Sakamoto and O. Ishitani, *Organometallics* **1997**, *16*, 5724–5729.

8. P. Kurz, B. Probst, B. Spingler and R. Alberto, *Eur. J. Inorg. Chem.* **2006**, *15*, 2966–2974.

9. H. Takeda, K. Koike, H. Inoue and O. Ishitani, *J. Am. Chem. Soc.* **2008**, *130*, 2023–2031.

10. C. Riplinger, M. D. Sampson, A. M. Ritzmann, C. P. Kubiak and E. A. Carter, *J. Am. Chem. Soc.* **2014**, *136*, 16285–16298.

11. H. Hori, F. P. A. Johnson, K. Koike, O. Ishitani and T. Ibusuki, *J. Photochem. Photobiol. A: Chem.* **1996**, *96*, 171–174.

12. A. L. Lee, *Chem. Rev.* **1987**, *87*, 711–743.

13. M. K. Itokazu, A. S. Polo and N. Y. Murakami Iha, *Inorg. Chem. Acta* **2001**, *313*, 149–155.

14. A. Ito, Y. Kang, E. Sakuda and N. Kitamura, *Inorg. Chem.* **2012**, *51*, 7722–7732.

15. G. Maerker and F. H. Case, *J. Am. Chem. Soc.* **1958**, *80*, 2745–2748.

16. D. A. M. Egbe, A. M. Amer and E. Klemm, *Des. Monomers Polym.* **2001**, *4*, 169–175.

17. J. V. Caspar and T. J. Meyer, *J. Phys. Chem.* **1983**, *87*, 952–957.

18. Z. M. Hudson and S. Wang, *Dalton Trans.* **2011**, *40*, 7805–7816.

19. E. Sakuda, Y. Ando, A. Ito and N. Kitamura, *Inorg. Chem.* **2011**, *50*, 1603–1613

20. M. J. Frisch, G. W. Trucks, H. B. Schlegel, G. E. Scuseria, M. A. Robb, J. R. Cheeseman, G. Scalmani, V. Barone, B. Mennucci, G. A. Petersson, H. Nakatsuji, M. Caricato, X. Li, H. P. Hratchian, A. F. Izmaylov, J. Bloino, G. Zheng, J. L. Sonnenberg, M. Ada, M. Ehara, K. Toyota, R. Fukuda, J. Hasegawa, M. Ishida, T. Nakajima, Y. Honda, O. Kitao, H. Nakai, T. Vreven, J. A. Jr. Montgomery, J. E. Peralta, F. Ogliaro, M. Bearpark, J. J. Heyd, E. Brothers, K. N. Kudin, V. N. Staroverov, R. Kobayashi, J. Normand, K. Raghavachari, A. Rendell, J. C. Burant, S. S. Iyengar, J. Tomasi, M. Cossi, N. Rega, N. J. Millam, M. Klene, J. E. Knox, J. B. Cross, V. Bakken, C. Adamo, J. Jaramillo, R. Gomperts, R. E. Stratmann, O. Yazyev, A. J. Austin, R. Cammi, C. Pomelli, J. W. Ochterski, R. L. Martin, K. Morokuma, V. G. Zakrzewski, G. A. Voth, P. Salvador, J. J. Dannenberg, S. Dapprich, A. D. Daniels, Ö. Farkas, J. B. Foresman, J. V. Ortiz, J. Cioslowski and D. J. Fox, *Gaussian, Inc.: Wallingford CT* **2009**.

21. P. J. Hay and W. R. Wadt, *J. Chem. Phys.* **1985**, *82*, 270–283.

22. W. R. Wadt and P. J. Hay, *J. Chem. Phys.* **1985**, *82*, 284–298.

23. P. J. Hay and W. R. Wadt, *J. Chem. Phys.* **1985**, *82*, 299–310.

24. A. D. Becke, *J. Chem. Phys.* **1993**, *98*, 5648–5652.

25. C. Lee, W. Yang and R. G. Parr, *Phys. Rev. B.* **1988**, *37*, 785–789.

26. J. Tomasi, B. Mennucci and R. Cammi, *Chem. Rev.* **2005**, *105*, 2999–3094.

27. R. Dennington, T. Keith and J. Millam, *GaussView, Version5, SemichemInc: Shawnee Mission KS* **2009**.

28. G. H. Allen, R. P. White, D. P. Rillema and T. J. Meyer, *J. Am. Chem. Soc.* **1984**,

106, 2613–2620.

29. J. V. Caspar, T. D. Westmoreland, G. H. Allen, P. G. Bradley, T. J. Meyer and W. H. Woodruff, *J. Am. Chem. Soc.* **1984**, *106*, 3492–3500.
30. H. -B. Kim, N. Kitamura and S. Tazuke, *J. Phys. Chem.* **1990**, *94*, 7401–7405.
31. K. Nozaki, K. Takamori, Y. Nakatsugawa and T. Ohno, *Inorg. Chem.* **2006**, *45*, 6161–6178.
32. K. Huang and A. Rhys, *Proc. R. Soc. London, Ser. A* **1950**, *204*, 406–423.
33. C. A. Parker and W. T. Rees, *Analyst* **1960**, *85*, 587–600.
34. B. Valeur, *Molecular Fluorescence: Principles and Applications. Wiley-VCH: Weinheim: New York* **2006**.
35. D. Fylstra, L. Lasdon, J. Watson and A. Waren, *Interfaces* **1998**, *28*, 29–55.
36. J. L. Jin, H. B. Li, T. Lu, Y. A. Duan, Y. Geng, Y. Wu and Z. M. Su, *J. Mol. Model.* **2013**, *19*, 3437-3446.
37. M. S. Wrighton, *Chem. Rev.* **1974**, *74*, 401–430.
38. A. Ito and T. J. Meyer, *Phys. Chem. Chem. Phys.* **2012**, *14*, 13731–13745.
39. L. S. Forster, *Coord. Chem. Rev.* **2002**, *227*, 59–92.
40. L. Wallace, D. C. Jackman, D. P. Rillema and J. W. Merkert, *Inorg. Chem.* **1995**, *34*, 5210–5214.
41. D. S. Striplin and G. A. Crosby, *Chem. Phys. Lett.* **1994**, *221*, 426–430.

Chapter 3. Spectroscopic and Photophysical Properties of Tricarbonyl Rhenium(I) Complexes Having Multiple Arylborane Charge Transfer Units

3-1 Introduction

As described in chapter 2, the introduction of an arylborane charge transfer unit into a tricarbonyl rhenium(I) complex (i.e., **ReBphen** and **ReBbpy**) has a significant impact on the spectroscopic and photophysical properties of the complex such as low-energy/intense absorption and low-energy/long-lived emission. The changes in the photophysical properties by introducing the arylborane unit in the periphery of the diimine ligand were shown to be originated from the synergistic interactions between metal-to-ligand charge transfer (MLCT) in the rhenium(I) complex and π(aryl)-p(B) CT in the arylborane charge transfer unit. Since the intense absorption and relatively long-lived excited states observed for **ReBphen** and **ReBbpy** are highly advantageous for an efficient photocatalytic system, further investigation and understanding of the rhenium(I)–arylborane complexes are of primary importance. Although a variety of transition metal complexes with a triarylborane-appended ligand have been reported as mentioned in Chapter 1,[1–12] the number of the report on the transition metal complex with multiple arylborane charge transfer units is still limited.[13–15] Recently, Nakagawa et al. have reported ruthenium(II) complexes with multiple arylborane centers show successive increases in the molar absorption coefficient of the MLCT absorption band (ε(MLCT)) and the radiative rate constant (k_r) upon increasing the number of the arylborane unit (n) in the complex. The results indicate a possibility for further modulation of the spectroscopic and photophysical properties of **ReBphen** or **ReBbpy**

by introduction an additional arylborane charge transfer unit to **ReBphen** and **ReBbpy**.

In this chapter, the synthesis, electrochemical, spectroscopic and photophysical properties of the novel rhenium(I) complexes having two (dimesitylboryl)durylethynyl (DBDE) groups, whose structures are shown in Schemes 3-1 and 3-2, are described. The DBDE groups are introduced to the 4- and 7-positions of 1,10-phenanthroline (*fac*-[Re(CO)$_3$(4,7-DBDE$_2$-phen)Br]: **ReB$_2$phen**) or 4- and 4'-positions of 2,2'-bipyridine (*fac*-[Re(CO)$_3$(4,4'-DBDE$_2$-bpy)Br]: **ReB$_2$bpy**). On the basis of the introduction of the two DBDE groups, **ReB$_2$phen** and **ReB$_2$bpy** showed lower-energy/more intense absorption compared to **ReBphen** and **ReBbpy**, respectively, while the two DBDE groups in **ReB$_2$bpy** showed more effective influence on the spectroscopic and photophysical properties compared to those in **ReB$_2$phen**. The conclusion described above indicates that the introduction of multiple-arylborane units to a diimine ligand gives rise to the intriguing effects on the spectroscopic and photophysical properties of a tricarbonyl rhenium(I) complex.

.

3-2 Experimental

The chemicals used in the synthesis of **ReB$_2$phen** and **ReB$_2$bpy** were purchased from available companies and used as supplied or purified prior to use as described in Chapter 2. Physical measurements and theoretical calculations were conducted by the same apparatus and methods, respectively, with those described in Chapter 2 otherwise noted.

3-2-1 Synthesis

Schemes 3-1 and 3-2 show the synthetic routes for **ReB$_2$phen** and **ReB$_2$bpy**, respectively. The complexes were synthesized by the Sonogashira–Hagihara cross

coupling reaction between (ethynylduryl)dimesitylborane (EDDB) and a dibromo-precursor rhenium(I) complex (i.e., *fac*-[Re(CO)$_3$(4,7-Br$_2$-phen)Br] or *fac*-[Re(CO)$_3$(4,4'-Br$_2$-bpy)Br] where 4,7-Br$_2$-phen = 4,7-dibromo-1,10-phenanthroline and 4,4'-Br$_2$-bpy = 4,4'-dibromo-2,2'-bipyridine). 4,7-Br$_2$-phen was synthesized according to the reported procedures.[16]

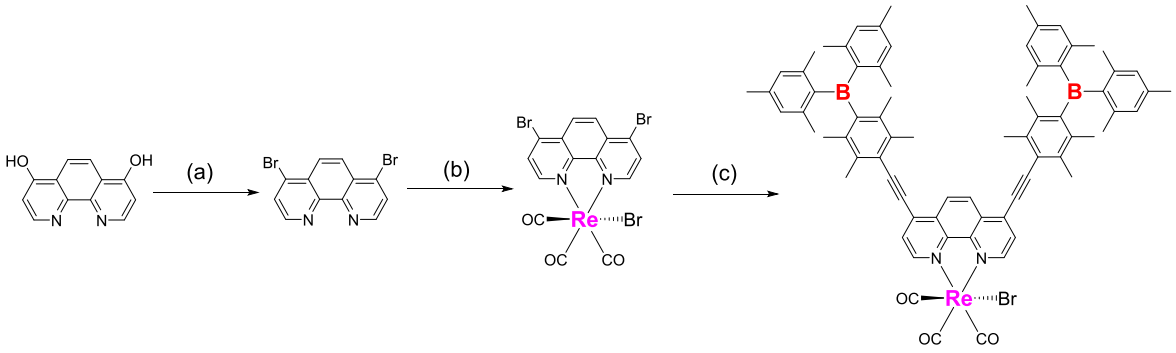

Scheme 3-1 Synthetic routes for **ReB$_2$phen**: (a) PBr$_3$, POBr$_3$, 110^{o}C, 8 h, (b) [Re(CO)$_5$Br], toluene, reflux, 2 h, (c) EDDB, Pd(PPh$_3$)$_2$Cl$_2$, CuI, THF/Et$_3$N, 50^{o}C, 2 h.

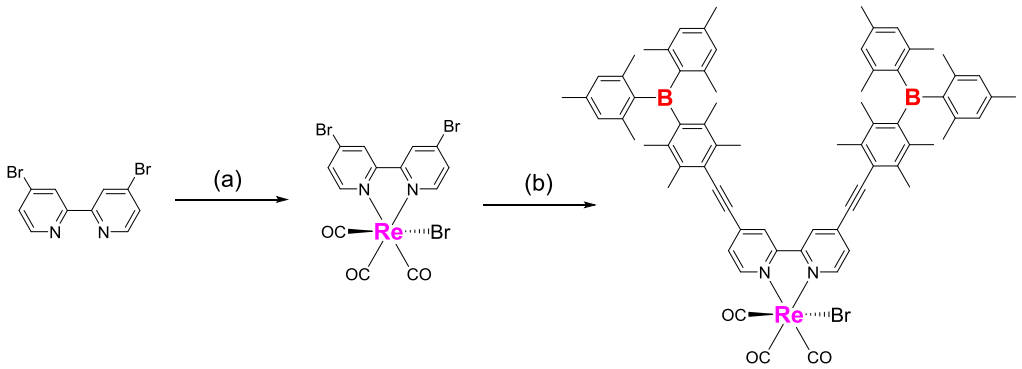

Scheme 3-2 Synthetic routes for **ReB$_2$bpy**: (a) [Re(CO)$_5$Br], toluene, reflux, 2 h, (b) EDDB, Pd(PPh$_3$)$_2$Cl$_2$, CuI, THF/Et$_3$N, 50^{o}C, 2 h.

Synthesis of 4,7-Dibromo-1,10-phenanthroline (4,7-Br_2-phen)

4,7-Dihydroxy-1,10-phenanthroline (380 mg, 1.80 mmol), PBr_3 (530 mg, 1.96 mmol) and $POBr_3$ (2.4 g, 8.4 mmol) were reflux at 110°C for 8 h under Ar-gas atmosphere. After the reaction was completed, ice (100 g) was poured into the mixture and the solution pH was adjusted to 8 with an aqueous 10% NaOH solution. The mixture was then extracted with CH_2Cl_2 (100 mL) for three times. The combined organic phase was dried over anhydrous $MgSO_4$ and evaporated to dryness under reduced pressure. The resulting products were purified by column chromatography (SiO_2, $CHCl_3$), affording pure 4,7-Br_2-phen (151 mg, 25%). R_f = 0.40 (SiO_2, $CHCl_3$). ^{1}H NMR (270 MHz, $CDCl_3$): δ 7.97 (d, 2H, J = 4.8 Hz, 3,8-Ar-H), 8.33 (s, 2H, 5,6-Ar-H), 8.95 (d, 2H, J = 4.8 Hz, 2,9-Ar-H). ESI-MS m/z 339 ($[M+H]^+$).

Synthesis of *fac*-Bromotricarbonyl(4,7-bromo-1,10-phenanthroline)rhenium(I) ([$Re(CO)_3$(4,7-Br_2-phen)Br])

[$Re(CO)_5Br$] (247 mg, 0.60 mmol) and 4,7-Br_2-phen (202 mg, 0.60 mmol) were stirred in toluene (25 mL) until all of the reactants were dissolved completely. After refluxing the mixture for 2 h under Ar-gas atmosphere, the solvent was removed by evaporation under reduced pressure. The crude product was washed with a large amount of *n*-hexane, affording the *facial* isomer of [$Re(CO)_3$(4,7-Br_2-phen)Br] as a dark yellow powder (408 mg, 91%). The purity of the complex was determined to be more than >95%, which was thought to be pure enough to employ in the following reaction. ^{1}H NMR (270 MHz, $CDCl_3$): δ 8.15 (d, 2H, J = 5.6 Hz, 3,8-Ar-H), 8.46 (s, 2H, 5,6-Ar-H), 9.20 (d, 2H, J = 5.6 Hz, 2,9-Ar-H). ESI-MS m/z 710 ($[M+Na]^+$)

Synthesis of *fac*-Bromotricarbonyl[4,7-(dimesitylboryl)durylethynyl-1,10-phenanthroline]rhenium(I) (ReB_2phen)

An oven-dried Schlenk tube was evacuated and filled with an Ar-gas. After adding $[Re(CO)_3(4,7\text{-}Br_2\text{-}phen)Br]$ (207 mg, 0.30 mmol), CuI (27 mg, 0.14 mmol) and $Pd(PPh_3)_2Cl_2$ (34 mg, 0.048 mmol), the reaction vessel was additionally evacuated and filled with an Ar-gas. An Ar-gas-purged tetrahydrofuran (THF)/triethylamine (9.0 mL/3.9 mL) mixture was added and, then, the mixture was stirred at room temperature for 15 min. A THF (6.3 mL) solution of EDDB (270 mg, 0.66 mmol) was added dropwise to the mixture. After stirring at 50 ℃ for 2 h, the reaction mixture was allowed to cool to room temperature. The insoluble solids were removed by filtration through Celite® and washed with THF. The crude product obtained by evaporation of the solution was purified by washing with *n*-hexane, column chromatography (LH-20, $CHCl_3$/ethanol = 2/1, v/v) and gel permeation chromatography (GPC), followed by binary phase diffusion of the CH_2Cl_2 solution of the product to *n*-hexane. The *facial* isomer of **ReB_2phen** was obtained as orange crystals (280 mg, 69 %). ^1H NMR (270 MHz, CD_3CN): δ/ppm 1.98 (24H, s, *ortho*-CH_3 of mesityl), 2.07 (12H, s, *ortho*-CH_3 of duryl), 2.28 (12H, s, *para*-CH_3 of mesityl), 2.53 (12H, s, *meta*-CH_3 of duryl), 6.77 (8H, s, Ar-H of mesityl), 7.92 (d, 2H, J = 5.5 Hz, 3,8-Ar-H), 8.58 (s, 2H, 5,6-Ar-H), 9.33 (d, 2H, J = 5.4 Hz, 2,9-Ar-H). ESI-MS *m/z* 1360 ($[M+Na]^+$). Analysis: $C_{75}H_{74}B_2BrN_2O_3Re$. Calc.: C, 67.27; H, 5.57; N, 2.09; Br, 5.97. Found: C, 67.08; H, 5.65; N, 2.03; Br, 4.00.

Synthesis of *fac*-Bromotricarbonyl(4,4'-bromo-2,2'-bipyridine)rhenium(I) ($[Re(CO)_3(4,4'\text{-}Br_2\text{-}bpy)Br]$)

$[Re(CO)_5Br]$ (408 mg, 1.01 mmol) and 4,4'-bromo-2,2'-bipyridine (314 mg, 1.00

mmol) were stirred in toluene (42 mL) until the reactants were completely dissolved. After refluxing the mixture for 2 h under Ar-gas atmosphere, the solvent was removed by evaporation under reduced pressure. The crude product was washed with a large amount of *n*-hexane, afforded the *facial* isomer of [$Re(CO)_3$(4,4'-Br_2-bpy)Br] as a dark yellow powder with a high purity (600 mg, 91%). ^{1}H NMR (270 MHz, $CDCl_3$): δ/ppm 7.72 (d, 2H, J = 6.0 Hz, 5,5'-Ar-H), 8.30 (d, 2H, J = 1.9 Hz, 3,3'-Ar-H), 8.87 (d, 2H, J = 5.9 Hz, 6,6'-Ar-H). ESI-MS m/z 687 ($[M+Na]^+$).

Synthesis of *fac*-Bromotricarbonyl[4,4'-(dimesitylboryl)durylethynyl-2,2'-bipyridine]rhenium(I) (ReB_2bpy)

After an oven-dried Schlenk tube was evacuated and filled with an Ar-gas, [$Re(CO)_3$(4,4'-Br_2-bpy)Br] (66 mg, 0.10 mmol), CuI (12 mg, 0.063 mmol), and $Pd(PPh_3)_2Cl_2$ (10 mg, 0.014 mmol) were added. The tube was evacuated and filled with an Ar-gas one more time, an Ar-gas-purged THF/triethylamine (3 mL/1.3 mL) mixture was added to the tube and stirred for 15 min at room temperature. A THF (2.1 mL) solution of EDDB (87 mg, 0.21 mmol) was added dropwise to the reaction mixture. The mixture was stirred at 50 ℃ for 2 h under Ar-gas atmosphere and, then, allowed to cool to room temperature. The insoluble solids were removed by filtration through Celite® and washed with toluene. The crude product was purified successively by column chromatography (LH-20, ethanol/chloroform = 1/2, v/v) and GPC. The resulting products were purified further by column chromatography (SiO_2, CH_3CN/*n*-hexane = 1/9, v/v), affording the pure *facial*-isomer of **ReB_2bpy** as an orange powder (90 mg, 69 %). R_f = 0.42 (Al_2O_3, chloroform). δ/ppm 1.97 (24H, s, *ortho*-CH_3 of mesityl), 2.04 (12H, s, *ortho*-CH_3 of duryl), 2.27 (12H, s, *para*-CH_3 of mesityl), 2.43 (12H, s,

meta-CH_3 of duryl), 6.76 (8H, s, Ar-H of mesityl), 7.56 (d, 2H, J = 5.7 Hz, 5,5'-Ar-H), 8.21 (s, 2H, 3,3'-Ar-H), 9.00 (d, 2H, J = 5.8 Hz, 6,6'-Ar-H). ESI-MS *m/z* 1235 ([M–Br]$^+$). Analysis: $C_{73}H_{74}BBrN_2O_3Re$ 0.25$CHCl_3$. Calc.: C, 65.41; H, 5.56; N, 2.08; Br, 5.94. Found: C, 65.32; H, 5.45; N, 2.22; Br, 4.44.

3-2-2 X-ray crystallography

The X-ray crystallographic data on **ReB$_2$phen** were collected by a Mercury CCD area detector coupled with a Rigaku AFC-7R diffractometer, by using CrystalClear (Rigaku Co.) with graphite-monochromated MoKα radiation (0.7107 Å). The structures were solved by CrystalStucture 3.6.0[17] and SHELX97.[18] Full-matrix least-square refinements were employed against F^2.

3-3 Results and Discussion

*3-3-1 X-ray Crystal Structure of **ReB$_2$phen**.*

Since recrystallization of **ReB$_2$phen** from a CH_2Cl_2/*n*-hexane mixture gave orange single crystals, X-ray crystallographic analysis of the complex was conducted. While one of the dimesitylboryl group was disordered presumably due to the presence of the diastereomers originated from the helicity around the two boron centers, the structure was adequately solved. Figure 3-1 shows the ORTEP images of **ReB$_2$phen**, in which one of the disordered dimesitylboryl groups is ignored, and the crystallographic data are summarized in Table 3-1. As the selected bond distances and angles are summarized in Tables 3-2 and 3-3, respectively, the results agree very well with the predicted structure of **ReB$_2$phen**, where the rhenium(I) center adopts a nearly octahedral coordination geometry and the carbonyl ligands are arranged in a *facial* orientation. One of the Re–N bond distances (2.182(5) and 2.151(5) Å for Re–N(1) and Re–N(2), respectively) is

shorter than the typical values for related tricarbonyl rhenium(I) diimine complexes, while the N–Re–N bidentate bite angle (75.9(2) °) is comparable to those hitherto reported: the Re–N distances are 2.181(5) and 2.186(5) Å, and the N–Re–N bite angle is 75.8(2) ° for [$Re(CO)_3$(phen)Cl].[19–25] The Re–Br bond length of **ReB_2phen** (2.585 (1) Å) is also shorter than that hitherto reported: 2.618(1) Å for [$Re(CO)_3$(tppz)Br] where tppz is 2,3,5,6-tetra(2-pyridyl)phyrazine.[26] These shortened Re–Br and Re–N(2) bonds could be explained by the electron-withdrawing characters of the DBDE groups: inductive effect by the electron-withdrawing ability. The Re–C15 bond length is 1.940(2) Å, which is longer that those of Re–C13 and Re–C14 (1.917(9) and 1.904(6) Å, respectively), due to the *trans* effect by the Br^- ligand.[27]

The carbon (C) – boron (B2) – carbon (C) angle (angle C–B–C) in the DBDE group is 120^o (118.9 (7), 121.1 (7) or 120.0 (7)^o), which is readily understood by the sp^2-like configuration around the boron center. Due to the disordered structure, it was difficult to determine another C–B–C angle. These results suggest that **ReB_2phen** might be asymmetry in solution.

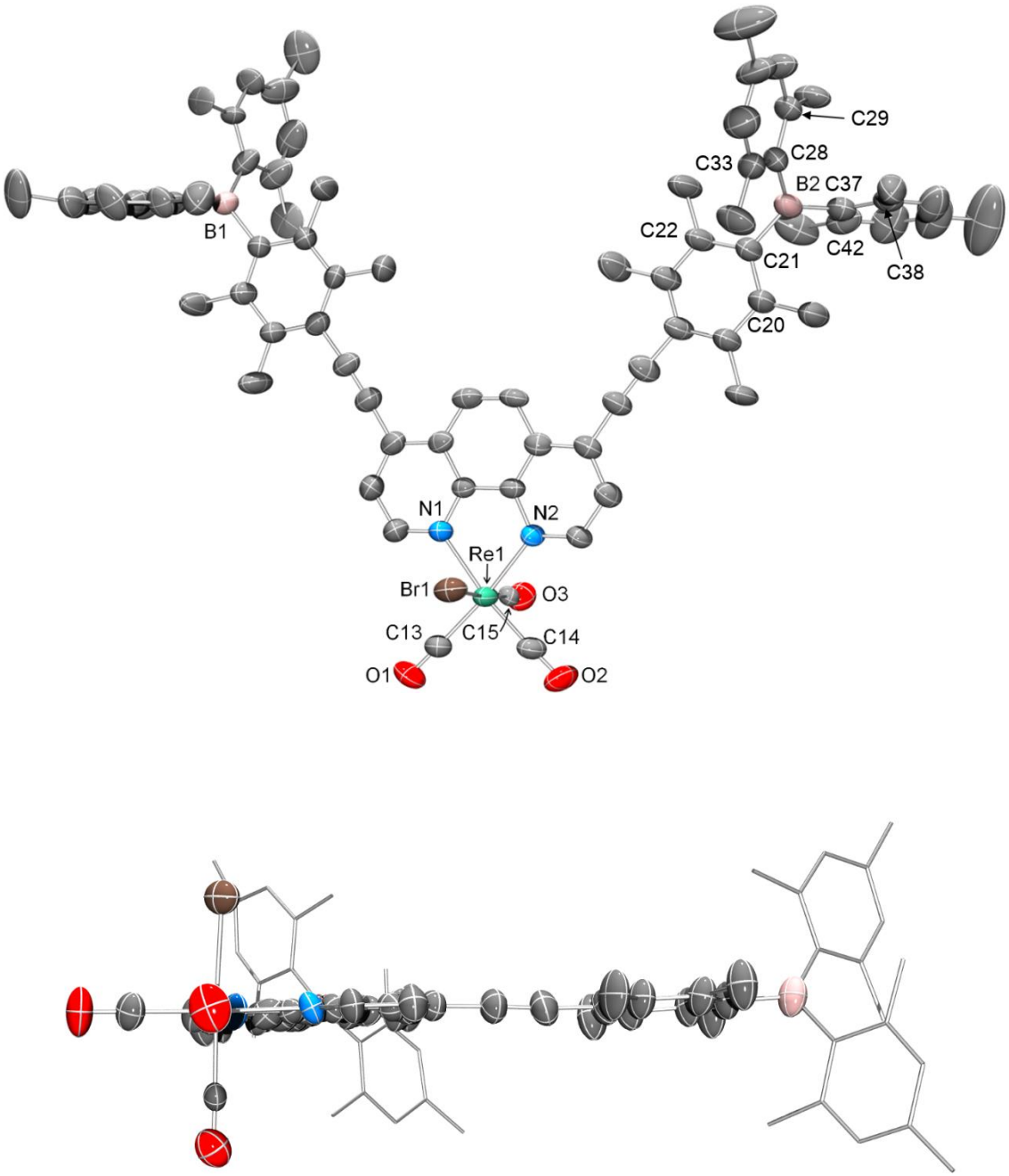

Figure 3-1 ORTEP drawings of **ReB_2phen**: top view (top) and side view (bottom).

Table 3-1 Crystallographic data for **ReB_2phen**.

Crystal-form	
Formula	$C_{75}H_{74}N_2O_3ReB_2Br$
F.W.	1339.09
size, mm	0.47×0.07×0.05
T, K	173.1
crys syst	Triclinic
space group	$P\bar{1}$
cell constant	
a, Å	11.849(16)
b, Å	18.679(3)
c, Å	20.482(3)
α, deg	66.047(6)
β, deg	74.632(8)
γ, deg	77.597(8)
V, Å^3	3965.1(10)
Z	2
ρ_{calc}, g/cm^3	1.122
μ, cm^{-1}	2.076
λ(Mo, Kα), Å	0.7107
*R*1%	0.059
w*R*2%	0.1427

$$R1 = \sum \big||F_o| - |F_c|\big| / \sum |F_o| \quad wR2 = [\sum (|F_o| - |F_c|)^2 / \sum w|F_o|^2]^{1/2}$$

Table 3-2 Selected bond distances for **ReB_2phen**.

atom	atom	distance (Å)
Re(1)	N(1)	2.182(5)
Re(1)	N(2)	2.151(5)
Re(1)	C(13)	1.917(9)
Re(1)	C(14)	1.904(6)
Re(1)	C(15)	1.940(2)
Re(1)	Br(1)	2.585(1)
C(21)	B(2)	1.550(1)
C(28)	B(2)	1.570(1)
C(37)	B(2)	1.570(1)
C(8)	C(16)	1.420(1)
C(16)	C(17)	1.180(1)
C(17)	C(18)	1.430(1)

Table 3-3 Selected bond angles for **ReB_2phen**.

atom	atom	atom	angle (^{o})
Br(1)	Re(1)	N(1)	85.3(1)
Br(1)	Re(1)	N(2)	84.8(1)
N(1)	Re(1)	N(2)	75.9(2)
C(21)	B(2)	C(28)	121.1(7)
C(21)	B(2)	C(37)	118.9(7)
C(28)	B(2)	C(37)	120.0(7)
B(2)	C(28)	C(29)	121.0(7)
B(2)	C(37)	C(38)	120.9(7)
B(2)	C(21)	C(22)	121.9(7)
B(2)	C(21)	C(20)	120.6(6)
B(2)	C(28)	C(33)	121.8(7)
B(2)	C(37)	C(42)	121.5(7)
C(7)	C(8)	C(16)	120.6(6)
C(16)	C(8)	C(9)	121.5(6)
C(17)	C(18)	C(19)	118.0(7)
C(23)	C(18)	C(17)	121.4(7)

3-3-2 Cyclic and Differential Pulse Voltammograms

As described in Chapter 2, the (dimesitylboryl)durylethynyl (DBDE) group in the phen or bpy ligand plays important role in the redox and excited-state behaviors of a $[Re(CO)_3LX]$-type complex. Therefore, the effects of the two DBDE groups on the electrochemical properties are worth evaluating. Figure 3-2 shows the cyclic and differential pulse voltammograms of **ReB$_2$phen** in *N*,*N*-dimethylformamide (DMF), together with those of the reference complexes (**ReBphen** and **Rephen**), and the redox potentials of the complexes are summarized in Table 3-4. Unfortunately, since the solubility of **ReB$_2$bpy** in DMF was very low, it was impossible to determine the redox potential of the complex. Thus, the data on **ReB$_2$bpy** are not shown here.

The metal oxidation potential of **ReB$_2$phen** ($E_{1/2}(Re^{II/I})$ = +1.48 V vs. SCE) is more positive compared to those of **ReBphen** ($E_{1/2}(Re^{II/I})$ = +1.45 V vs. SCE) and **Rephen** ($E_{1/2}(Re^{II/I})$ = +1.42 V vs. SCE), indicating that the two electron-withdrawing DBDE groups slightly decrease the electron density on the Re(I) ion. The results are in good accordance with the shorter Re–Br and Re–N(2) bond lengths in the X-ray crystal structure of **ReB$_2$phen** compared to those observed for $[Re(CO)_3(tppz)Br]$ as described above. On the other hand, **ReB$_2$phen** exhibited the first ($E_{1/2}(Re^{I/0})$) and second reduction waves ($E_{1/2}(Re^{I/0})$) at –0.95 V and –1.18 V, respectively. The two reduction waves were shifted to the positive potential direction compared to the relevant values of **ReBphen** and **Rephen**. These results can be explained by the increase in the electron-accepting abilities of the two arylborane charge transfer units. Furthermore, **ReB$_2$phen** showed the third reduction wave at $E_{1/2}(Re^{-I/-II})$ = –1.47 V ascribed to the reduction of the boron units, similar to **ReBphen**. It is worth pointing out that, upon the introduction of the two DBDE groups, the third reduction wave was shifted to the

positive direction by 140 mV compared to that of **ReBphen**, suggesting electron conjugation between the two boron centers. The results demonstrate that the two DBDE groups in **ReB$_2$phen** are reduced more easily than that in **ReBphen**. Such electrochemical characteristic of **ReB$_2$phen** should reflect on the excited-state properties of the complexes, which will be described in the following sections.

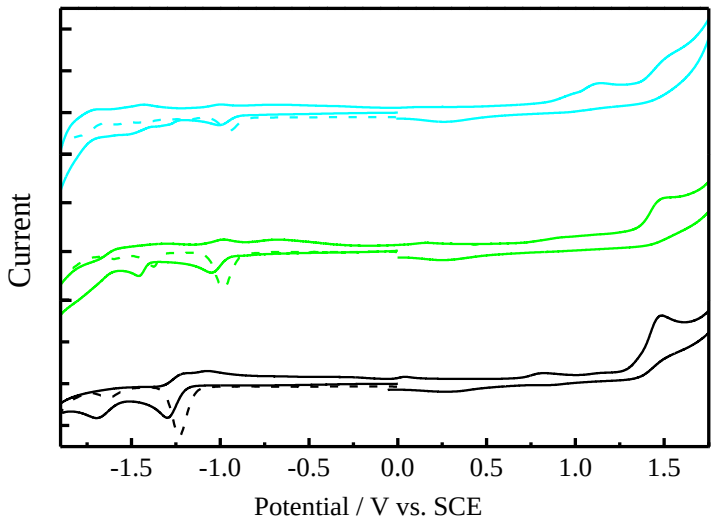

Figure 3-2 Cyclic (solid curve) and differential pulse voltammograms (broken curve) of **ReB$_2$phen** (blue), **ReBphen** (green) and **Rephen** (black) in DMF.

Table 3-4 Redox potentials of the complexes in DMF (0.1 M $TBAPF_6$).

complex	$E_{1/2}$ / V vs. SCE			
	$Re^{-I/-II}$	$Re^{0/-I}$	$Re^{I/0}$	$Re^{II/I}$
ReB$_2$phen[a]	–1.47	–1.18	–0.95	+1.48
ReBphen[b]	–1.61	–1.38	–0.98	+1.45
Rephen[b]		–1.63	–1.23	+1.42

a) Determined under saturated concentration conditions,

b) Data compiled from Chapter 2.

3-3-3 Absorption Spectra in Toluene and Time-Dependent Functional Theory (TD-DFT) Calculations

The absorption spectra of **ReB$_2$phen** and **ReB$_2$bpy** in toluene at 298 K are shown in Figure 3-3, together with those of the corresponding reference complexes. The absorption maximum wavelengths (λ^{abs}) and the relevant molar absorption coefficients (ε) of the complexes are summarized in Table 3-5. The broad and intense absorption bands are observed for **ReB$_2$phen** in 270–550 nm. On the basis of the electrochemical data in Table 3-4, the absorption band of **ReB$_2$phen** at 325 nm (ε_{325} = 4.95 × 10^4 M^{-1}cm^{-1}) can be ascribed to the $^1\pi\pi^*$ transition in the phen ring. The absorption band at around 330–410 nm observed for **ReB$_2$phen** (λ^{abs} = 387 nm, ε_{387} = 5.57 × 10^4 M^{-1}cm^{-1}) is assigned to the LC transitions, composed of the $^1\pi\pi^*$ transition(s) in the durylethynyl-diimine unit(s) and the π(aryl)-p(B) CT transition(s) in the DBDE group(s) as judged by the similarity of the spectral band shape with that of **ReBphen**. While the ^{1}MLCT absorption band of **ReB$_2$phen** has not been observed clearly due to the spectral overlap with the intense ^{1}LC band, the spectral shoulder at 443 nm (ε_{443} = 2.19 × 10^4 M^{-1}cm^{-1}) is assigned to ^{1}MLCT absorption. Both $^1\pi\pi^*$ and ^{1}MLCT absorption bands of **ReB$_2$phen** are shifted to the lower energy and the relevant ε values increase obviously with the increase in the number of the DBDE group in the complex compared to those of **ReBphen** and **Rephen** (see Figure 3-3), demonstrating that the number of the arylborane charge transfer unit influence largely the spectroscopic characteristics of the complex.

ReB$_2$bpy also shows broad and intense absorption bands in 270–550 nm. The $^1\pi\pi^*$ transition in the bpy ring and the LC transition(s) in the DBDE group(s) are observed at around 299 nm and 320–400 nm (λ^{abs} = 374 nm, ε_{374} = 5.44 × 10^4 M^{-1}cm^{-1}), respectively.

Furthermore, the ^{1}MLCT transition of **ReB$_2$bpy** is observed at around 450 nm as an absorption peak, while that of **ReB$_2$phen** is observed as a shoulder as described above. As pointed out in Chapter 2, since 1,10-phenanthroline possesses an expanded π-electron system and a larger molecular orbital (MO) population at the 4-position compared to 2,2'-bopyridine, the LC absorption transitions of **ReB$_2$phen** extend to the longer wavelength compared to those of **ReB$_2$bpy**. This will be the primary reason for the difference in the MLCT absorption band structures between the two complexes. It is shown from Figure 3-3 and Table 3-5, furthermore, that the ^{1}MLCT absorption band of **ReB$_2$bpy** is shifted to the lower energy compared to that of **ReBbpy** (22 nm = 1140 cm^{-1}), which is much larger than the spectral shift observed for the phen-type complexes (**ReB$_2$phen**/**ReBphen**, 5 nm = 260 cm^{-1}), indicating more significant effects of the two arylborane charge transfer units on the MLCT absorption behaviors of the bpy-type complexes. This has been also confirmed by TD-DFT calculations as described later again.

To reveal more details about the absorption spectra, TD-DFT calculations were conducted for the complexes. Although similar calculations on **ReBphen**, **Rephen**, **ReBbpy**, and **Rebpy** in DMF have been conducted as described in Chapter 2, the absorption characteristics of the complexes are worth reinvestigating in toluene, whose results are summarized in Tables 3-6 ~ 3-9.

The data demonstrate that the lowest-energy absorption transitions of all of the complexes are ascribed to the HOMO (highest-energy occupied MO) → LUMO (lowest-energy unoccupied MO) transitions except for **ReBphen**: HOMO → LUMO (84%)/HOMO → LUMO+1 (16%). On the basis of the contours of the frontier molecular orbitals (i.e., HOMO and LUMO) shown in Figure 3-4 and the contribution

of each atom in the relevant MO in Table 3-8, it is predicted that the electron of **ReB$_2$phen** in HOMO distributes to the d-orbital of the Re(I) center and bromide. On the other hand, LUMO of **ReB$_2$phen** is best characterized by the electron distributions on the π*-orbital of phen and p(B), which are similar to that of **ReBphen**. Therefore, it is feasible to assign the lowest-energy excited singlet state of **ReB$_2$phen** to the synergistic MLCT/π(aryl)-p(B) CT state, similar to that of **ReBphen**. On the other hand, the lowest-energy excited singlet state of **Rephen** possesses almost pure MLCT characters as described in Chapter 2, and this is also confirmed by the TD-DFT calculations on the complex in toluene.

Similar behaviors to those of the phen-type complexes are also observed for the bpy-type complexes. The lowest-energy excited states of **ReB$_2$bpy** and **ReBbpy** are ascribed to the synergistic MLCT/π(aryl)-p(B) CT states while **Rebpy** possesses almost pure MLCT characters. Furthermore, it is worth noting that the introduction of the two arylborane charge transfer units to the periphery of the diimine ligand results in the slightly high boron and low phen population percentages in LUMO of **ReB$_2$phen** and **ReB$_2$bpy** compared to the relevant values of **ReBphen** and **ReBbpy**, respectively. Such contributions of the π(aryl)-p(B) CT to LUMO enhances the transition dipole moments of the MLCT absorption of **ReB$_2$phen** and **ReB$_2$bpy**, and the theoretical calculations described above are consistent with the experimental observations that the ε values of the MLCT/π(aryl)-p(B) bands increase with an increase in the number of the arylborane charge transfer unit in the complex.

Furthermore, the absorption transition energy to the lowest-energy excited singlet state of **ReB$_2$phen** (2.2682 eV) is lower than the corresponding value of **ReBphen** (2.3151 eV), while the value is also lower for **ReB$_2$bpy** (2.2718 eV) compared to that of

ReBbpy (2.3392 eV). These results are in good agreement with the low-energy shifts of the experimentally observed ^{1}MLCT absorption data on the complexes with the two arylborane charge transfer units compared to the relevant values of the complexes with a single DBDE group in Figure 3-3 and Table 3-5. The difference in the absorption transition energy between **ReB$_2$bpy** and **ReBbpy** ($\Delta E_{MLCT}(B_2/B)$ = 0.0674 eV = 540 cm^{-1}) is larger than that between **ReB$_2$phen** and **ReBphen** (0.0469 eV = 380 cm^{-1}). Although the $\Delta E_{MLCT}(B_2/B)$ values described above are not coincide with the observed values ($\Delta E_{MLCT}(B_2/B)$ = 1140 and 260 cm^{-1} for the bpy and phen series, respectively), the characteristic properties of the absorption transitions for the bpy- and phen-type complexes can be explained by the present theoretical calculations.

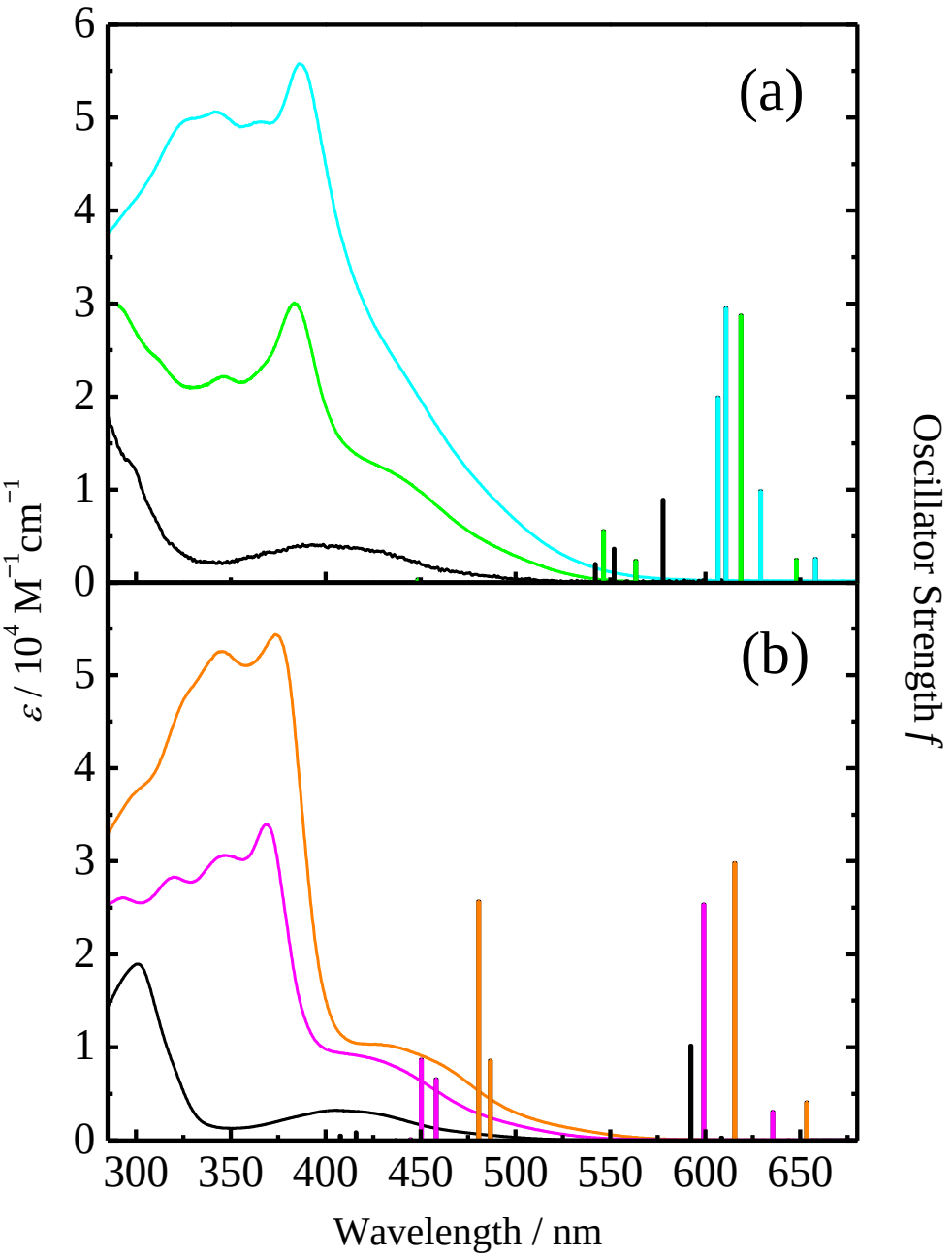

Figure 3-3 Absorption spectra of (a) **ReB$_2$phen** (blue), **ReBphen** (green), and **Rephen** (black), and (b) **ReB$_2$bpy** (orange), **ReBbpy** (pink), and **Rebpy** (black) in toluene at 298 K. The perpendicular bars represent the oscillator strengths of the absorption transitions calculated by TD-DFT in toluene.

Table 3-5 Absorption maxima (λ^{abs}) and corresponding molar absorption coefficients (ε) of the complexes in toluene at 298 K.

complex	λ^{abs}/ nm (ε / 10^4 $M^{-1}cm^{-1}$)		
	$\pi\pi^*$	π(aryl)-p(B) CT	MLCT
ReB$_2$phen	325 (4.95)	387 (5.57)	443 (2.19)
ReBphen	288 (2.99)	384 (3.00)	438 (1.15)
Rephen	n.d.[a]		392 (0.41)
ReB$_2$bpy	299 (3.72)	374 (5.44)	450 (0.91)
ReBbpy	292 (2.60)	369 (3.39)	428 (0.86)
Rebpy	301 (1.89)		410 (0.31)

a) not determined due to superposition with absorption of the solvent.

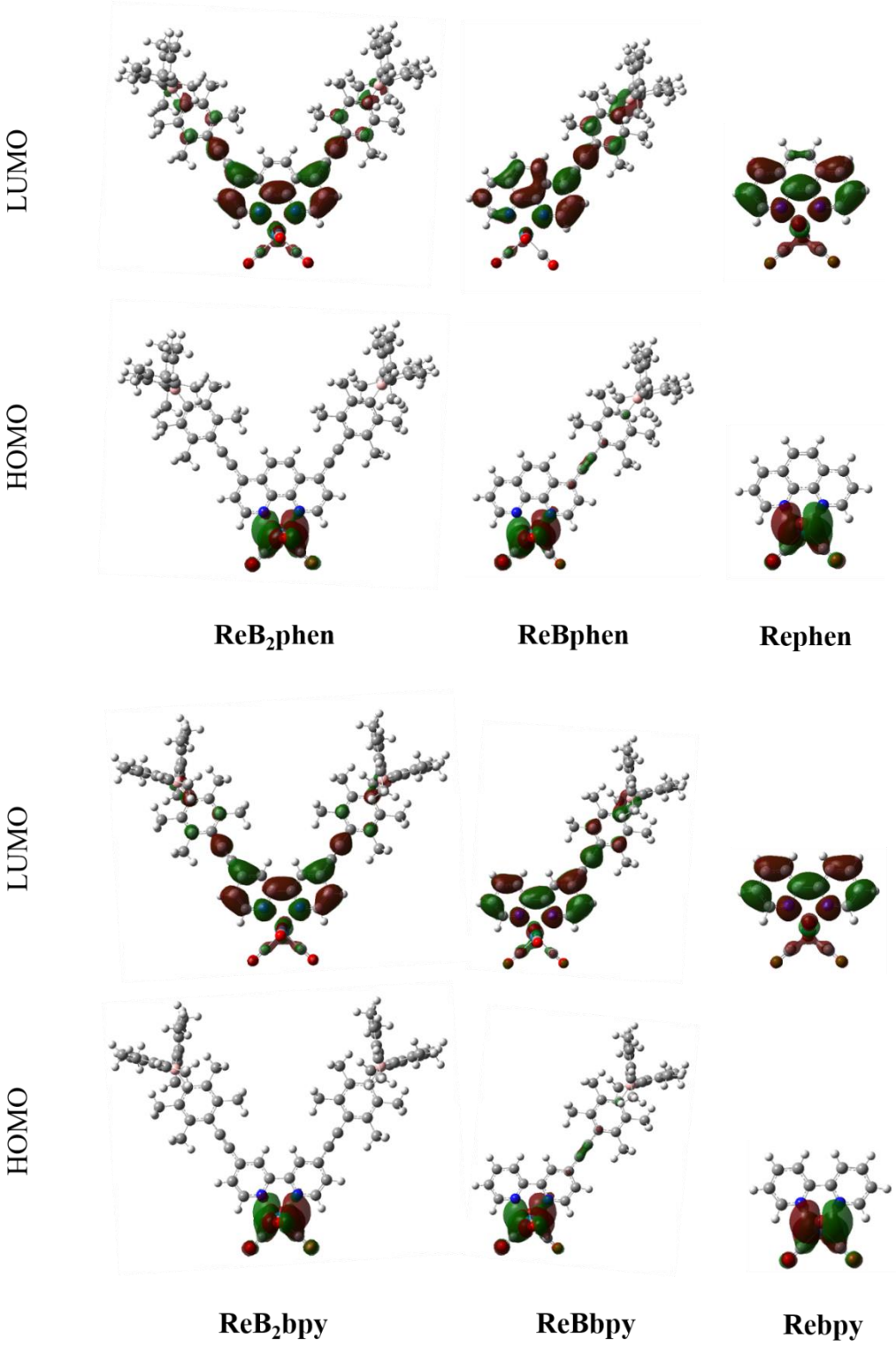

Figure 3-4 Frontier molecular orbitals (contour = 0.03 eÅ^{-3}) of the complexes.

Table 3-6 Calculated excited states of **ReB_2phen**, **ReBphen** and **Rephen** in toluene.

Excited state	Transition	Energy (Wavelength)	Oscillator Strength
	ReB_2phen		
1	HOMO → LUMO	2.2682 eV (546.62 nm)	0.0139
2	HOMO–1 → LUMO	2.3443 eV (528.88 nm)	0.1195
3	HOMO–1 → LUMO (22 %) HOMO → LUMO+1 (78 %)	2.4389 eV (508.37 nm)	0.0888
4	HOMO–1 → LUMO+1	2.4521 eV (505.63 nm)	0.1583
5	HOMO–3 → LUMO (24 %) HOMO–2 → LUMO+1 (76 %)	2.8596 eV (433.57 nm)	0.8749
	ReBphen		
1	HOMO → LUMO (84 %) HOMO → LUMO+1 (16 %)	2.3151 eV (535.54 nm)	0.0192
2	HOMO–1 → LUMO (71 %) HOMO → LUMO (29 %)	2.3915 eV (518.44 nm)	0.1492
3	HOMO → LUMO+1	2.6347 eV (470.59 nm)	0.0211
4	HOMO–1 → LUMO+1	2.7017 eV 458.91 nm)	0.0218
5	HOMO → LUMO	2.9282 eV (423.42 nm)	1.0768
	Rephen		
1	HOMO → LUMO	2.4618 eV (503.63 nm)	0.0011
2	HOMO–1 → LUMO	2.5604 eV (484.25 nm)	0.0358
3	HOMO → LUMO+1	2.7218 eV (455.52 nm)	0.0095
4	HOMO–1 → LUMO+1	2.7714 eV 447.37 nm)	0.0086
5	HOMO–2 → LUMO	3.1742 eV (390.59 nm)	0.0000

Table 3-7 Calculated excited states of **ReB_2bpy**, **ReBbpy** and **Rebpy** in toluene.

Excited state	Transition	Energy (Wavelength)	Oscillator Strength
	ReB_2bpy		
1	HOMO → LUMO	2.2718 eV (545.76 nm)	0.0223
2	HOMO–1 → LUMO	2.3703 eV (523.08 nm)	0.1454
3	HOMO–2 → LUMO	2.9387 eV (421.91 nm)	0.6444
4	HOMO → LUMO+1	2.9574 eV (419.24 nm)	0.0241
5	HOMO–12→ LUMO (84 %) HOMO–10→ LUMO (16 %)	2.9805 eV (415.98 nm)	0.2492
	ReBbpy		
1	HOMO → LUMO	2.3392 eV (530.02 nm)	0.0204
2	HOMO–1 → LUMO (80 %) HOMO → LUMO (20 %)	2.4405 eV (508.02 nm)	0.1144
3	HOMO–2 → LUMO	3.0069 eV (412.34 nm)	0.8621
4	HOMO–7 → LUMO	3.0474 eV 406.86 nm)	0.0039
5	HOMO → LUMO+1	3.1268 eV (396.52 nm)	0.0753
	Rebpy		
1	HOMO → LUMO	2.4192 eV (512.49 nm)	0.0014
2	HOMO–1 → LUMO	2.5293 eV (490.19 nm)	0.0346
3	HOMO–2 → LUMO	3.1231 eV (396.99 nm)	0.0000
4	HOMO → LUMO+1	3.4279 eV 361.69 nm)	0.0029
5	HOMO–1 → LUMO+1	3.4896 eV (355.30 nm)	0.0007

Table 3-8 Molecular-orbital contributions of **ReB$_2$phen**, **ReBphen** and **Rephen** in toluene.

Complex	Molecular Orbital	Eigenvalues / Hartrees	Contribution / %							
			rhenium	diimine					CO	bromide
				phen	ethynyl	duryl	boron	mesityl		
ReB$_2$phen	315 (LUMO+3)	–0.06602	0.01	9.03	1.09	16.74	27.89	45.22	0.02	0.00
	314 (LUMO+2)	–0.06626	0.17	7.42	1.24	17.36	28.15	45.35	0.18	0.13
	313 (LUMO+1)	–0.09708	0.25	70.37	11.29	13.48	1.69	2.30	0.62	0.00
	312 (LUMO)	–0.09918	3.91	68.55	8.89	9.60	1.22	1.69	3.71	2.43
	311 (HOMO)	–0.20657	31.81	3.20	0.59	0.87	0.02	0.11	16.16	47.24
	310 (HOMO–1)	–0.20689	29.61	6.99	3.03	3.94	0.07	0.51	13.37	42.48
	309 (HOMO–2)	–0.22116	0.72	19.55	14.45	33.14	0.58	6.80	1.37	23.29
	308 (HOMO–3)	–0.22585	0.32	12.51	16.48	46.15	0.87	15.37	0.28	8.02
ReBphen	206 (LUMO+3)	–0.04361	0.80	76.64	5.13	8.01	1.55	6.74	0.70	0.43
	205 (LUMO+2)	–0.06684	0.06	8.60	1.28	17.46	27.87	44.61	0.07	0.05
	204 (LUMO+1)	–0.08758	1.63	93.78	0.45	0.90	0.11	0.14	1.91	1.08
	203 (LUMO)	–0.10042	2.67	70.50	9.42	10.24	1.21	1.69	2.66	1.61
	202 (HOMO)	–0.20858	31.59	3.57	0.91	1.38	0.03	0.18	15.80	46.54
	201 (HOMO–1)	–0.20999	29.59	5.07	0.84	1.00	0.02	0.14	13.46	49.88
	200 (HOMO–2)	–0.22465	0.39	16.64	15.38	39.48	0.71	10.49	0.86	16.05
	199 (HOMO–3)	–0.22711	0.00	0.04	0.07	9.83	1.07	88.97	0.00	0.02
Rephen	97 (LUMO+3)	–0.02570	22.51	27.52					47.89	2.08
	96 (LUMO+2)	–0.04182	2.61	92.61					2.96	1.82
	95 (LUMO+1)	–0.08774	0.15	99.26					0.58	0.01
	94 (LUMO)	–0.09356	3.97	89.40					3.93	2.70
	93 (HOMO)	–0.21111	31.51	2.64					15.93	49.92
	92 (HOMO–1)	–0.21273	29.21	4.77					12.98	53.04
	91 (HOMO–2)	–0.23921	68.01	2.78					28.91	0.30
	90 (HOMO–3)	–0.24954	23.22	24.31					11.68	40.79

Table 3-9 Molecular-orbital contributions of **ReB$_2$bpy**, **ReBbpy** and **Rebpy** in toluene.

Complex	Molecular Orbital	Eigenvalues / Hartrees	Contribution / %							
			rhenium	diimine					CO	bromide
				bpy	ethynyl	duryl	boron	mesityl		
ReB$_2$bpy	309 (LUMO+3)	–0.06078	0.09	18.47	3.02	10.48	23.39	44.17	0.38	0.00
	308 (LUMO+2)	–0.06928	0.21	46.56	2.82	13.55	14.75	21.91	0.10	0.10
	307 (LUMO+1)	–0.08046	0.30	43.96	14.20	22.26	8.03	10.36	0.88	0.01
	306 (LUMO)	–0.09949	4.10	69.44	8.38	8.79	1.18	1.65	3.90	2.56
	305 (HOMO)	–0.20733	32.02	3.32	0.84	1.27	0.02	0.17	16.19	46.17
	304 (HOMO–1)	–0.20856	30.16	4.76	2.39	2.81	0.05	0.39	13.46	45.98
	303 (HOMO–2)	–0.22399	0.16	11.98	18.00	46.63	0.85	12.74	0.23	9.41
	302 (HOMO–3)	–0.22404	0.66	11.55	15.59	40.60	0.73	11.17	1.20	18.50
ReBbpy	200 (LUMO+3)	–0.05608	1.27	92.49	0.52	0.65	0.77	1.79	1.85	0.66
	199 (LUMO+2)	–0.06157	0.35	29.93	2.30	8.97	20.13	37.82	0.35	0.15
	198 (LUMO+1)	–0.07451	0.34	55.99	6.35	14.74	9.18	12.62	0.62	0.16
	197 (LUMO)	–0.09815	3.95	74.75	6.18	6.55	0.92	1.28	3.86	2.51
	196 (HOMO)	–0.20924	31.97	3.29	0.88	1.35	0.02	0.19	16.01	46.29
	195 (HOMO–1)	–0.21109	29.54	4.36	0.98	1.07	0.02	0.15	13.27	50.61
	194 (HOMO–2)	–0.22487	0.34	11.50	16.33	43.43	0.79	12.32	0.69	14.60
	193 (HOMO–3)	–0.22679	0.00	0.02	0.07	10.22	1.06	88.61	0.00	0.02
Rebpy	91 (LUMO+3)	–0.02575	23.15	24.71					50.03	2.11
	90 (LUMO+2)	–0.05446	0.39	97.57					2.01	0.30
	89 (LUMO+1)	–0.06049	1.90	95.52					1.52	1.06
	88 (LUMO)	–0.09529	3.93	89.39					3.98	2.70
	87 (HOMO)	–0.21161	31.77	2.68					16.01	49.54
	86 (HOMO–1)	–0.21358	29.08	4.37					12.87	53.68
	85 (HOMO–2)	–0.23931	67.67	3.09					28.92	0.32
	84 (HOMO–3)	–0.25189	31.38	9.73					13.76	45.13

3-3-5 Emission Spectra and Photophysical Properties

Figure 3-5 displays the corrected emission spectra of **ReB$_2$phen** and **ReB$_2$bpy** in toluene at 298 K, together with those of the corresponding reference complexes. Note that, in Figure 3-5, the emission intensities are normalized to those at the maximum wavelengths (λ^{em}). All of the complexes in toluene showed broad and structureless emission from the MLCT excited triplet states, and the emission decay profiles of the complexes were fitted by single exponential functions as shown in Figure 3-6. The photophysical parameters of the complexes thus obtained are summarized in Table 3-10: emission maximum wavelength = λ^{em}, emission quantum yield = Φ^{em}, and emission lifetime = τ^{em}.

The emission maxima of **ReB$_2$phen** (λ^{em} = 669 nm) and **ReBphen** (λ^{em} = 669 nm) were identical with each other, while the full width at half-maximum (fwhm) of **ReB$_2$phen** ($\tilde{\nu}_{1/2}$ = 3250 cm^{-1}) was smaller than that of **ReBphen** ($\tilde{\nu}_{1/2}$ = 3430 cm^{-1}) by 180 cm^{-1}. However, the emission spectrum of **ReB$_2$bpy** (λ^{em} = 653 nm) was red-shifted compared to that of **ReBbpy** (λ^{em} = 641 nm), while the difference in the fwhm value between **ReB$_2$bpy** ($\tilde{\nu}_{1/2}$ = 3280 cm^{-1}) and **ReBbpy** ($\tilde{\nu}_{1/2}$ = 3650 cm^{-1}) was almost twice larger (370 cm^{-1}) than that between **ReB$_2$phen** and **ReBphen**: 180 cm^{-1}. The differences in the emission maximum energy ($\Delta\tilde{\nu}^{em}$) and fwhm between the double and single boron center(s) complexes are much larger for the bpy-type complexes (**ReB$_2$bpy** vs. **ReBbpy**) than those for the phen-type (**ReB$_2$phen** vs. **ReBphen**), indicating the more effective influence of the two arylborane charge transfer units to the photophysical properties of the bpy-type complex. These results are consistent with the absorption and TD-DFT calculation data on the complexes as described before.

The emission lifetime of **ReB$_2$phen** in toluene (τ^{em} = 1.2 μs) was 1.3-times shorter than that of **ReBphen** (τ^{em} = 1.6 μs) while the emission quantum yield of **ReB$_2$phen** (Φ^{em} = 0.057) was 1.7-times higher than that of **ReBphen** (Φ^{em} = 0.033). The introduction of the two DBDE groups into the phen ligand increased both radiative (k_r) and nonradiative rate constants (k_{nr}) with the factors of 2.3 and 1.3, respectively: see Table 3-9. On the other hand, the emission lifetime of **ReB$_2$bpy** in toluene (τ^{em} = 0.14 μs) was also 1.2-times shorter than that of **ReBbpy** (τ^{em} = 0.17 μs), while the emission quantum yield of **ReB$_2$bpy** (Φ^{em} = 0.039) was twice higher than that of **ReBbpy** (Φ^{em} = 0.020). Both k_r and k_{nr} values increased with the factors of 2.3 and 1.2, respectively, by the introduction of the two DBDE groups into the bpy ligand (see Table 3-9). It is interesting to point out that the k_r value increases 2.3-times by the introduction of the two DBDE units compared to those of the complexes with a single DBDE group in the complex, irrespective of the diimine ligand. Since the ε value of the MLCT absorption band (ε(MLCT)) of **ReB$_2$bpy** is also obviously larger than that of **ReBbpy**, the positive correlation between k_r and ε(MLCT) might be explained by the Strickler–Berg relation for the fluorescence transition of a molecule given by Eq. (3-1).[28]

$$k_r^0 = 2.880 \times 10^{-9} D_s^2 \frac{g_1}{g_u} \frac{\int I(\tilde{\nu}) d\tilde{\nu}}{\int \tilde{\nu}^{-3} I(\tilde{\nu}) d\tilde{\nu}} \int \frac{\varepsilon(\tilde{\nu})}{\tilde{\nu}} d\tilde{\nu} \qquad (3\text{-}1)$$

In Eq. (3-1), k_r^0 is the intrinsic (or natural) S_1–S_0 fluorescence rate constant of a molecule. $I(\tilde{\nu})$ and $\varepsilon(\tilde{\nu})$ are the fluorescence intensity and the ε value of the absorption band of a molecule responsible for the (S_1–S_0) fluorescence transition at a given wavenumber ($\tilde{\nu}$), respectively. D_s is the refractive index of a medium and, g_1 and g_u are the electronic degeneracies in the ground and excited states, respectively. The Strickler-Berg relation demonstrates that, with an increase in the ε value of a molecule, the relevant fluorescence rate constant (k_r^0) and, thus, the fluorescence quantum yield

should increase in accord with the ε value: $\Phi^{em} \propto \varepsilon(S_1–S_0)$. The ε(MLCT) value of **ReB$_2$bpy** is 1.1-times larger than that of **ReBbpy**, while that of **ReB$_2$phen** is 1.9-times larger than ε(MLCT) of **ReBphen** as seen in Table 3-5. Since the k_r values increase 2.3-times for both **ReB$_2$phen** and **ReB$_2$bpy**, both phen- and bpy-type complexes are considered qualitatively or phenomenologically to follow the Strickler-Berg-type relation.

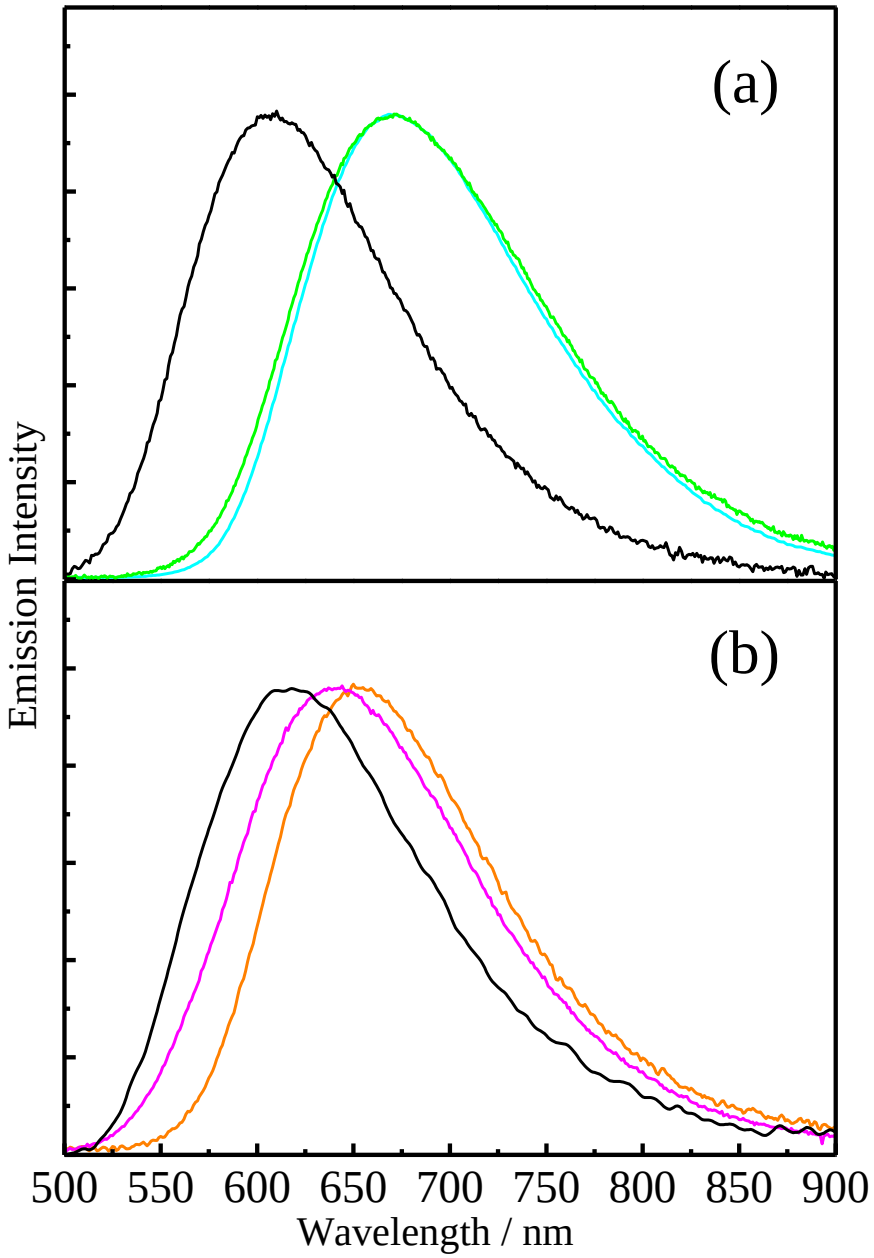

Figure 3-5 Corrected emission spectra of (a) **ReB$_2$phen** (blue), **ReBphen** (green), and **Rephen** (black), (b) **ReB$_2$bpy** (orange), **ReBbpy** (pink) and **Rebpy** (black) in toluene at 298 K.

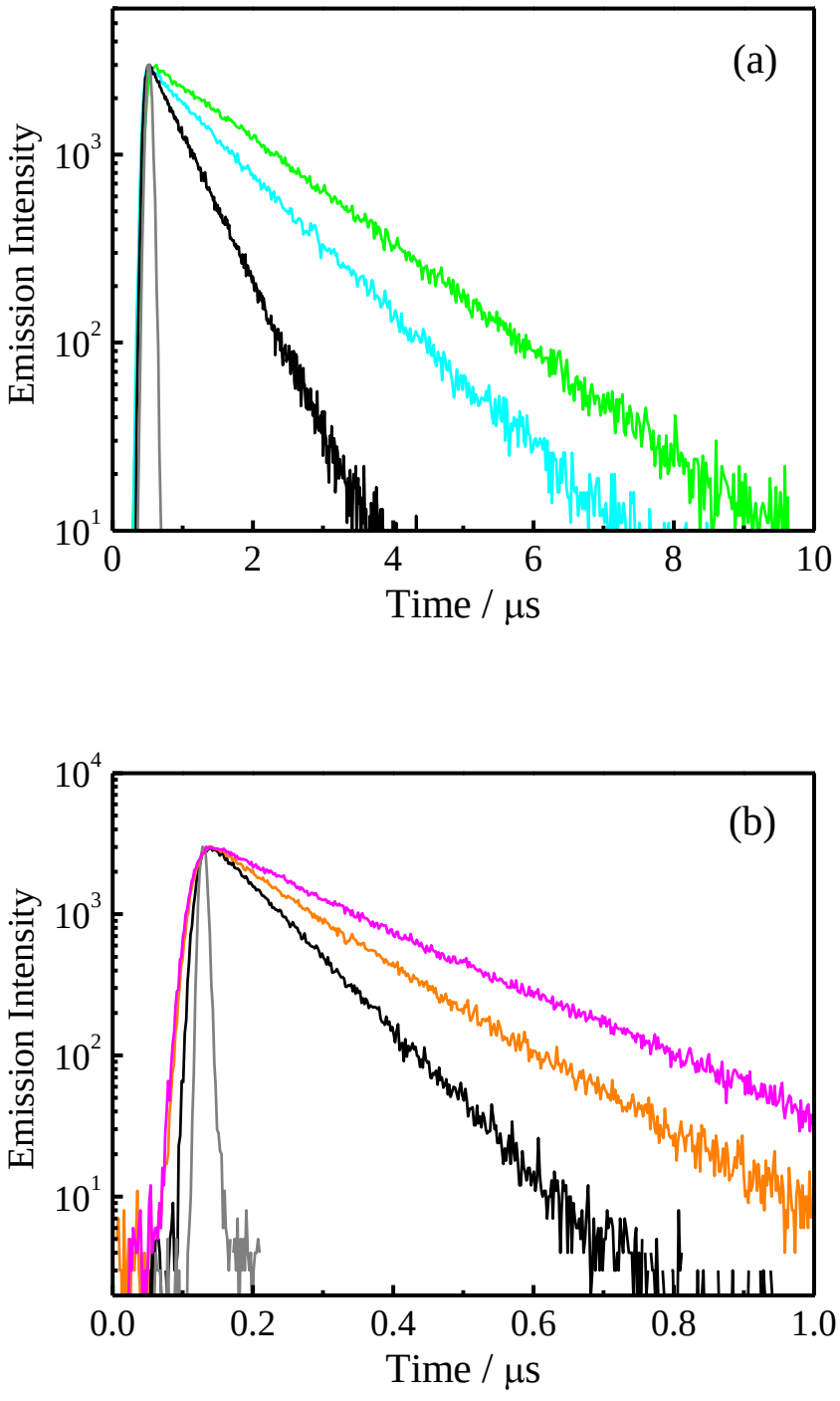

Figure 3-6 Emission decay profiles of (a) **ReB$_2$phen** (blue), **ReBphen** (green), and **Rephen** (black), (b) **ReB$_2$bpy** (orange), **ReBbpy** (pink), and **Rebpy** (black) in toluene. Gray curves represent those of the instrumental response function (IRF).

Table 3-10 Spectroscopic and photophysical properties of the complexes in toluene at 298 K.

complex	λ^{em} / nm	Φ^{em}	τ^{em} / μs	k_r / 10^5 s^{-1}	k_{nr} / 10^5 s^{-1}	$\tilde{\nu}_{1/2}$ / cm^{-1}
ReB_2phen	669	0.057	1.2	0.48	7.9	3250
ReBphen	669	0.033	1.6	0.21	6.0	3430
Rephen	605	0.070	0.56	1.3	17	3680
ReB_2bpy	653	0.039	0.14	2.8	69	3280
ReBbpy	641	0.020	0.17	1.2	58	3650
Rebpy	614	0.020	0.090	2.2	110	3820

3-3-6 Temperature Dependence of the Emission Lifetime

The spectroscopic and photophysical properties of the complexes in Table 3-10 demonstrate that the k_{nr} value of **ReB$_2$bpy** is larger than that of **ReBbpy** in accord with the prediction from the energy gap law of k_{nr}: the natural logarithms of k_{nr} of the ^{3}MLCT excited state of a transition metal complex increases linearly with a decrease in the emission energy ($\tilde{\nu}^{em}$). However, the k_{nr} value of **ReB$_2$phen** is larger than that of **ReBphen** despite the same emission energies of the two complexes. Furthermore, **ReB$_2$bpy** and **ReBbpy** with shorter-wavelength emission (λ^{em} = 653 and 641 nm, respectively) show larger k_{nr} values ((58~69) x 10^5 s^{-1}) than **ReB$_2$phen** and **ReBphen** (λ^{em} = 669 nm and k_{nr} ~ 10^5 s^{-1}), which cannot be explained by the prediction by the energy gap law of k_{nr}.

As described in Chapter 2, the small k_{nr} values observed for **ReBphen** and **ReBbpy** were explained by the smaller contributions of the non-emitting states (i.e., excited triplet dd state (^{3}dd*) or 4th ^{3}MLCT excited state) to excited-state decay due to the large thermal activation energies (ΔE) to the non-emitting states and, thus, the emission lifetimes of the complexes were less sensitive to temperature (T) compared to those of the corresponding reference complexes. Therefore, the T-controlled emission decay measurements were carried out for **ReB$_2$phen** and **ReB$_2$bpy** in propylene carbonate (PC). As shown in Figure 3-7, while the emission decay profile of **ReB$_2$phen** could be analyzed by a single exponential function irrespective of T (220–330 K), that of **ReB$_2$bpy** required two exponential functions (τ_1 and τ_2) below 330 K. Although the origin of double exponential decay of **ReB$_2$bpy** is still unknown, one possible reason might be dual emission nature of the complex. In practice, it has been known that ruthenium(II) polypyridine complexes having an arylethynyl-1,10-phenanthroline

ligand(s) including $[Ru(phen)_2(phen\text{-}DBDE)]^{2+}$ show dual emission at room temperature[29,30] or low temperature.[31] The Re(I) tricarbonyl complex having a 4,7-disubstituted-phen ligand has been also reported to show dual emission at low temperature.[32–34] It is worth pointing out that the short lifetime component (τ_2) of **ReB$_2$bpy** decreases with an increase in *T*, while the long lifetime component (τ_1) is insensitive to *T*: see Figure 3-8. Such *T*-dependent emission behaviors have been also observed for $[Ru(phen)_2(phen\text{-}DBDE)]^{2+}$, suggesting dual emission nature of **ReB$_2$bpy**.[35] Among the four rhenium(I) tricarbonyl complexes studied in this thesis (i.e., **ReB$_2$phen**, **ReBphen**, **ReB$_2$bpy**, and **ReBbpy**), although **ReB$_2$bpy** alone shows double exponential decay in the *T* range studied ($220 < T < 330$ K), other complexes might also exhibit dual emission below 220 K, which should be cleared in future studies.

Although the origin of double exponential decay of **ReB$_2$bpy** is not clear in the present stage of the investigation as described above, the *T*-dependent τ_2 component is employed for the following discussion. The *T*-dependent emission lifetimes of **ReB$_2$phen** and **ReB$_2$bpy** were then analyzed by an Arrhenius-type equation in Eq. (3-2)[34] with the parameters in Table 3-11.

$$[\tau^{\mathrm{em}}(T)]^{-1} = \frac{k_0 + k_1 \exp(-\Delta E/RT)}{1 + \exp(-\Delta E/RT)} \qquad (3\text{-}2)$$

In Eq. (3-2), k_0 is the sum of the *T*-independent radiative (k_r^0) and nonradiative decay rate constants (k_{nr}^0), and k_1 is the frequency factor for thermal activation from the emitting ^{3}MLCT excited state to the higher-energy non-emitting excited state(s) with the energy barrier between the two states being ΔE: see Scheme 3-3.

As shown in Table 3-11, the ΔE value of **ReB$_2$phen** (910 cm^{-1}) was 1.1-times smaller than that of **ReBphen** (960 cm^{-1}), while the ΔE value of **ReB$_2$bpy** (630 cm^{-1}) was 1.6-times smaller than that of **ReBbpy** (1000 cm^{-1}). Judging from the ΔE value

(630 ~ 1000 cm^{-1}) observed for each complex, the ΔE value is too small for the thermal activation energy from the emitting ^{3}MLCT excited state to the ^{3}dd* state and, thus, the value will be responsible for the thermal activation to the 4th ^{3}MLCT excited state. The presence of the two arylborane charge transfer units in the diimine ligand results in the decreases in the ΔE values of **ReB$_2$phen** and **ReB$_2$bpy** compared to those of **ReBphen** and **ReBbpy**, suggesting larger contributions of the 4th ^{3}MLCT excited states to excited decay of **ReB$_2$phen** and **ReB$_2$bpy**. Furthermore, the difference in the ΔE value between the complexes having the double and single DBDE group(s) is larger for the bpy-type complexes compared to that of the phen-type complexes. This is in accordance with the excited state properties of the complexes derived by the absorption/emission spectra and TD-DFT calculations.

It is worth pointing, nevertheless, that the k_1 value of **ReB$_2$phen**, corresponding to the frequency factor for the thermal activation from the emitting ^{3}MLCT state to the 4th ^{3}MLCT excited state, is 1.6-times larger than that of **ReBphen**, while the value is 4.1-times smaller for **ReB$_2$bpy** compared to that of **ReBbpy**. Thus, the ΔE and k_1 values of the phen- and bpy-type complexes show opposite trends with one another. Although the primary reason for this is not clear in the present stage of the investigations, the T-dependent emission lifetimes of the complexes are governed in balance with the ΔE and k_1 values. The present experiments demonstrate that the τ^{em} values of **ReB$_2$phen** and **ReB$_2$bpy** are more sensitive to T compared to those of **ReBphen** and **ReBbpy**.

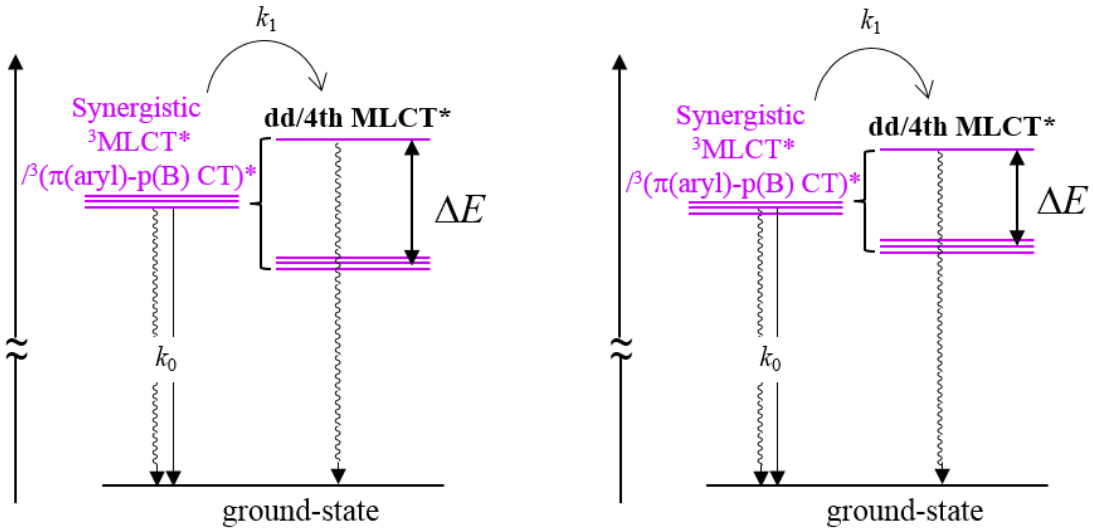

Scheme 3-3 Energy diagrams for the temperature-dependent emission lifetimes of the complexes.

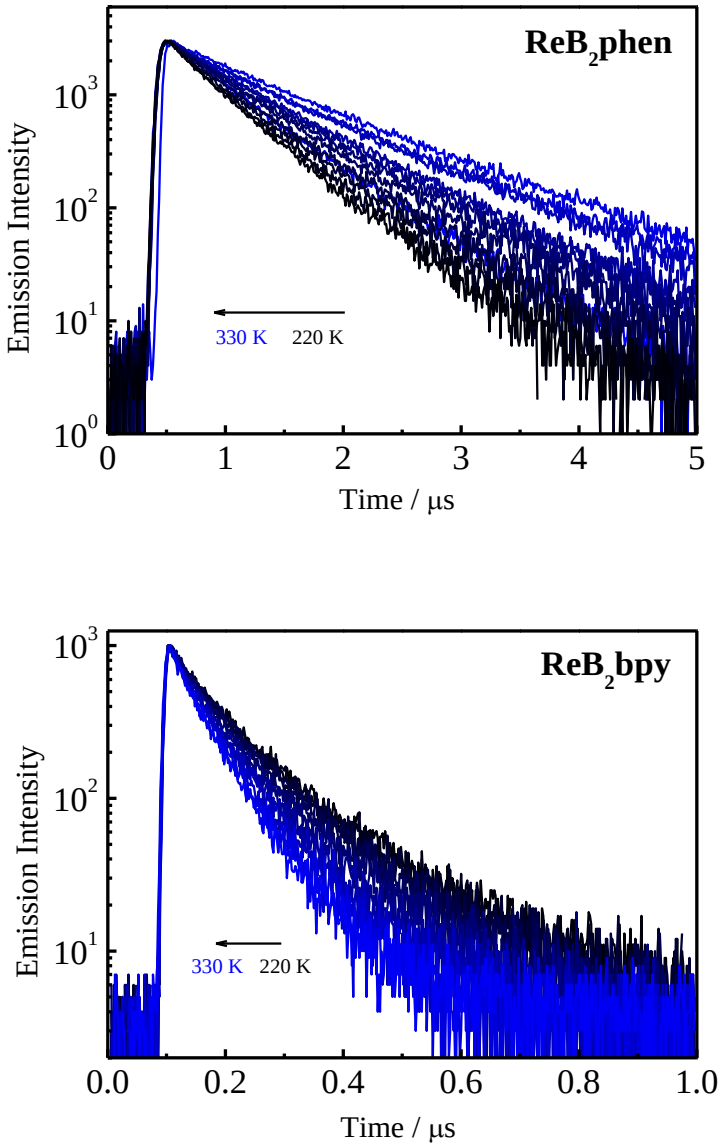

Figure 3-7 Temperature (T = 220–330 K) dependent emission decay profiles of **ReB$_2$phen** and **ReB$_2$bpy** in propylene carbonate.

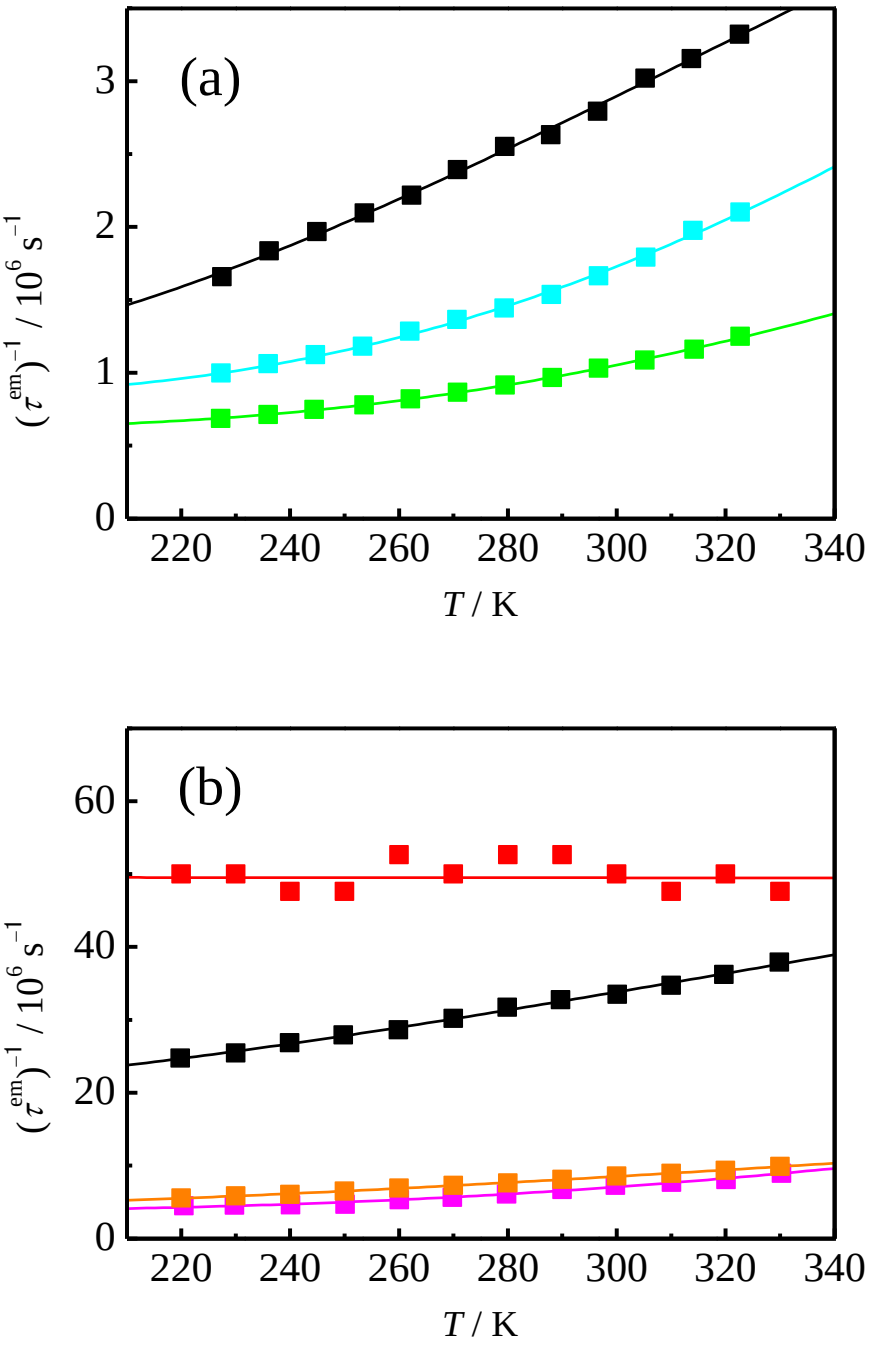

Fig 3-8 Temperature dependences of the emission lifetimes of the (a) **ReB$_2$phen** (blue), **ReBphen** (green) and **Rephen** (black), (b) **ReB$_2$bpy** (τ_2: orange, τ_1: red), **ReBbpy** (pink) and **Rebpy** (black) in propylene carbonate. The results on **ReBphen**/**Rephen** and **ReBbpy**/**Rebpy** are compiled from Chapter 2.

Table 3-11 Temperature dependent emission parameters of the complexes in propylene carbonate.

complex	ΔE / cm^{-1}	k_0 / 10^6 s^{-1}	k_1 / 10^8 s^{-1}
ReB$_2$phen	910	0.82	0.70
ReBphen[a]	960	0.61	0.43
Rephen[a]	560	0.94	0.30
ReB$_2$bpy[b]	630	3.9	1.0
ReBbpy[a]	1000	3.7	4.1
Rebpy[a]	560	19	2.6

a) The data compiled from Chapter 2. b) calculated by τ_2.

3-4 Conclusions

In this chapter, two novel rhenium(I) complexes having multiple arylborane charge transfer units were synthesized and the effects of the number of the arylborane charge transfer unit in the complex on the redox, spectroscopic and photophysical properties were described in detail. **ReB$_2$phen** and **ReB$_2$bpy** showed low-energy and more intense absorption compared to the corresponding reference complexes having a single arylborane unit. The molar absorption coefficients of the MLCT absorption bands of **ReB$_2$phen** and **ReB$_2$bpy** were also largely enhanced owing to the synergistic interactions between MLCT and π(aryl)-p(B) CT caused by the presence of the two arylborane units in the periphery of the diimine ligands. The k_r values of **ReB$_2$phen** and **ReB$_2$bpy** were almost twice larger than the relevant values of **ReBphen** and **ReBbpy**, which could be explained by the Strickler-Berg-type relation for the fluorescence transition of a molecule. Furthermore, **ReB$_2$bpy** displayed more effective influences on the spectroscopic and photophysical properties compared to **ReB$_2$phen**, which was also confirmed by TD-DFT calculations and *T*-dependent emission lifetimes of the complexes.

In this chapter, it is demonstrated that synthetic control/tuning of the electrochemical, spectroscopic and photophysical properties of a Re(I) complex is achieved by a triarylborane-appended π-chromophoric ligand.

3-5 References

1. E. Sakuda, A. Funahashi and N. Kitamura, *Inorg. Chem*. **2006**, *45*, 10670–10677.
2. N. Kitamura, E. Sakuda and Y. Ando, *Chem. Lett*. **2009**, *38*, 938–943.

3. Z. M. Hudson, C. Sun, K. J. Harris, B. E. Lucier, R. W. Schurko and S. Wang, *Inorg. Chem*. **2011**, *50*, 3447–3457.
4. A. Ito, T. Hirokawa, E. Sakuda and N. Kitamura, *Chem. Lett*. **2011**, *40*, 34–36.
5. Y. You and S. Y. Park, *Adv. Mater*. **2008**, *20*, 3820–3826.
6. R. S. Vadavi, K. M. Lee, T. Kim, J. Lee and M. H. Lee, *Organometallics* **2011**, *31*, 31–34.
7. C. R. Wade and F. P. Gabbai, *Inorg. Chem*. **2010**, *49*, 714–720.
8. Y. Sun, X. M. Hudson, Y. Rao and S. Wang, *Inorg. Chem*. **2011**, *50*, 3373–3378.
9. A. Ito, Y. Kang, E. Sakuda and N. Kitamura, *Inorg. Chem*. **2012**, *51*, 7722–7732.
10. S. -B. Zhao, T. McCormick and S. Wang, *Inorg. Chem*. **2007**, *46*, 10965–10967.
11. Y. Sun, N. Ross, S. -B. Zhao, K. Huszarik, W. -L. Jia and R. -Y. Wang, *J. Am. Chem. Soc*. **2007**, *129*, 7510–7511.
12. Z. M. Hudson and S. Wang, *Dalton Trans*. **2011**, *40*, 7805–7816.
13. A. Zhao, F. Li, S. Liu, M. Yu, Z. Liu, T. Yi and C. Huang, *Inorg. Chem*. **2008**, *47*, 9256–9264.
14. D. J. H. Emslie, L. E. Harrington, H. A. Jenkins, C. M. Robertson and J. F. Britten, *Organometallics* **2008**, *27*, 5317–5325.
15. A. Nakagawa, E. Sakuda, A. Ito and N. Kitamura, *Inorg. Chem*. **2015**, *54*, 10287–10295.
16. F. H. Case, *J. Org. Chem*. **1951**, *16*, 941–945.
17. Crystal Structure Analysis Package, Rigaku and Rigaku/MSC (**2000-2004**). 9009 NewTrails Dr. The Woodlands TX 77381 USA.
18. G. M. Sheldrick, A program for crystal structure determination and refinement, University of Göttingen, **1997**.

19. S. F. Haddad, J. A. Marshall, G. A. Grosby and B. Twamley, *Acta Cryst*. **2002**, *58*, m559–m561.

20. S. A. Moya, J. Guerrero, R. Pastene, R. Schmidt, R. Sariego, R. Sartori, J. Sanz-Aparicio, I. Fonseca and M. Martinez-Ripoll, *Inorg. Chem*. **1994**, *22*, 2341–2346.

21. W. B. Connick, A. J. Di Bilio, M. G. Hill, J. R. Winkler and H. B. Gray, *Inorg. Chim. Acta* **1995**, *240*, 169–173.

22. L. A. Lucia, K. Abboud and K. S. Schanze, *Inorg. Chem*. **1997**, *36*, 6224–6234.

23. J. Guerrero, O. E. Piro, E. Wolcan, M. R. Feliz, G. Ferraudi and S. A. Moya, *Organometallics* **2001**, *20*, 2842–2853.

24. K. K. -W. Lo, K. H. -K. Tsang, W. -K. Hui and N. Zhu. *Inorg. Chem*. **2005**, *44*, 6100–6110.

25. K. K. -W. Lo, K. H. -K. Tsang and N. Zhu, *Organometallics* **2006**, *25*, 3220–3227.

26. S. R. Banerjee, M. K. Levadala, N. Lazarova, L. Wei, J. F. Valliant, K. A. Stephenson, J. W. Babich, K. P. Maresca and J. Zubieta, *Inorg. Chem*. **2002**, *41*, 6417–6425.

27. S. F. Haddad, J. A. Marshall, G. A. Grosby and B. Twamley, *Acta Cryst*. **2002**, *58*, m559–m561.

28. S. J. Strickler and R. A. Berg, *J. Chem. Phys*. **1962**, *37*, 814–822.

29. E. C. Glazer, D. Magde and Y. Tor, *J. Am. Chem. Soc*. **2005**, **127**, 4190–4192.

30. E. C. Glazer, D. Magde and Y. Tor, *J. Am. Chem. Soc*. **2007**, *129*, 8544–8551.

31. E. Sakuda, Y. Ando, A. Ito and N. Kitamura, *Inorg. Chem*. **2011**, *50*, 1603–1613.

32. L. Wallace and D. P. Rillema, *Inorg. Chem*. **1993**, *32*, 3836–3843.

33. L. Wallace, C. Woods and D. P. Rillema, *Inorg. Chem*. **1995**, *34*, 2875–2882.

34. L. Wallace, D. C. Jackman, D. P. Rillema and J. Merkert, *Inorg. Chem*. **1995**, *34*, 5210–5214.

35. E. Sakuda, C. Matsumoto, Y. Ando, A. Ito, K. Mochida, A. Nakagawa and N. Kitamura, *Inorg. Chem*. **2015**, *54*, 3245–3252.

36. L. Wallace, D. C. Jackman, D. P. Rillema and J. W. Merkert, *Inorg. Chem*. **1995**, *34*, 5210–5214.

Chapter 4. Photocatalytic CO_2 Reduction by Tricarbonyl Rhenium(I) Complexes Having Arylborane Charge Transfer Units

4-1 Introduction

A class of tricarbonyl rhenium(I) complexes having a diimine ligand ([$Re(CO)_3LX$]) is known to act as a photocatalyst for CO_2 reduction, which selectively produces CO with a relatively high turnover number (TON).[1–8] Since the visible-light absorption intensity of [$Re(CO)_3LX$] is in general weak (e.g., 3.2×10^3 $M^{-1}cm^{-1}$ at 389 nm for [$Re(CO)_3(bpy)Cl$] in tetrahydrofuran, bpy = 2,2'-bipyridine),[9] a photosensitizer is often employed in a photocatalytic reaction system based on [$Re(CO)_3LX$]. As a typical example, polypyridine ruthenium(II) complexes represented by $[Ru(bpy)_3]^{2+}$ are frequently utilized as photosensitizers, since they show relatively intense visible-light absorption ascribed to the metal-to-ligand charge transfer (MLCT) transition: ε (molar absorption coefficient) = 13,000 $M^{-1}cm^{-1}$ at 451 nm for $[Ru(bpy)_3]^{2+}$ in CH_3CN.[10] In a $[Ru(bpy)_3]^{2+}$ – [$Re(CO)_3(bpy)Cl$] system, $[Ru(bpy)_3]^{2+}$ as a photosensitizer absorbs visible light and subsequent excitation energy transfer from the excited triplet MLCT state (^{3}MLCT*) of $[Ru(bpy)_3]^{2+}$ to [$Re(CO)_3(bpy)Cl$] produces the ^{3}MLCT* state of [$Re(CO)_3(bpy)Cl$]. Reductive quenching of the ^{3}MLCT* state of [$Re(CO)_3(bpy)Cl$] by an electron donor then generates the one-electron reduced species (OERs) of [$Re(CO)_3(bpy)Cl$], which triggers catalytic reduction of CO_2.[1] A combination of a photosensitizer and a photocatalyst has been extensively studied on the basis of the intra- and/or inter-molecular strategies to achieve an efficient CO_2 photoreduction system. As an example for the latter system, Hukkanen et al. have reported that a 1/1 (mol/mol) mixture of [$Re(bpy)(CO)_3Cl$] and $[Ru(bpy)_3]^{2+}$ efficiently reduces CO_2 by

visible-light irradiation in the presence of NEt_4Cl as a stabilizer for the chloride ion in $[Re(bpy)(CO)_3Cl]$.[11] Such bi- or multi-molecular systems are widely utilized in a variety of light-driven reactions.[6,12–16] Chemical bonding between a photosensitizer and a catalyst is another choice to construct a photosensitizer–catalyst system. Such intramolecular strategy can enhance the efficiency of the photoinduced reaction between the two moieties. In practice, Koike et al. reported Ru(II)–Re(I) binuclear complexes (Scheme 4-1) acted as CO_2 reduction photocatalysts and the reaction efficiency correlated to the length of the alkyl chain linked between the two moieties.[17]

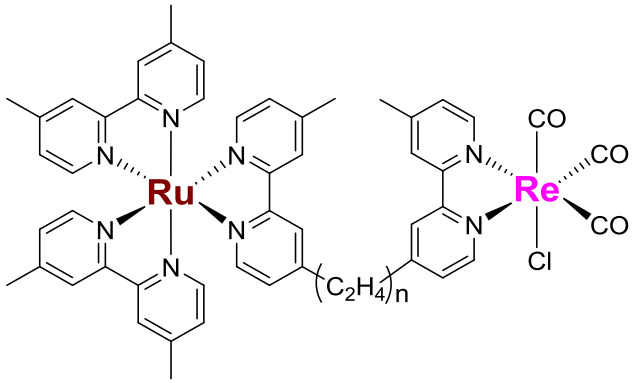

Scheme 4-1 Chemical structure of $[Re(dmb)_2–LL–Re(CO)_3Cl]^{2+}$ (dmb = 4,4'-dimethyl-2,2'-bipyridine and LL = bridging ligand having $(C_2H_4)_n$– spacer (n = 1–3).

As described in Chapters 2 and 3, the tricarbonyl rhenium(I) complexes having one or two arylborane charge transfer unit(s) show low-energy/intense absorption and low-energy/long-lived emission compared to the corresponding reference complexes without an arylborane charge transfer unit. In particular, their ^{1}MLCT and higher-energy absorption bands in the broad UV–visible regions (e.g., 22,700 $M^{-1}cm^{-1}$ at 438 nm for **ReBphen**) are more intense than those of the reference complexes and also comparable

with that of $[Ru(bpy)_3]^{2+}$. Such intense absorption of the complexes indicates that they act as a visible-light-driven CO_2 reduction catalyst without an additional photosensitizer(s). Furthermore, the long-lived excited states of the complexes are also advantageous for efficient photoinduced electron transfer to give the OER of $[Re(CO)_3LX]$, followed by catalytic CO_2 reduction. Although a large quantity of the reports on photocatalytic CO_2 reduction using transition metal complexes have been published,[6–8,17–22] photocatalytic CO_2 reduction by a transition metal complex with an arylborane charge transfer unit(s) has not been hitherto reported, except for the preliminary results on CO_2 photoreduction by the ruthenium(II) complex having an arylborane-appended ligand by Sakuda et al. In this chapter, emission quenching of the ^{3}MLCT* states of **ReBphen** and **ReBbpy** by triethanolamine (TEOA) and photocatalytic CO_2 reduction by these complexes are described. The turn over numbers of CO_2 photoreduction to CO by the complexes demonstrated the photocatalytic abilities of the rhenium(I)–arylborane complexes. The conclusions indicate future availability of the complexes in an efficient photocatalytic CO_2 reduction system.

4-2 Experimental

4-2-1 Chemicals and Measurements

Gas chromatography (GC) grade triethanolamine (TEOA) was purchased from Sigma-Aldrich Co., LLC. and used without further purification. *N*,*N*-Dimethylformamide (DMF) was distilled prior to use. A highly purified CO_2 gas (liquefied carbon dioxide, 99.999%) was purchased from NIPPON EKITAN Corporation and used as supplied.

Gas chromatography was conducted by using a 490 Micro-GC (GL Sciences, Inc.)

equipped with a molecular sieve column (Agilent). A carrier gas was a He- or Ar-gas for analysis of CO or H_2, respectively. The flow rate was set 0.2–0.4 mL/min. Electropherograms were recorded on a capillary electrophotoresis system (Tech. 7100, Agilent). Experimental conditions are as follows: capillary size = I.D. 75 μm, length = 80.5 cm, temperature = 25°C, migration solution = α-AFQ109 (pH = 9.0), sample injection = pressurization (50 mbar, 4 sec), applied voltage = –25 kV, detection wavelength: Sig = 400 nm (band width = 25 nm), and Ref = 265 nm (band width = 10 nm) (Indirect UV detection).

Spectroscopic and photophysical measurements described in this chapter were conducted under the similar conditions to those described in Chapter 2 otherwise noted.

4-2-2 Photocatalytic reactions

Photocatalytic reactions were carried out by 4-mL solutions of a complex (0.05 mM) in DMF/TEOA (v/v = 5/1) in 17-mL test tubes (9800-15-150 EX, 15 × 150 mm × 1.2, ASAHI GLASS CO., LTD.). After purging the reaction mixture with a CO_2 gas for 20 min, the solution was sealed by a septum (W-15) and, then, irradiated at $\lambda > 400$ nm using a 100-W high-pressure mercury lamp (SEN LIGHTS Corporation) equipped with a $NaNO_2$ solution filter (0.33 mol/L = 20 g/L, path length = 1 cm). CO was analyzed by a gas chromatograph equipped with a thermal conductivity detector and HCOOH was analyzed by a capillary electrophoresis system. In this study, a turn over number (TON) is defined as (mole amount of the product) / (mole amount of the photocatalyst).

4-3 Results and Discussion

4-3-1 Emission quenching by TEOA

Since reductive quenching of the excited triplet MLCT state of $[Re(CO)_3LX]$ giving OER of the complex is the primary reaction of CO_2 photoreduction as mentioned before, the photoredox abilities of the complexes are worth evaluating in detail using TEOA as a reductant. Figures 4-1 and 4-2 show the absorption and emission spectra of the complexes in the absence and presence of TEOA in DMF under Ar-gas atmosphere. The emission intensity of the complex decreased with an increase in the TEOA concentration ([TEOA]) in the solution, while the relevant absorption spectrum was unchanged in the presence of TEOA irrespective of the complex. The absorption spectra of the complexes in the absence and presence of TEOA indicate that there is no evidence for the interaction between the ground-state complex and TEOA. Since the emission spectral band shape of the complex in the absence and presence of TEOA resembles with each other, there is no or weak electronic interaction between the excited-state complex and TEOA as well. As shown in Figure 4-3, the emission decay profiles of the complexes in DMF were analyzable by single exponential functions irrespective of the concentration of TEOA, and the emission lifetime of the complex decreased upon an addition of TEOA. On the basis of such experimental results, it is concluded that the emissions from the complexes are quenched by electron transfer from TEOA to the excited states of the complexes, and the dynamic quenching is the predominant process. As demonstrated in Figures 4-2 and 4-3, a 5.9–14-times higher concentration of TEOA is required to obtain sufficient emission quenching of the bpy-type complexes compared to that of the phen-type complexes, presumably due to the difference in the excited-state lifetime of the complex, indicating that the interactions between the complex and the quencher is sensitive to the diimine structure of the Re(I) complex. Furthermore, it is worth pointing out that emission quenching of

the rhenium(I)–arylborane complexes proceeds more efficiently than that of **Rephen** or **Rebpy**. The origin of such characteristics is discussed in the following section.

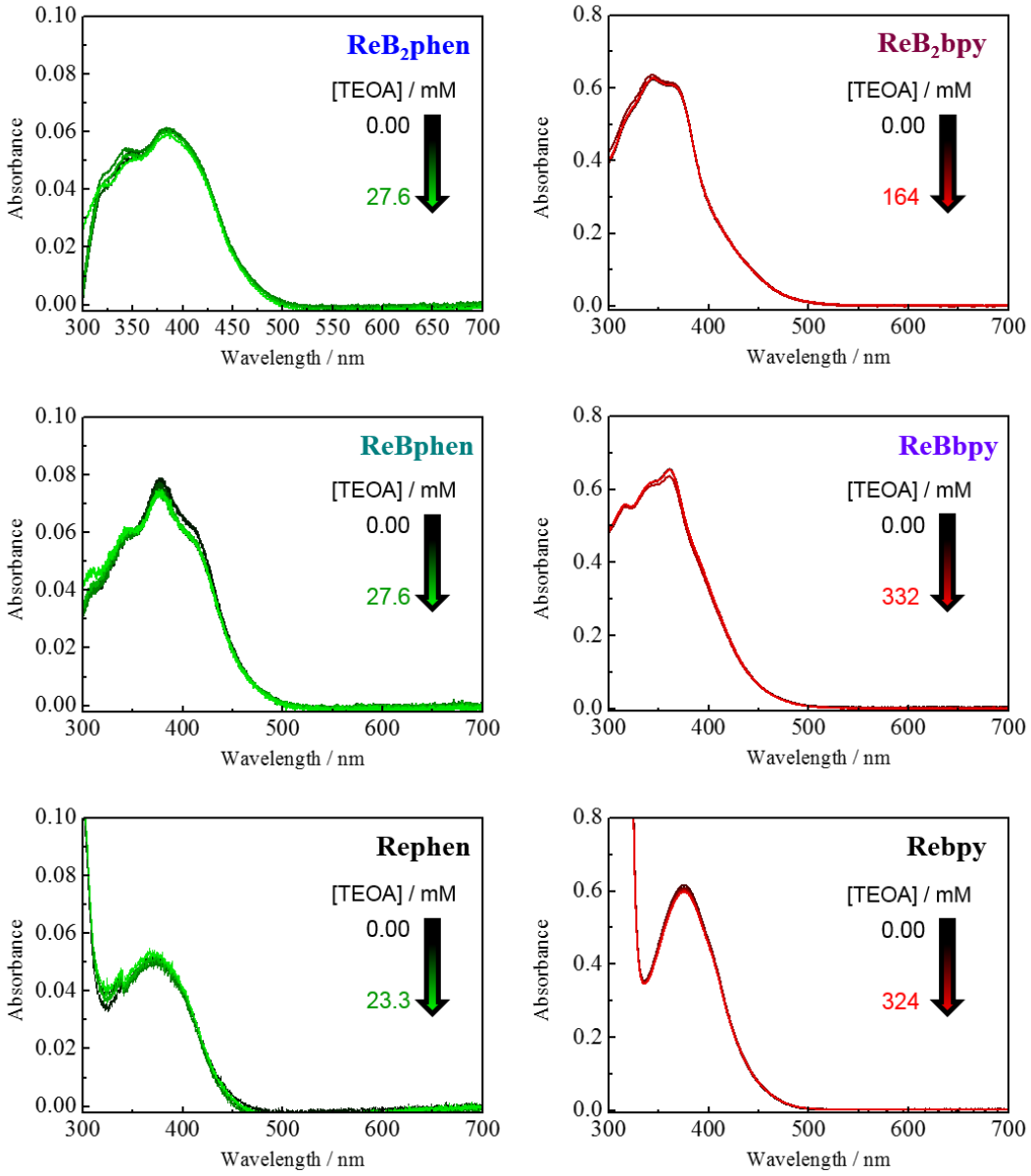

Figure 4-1 Absorption spectra of the complexes in the presence and absence of TEOA in DMF under Ar-gas atmosphere. The concentrations of the complexes are as follows, [**ReB$_2$phen**] = 1.2 $\times 10^{-6}$ M, [**ReBphen**] = 1.7 $\times 10^{-6}$ M, [**Rephen**] = 1.5 $\times 10^{-6}$ M, [**ReB$_2$bpy**] = 1.7 $\times 10^{-5}$ M, [**ReBbpy**] = 2.4 $\times 10^{-5}$ M, [**Rebpy**] = 2.0 $\times 10^{-3}$ M.

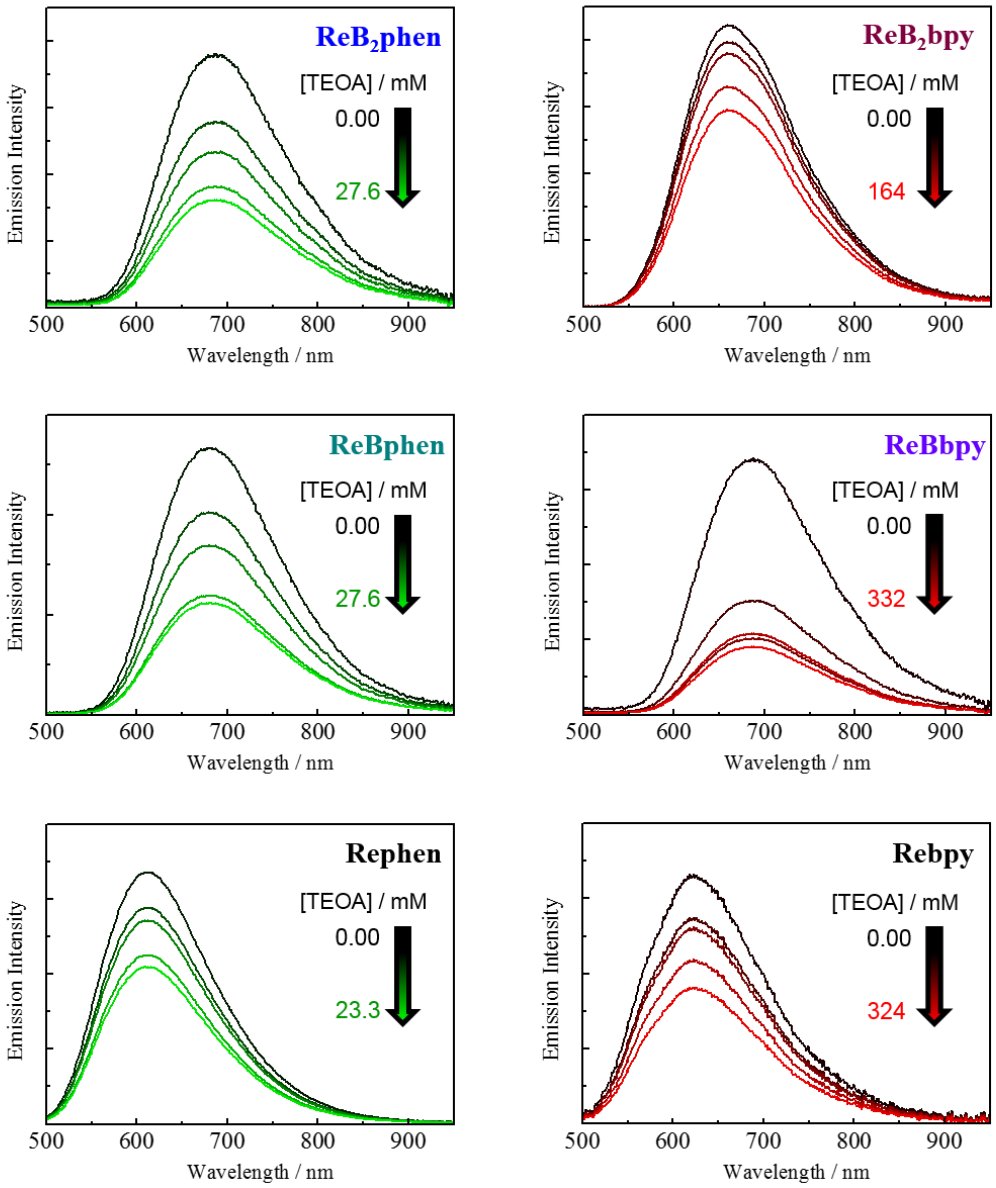

Figure 4-2 Emission spectra of the complexes in the presence and absence of TEOA in DMF in Ar-gas atmosphere. The concentrations of the complexes are as follows,

[**ReB$_2$phen**] = 1.2 $\times 10^{-6}$ M, [**ReBphen**] = 1.7 $\times 10^{-6}$ M, [**Rephen**] = 1.5 $\times 10^{-6}$ M,

[**ReB$_2$bpy**] = 1.7 $\times 10^{-5}$ M, [**ReBbpy**] = 2.4 $\times 10^{-5}$ M, [**Rebpy**] = 2.0 $\times 10^{-3}$ M.

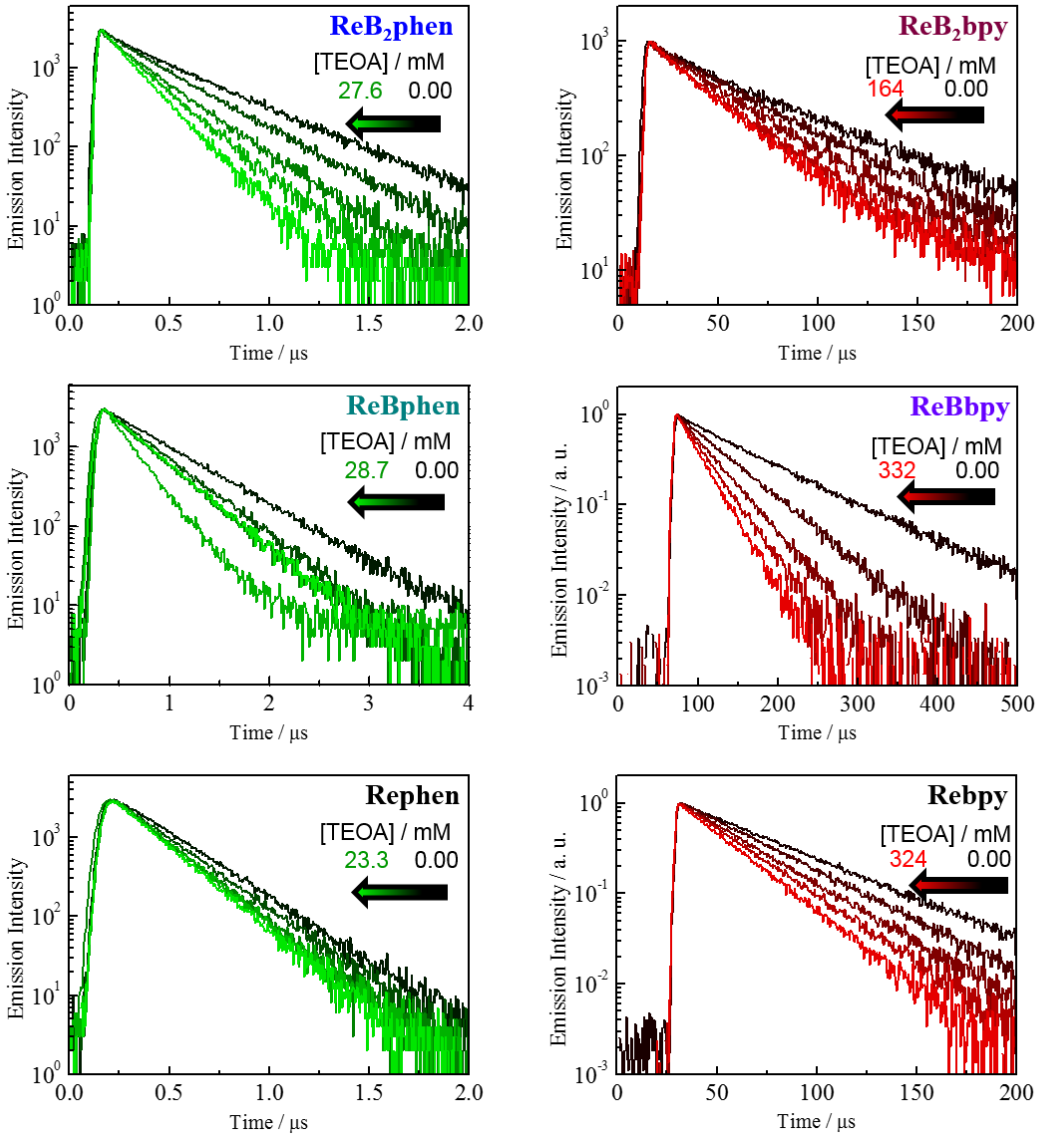

Figure 4-3 Emission decay profiles of the complexes in the presence and absence of TEOA in DMF under Ar-gas atmosphere. The concentrations of the complexes are as follows,

[**ReB$_2$phen**] = 1.2 $\times 10^{-6}$ M, [**ReBphen**] = 1.7 $\times 10^{-6}$ M, [**Rephen**] = 1.5 $\times 10^{-6}$ M,

[**ReB$_2$bpy**] = 1.7 $\times 10^{-5}$ M, [**ReBbpy**] = 2.4 $\times 10^{-5}$ M, [**Rebpy**] = 2.0 $\times 10^{-3}$ M.

4-3-2 Stern–Volmer Analysis

Since the emissions from the complexes are sufficiently quenched by TEOA as shown in Figures 4-2 and 4-3, the excited-state lifetimes of the complexes in the absence and presence of TEOA are analyzed on the basis of the Stern–Volmer relationship. Scheme 4-2 shows the kinetic scheme for photoinduced electron-transfer (ET) quenching of a tricarbonyl rhenium(I) complex (Re^{I}) by an electron donor (D). In Scheme 4-2, k_d and k_{-d} are the association and dissociation rate constants of the reactants and the encounter complex, respectively. k_{ET} and k_{-ET} represent the forward and backward ET rate constants within the encounter complex, respectively. k_{BET} is the backward ET rate constant giving the ground-state complex, and k''_{-d} is subsequent dissociation of the ground-state complex. k'_{-d} and k'_{d} are the rate constants for free ion formation and homogeneous recombination of the ions, respectively.[23–29] The emission quenching rate constant (k_q) of a rhenium complex by an electron donor is given by the Stern–Volmer equation in Eq. (4-1),[30–33]

$$\frac{\tau_0}{\tau} = 1 + k_q \tau_0 [D] \qquad (4\text{-}1)$$

where τ_0 and τ are the emission lifetimes of the complex in the absence and presence of D, respectively. [D] is the concentration of a quencher: TEOA.

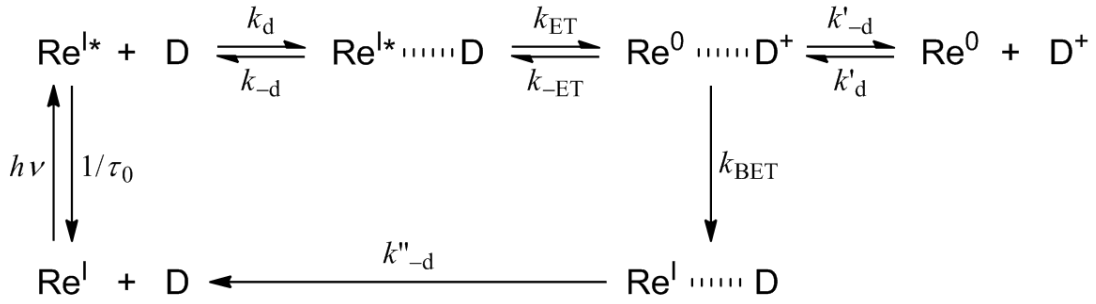

Scheme 4-2 Kinetic scheme for photoinduced ET quenching of the excited triplet MLCT state of a tricarbonyl rhenium(I) complex (Re^I) by an electron donor (D).

Figure 4-4 shows the Stern–Volmer plots for the complexes. Since the plot showed a good linear relationship between τ_0^{em}/τ^{em} and [TEOA] irrespective of the complex, the linear regression of each plot in Figure 4-4 by Eq. (4-1) gave the relevant k_q value as summarized in Table 4-1. The k_q value of **ReB$_2$phen** ($13 \times 10^7\ M^{-1}s^{-1}$) was larger than those of **ReBphen** ($8.9 \times 10^7\ M^{-1}s^{-1}$) and **Rephen** ($4.2 \times 10^7\ M^{-1}s^{-1}$). Similarly, the k_q value successively increased upon the introduction of the DBDE group into **Rebpy** ($k_q = 5.9 \times 10^7\ M^{-1}s^{-1}$) < **ReBbpy** ($7.6 \times 10^7\ M^{-1}s^{-1}$) < **ReB$_2$bpy** ($9.6 \times 10^7\ M^{-1}s^{-1}$).

Table 4-1 Emission quenching parameters of the complexes by TEOA in DMF.

complex	$\tau^{em}{}_0$ / ns	$\Delta G_{ET}{}^0$ / eV	k_q / $M^{-1}s^{-1}$	E_0 / cm^{-1}
ReB$_2$phen	390	–0.17	13×10^7	14640
ReBphen	800	–0.21	8.9×10^7	15850[b]
Rephen	300	–0.26	4.2×10^7	18180[b]
ReB$_2$bpy	60	n. d.[a]	9.6×10^7	15060
ReBbpy	100	–0.025	7.6×10^7	15590[b]
Rebpy	50	+0.049	5.9×10^7	16130[b]

a) not determined due to the lack of electrochemical data caused by the low solubility of the complex in DMF. b) compiled from chapter 2.

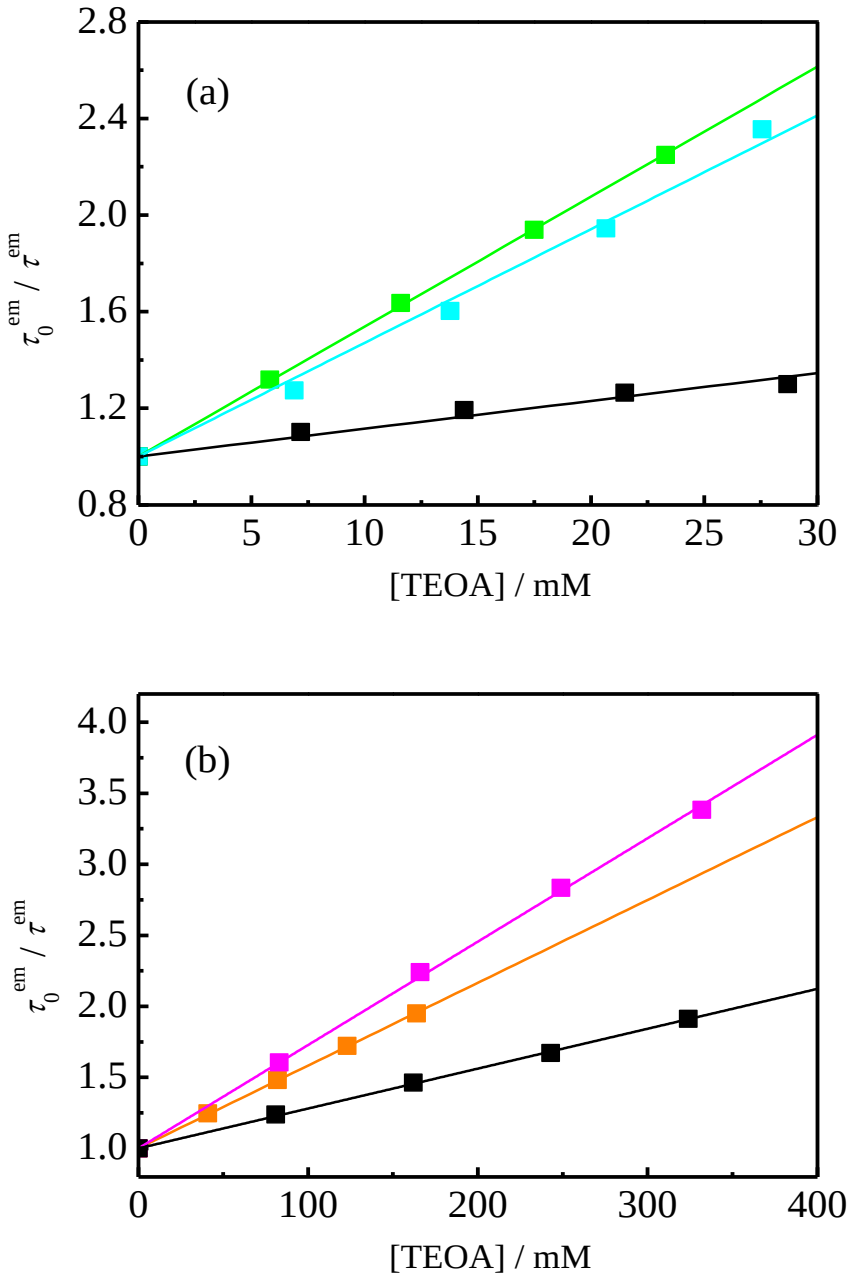

Figure 4-4 Stern–Volmer plots for emission quenching of (a) **ReB$_2$phen** (blue), **ReBphen** (green) and **Rephen** (black), (b) **ReB$_2$bpy** (orange), **ReBbpy** (pink) and **Rebpy** (black) by TEOA in DMF.

The emission quenching rate constant of a rhenium(I) complex by an amine is dependent on the Gibbs free energy change for the ET reaction (ΔG_{ET}^{0}).[33,34] ΔG_{ET}^{0} of a photoinduced ET (PET) reaction is calculated based on Eq. (4-2),[35–37]

$$\Delta G_{ET}^{0} = E_{1/2}(D^{I/0}) - E_{1/2}(Re^{I/0}) - E_0 + w_p - w_r \qquad (4\text{-}2)$$

where $E_{1/2}(D^{I/0})$ and $E_{1/2}(Re^{I/0})$ are the oxidation potential of a quencher and the reduction potential of a complex, respectively. E_0 is the excited-state energy of a complex and, w_p and w_r are the electrostatic works necessary to bring together the two product ions and the reactants from an infinite distance to the close-contact distance for PET, $d = (r_A + r_D)$, respectively, where r_A and r_D are the radii of an electron acceptor and an electron donor, respectively. The w_p and w_r values can be calculated by Eqs. (4-3),

$$w_p = \frac{Z_{D+} Z_{A-} e^2}{D_s d} \qquad (4\text{-}3a)$$

$$w_r = \frac{Z_D Z_A e^2}{D_s d} \qquad (4\text{-}3b)$$

where Z_{D+} and Z_{A-} are the charges of the two product ions, Z_D and Z_A are the charges of the two reactants, e and D_s are the elementary electric charge and the static dielectric constant of a medium, respectively.

The calculated ΔG_{ET}^{0} values are included in Table 4-1. While the ΔG_{ET}^{0} value of **ReB$_2$bpy** cannot be calculated due to the lack of the electrochemical data of the complex, the data indicate that all of the PET reactions are exergonic except for that of **Rebpy**. The PET reactions for **ReB$_2$phen** and **ReBphen** (ΔG_{ET}^{0} = –0.17 and –0.21 eV, respectively) are thermodynamically unfavorable compared to that of **Rephen** (ΔG_{ET}^{0} = –0.26 eV), while the k_q value shows an opposite trend.[33,34] The unusual efficient PET rate constants observed for **ReB$_2$phen** and **ReBphen** are presumably due to the large charge-separated excited states of the complexes and the electron-accepting ability of

the arylborane charge transfer unit(s). In practice, the PET quenching experiments for **ReBphen** using a series of an electron donor have revealed that **ReBphen** shows a smaller outer-sphere reorganization energy for the electron transfer than **Rephen**.[29] On the other hand, PET from TEOA to **ReBbpy** (ΔG_{ET}^{0} = –0.025 eV) is thermodynamically favorable compared to that to **Rebpy** (ΔG_{ET}^{0} = +0.049 eV) and, thus, it is acceptable that **ReB$_2$bpy** shows a larger k_q value compared to **ReBbpy**.

These results indicate that the presence of an "electron-accepting" arylborane charge transfer unit(s) in the periphery of the diimine ligand in [Re(CO)$_3$LX] is highly effective for the "reductive" electron transfer reaction from TEOA to the excited triplet MLCT state of the complex. Owing to the long-lived excited states and the efficient electron transfer reactions of the rhenium(I)–arylborane complexes, the complexes are expected to produce OER more efficiently compared to the corresponding reference complexes without an arylborane group.

4-3-3 Photocatalytic CO_2 Reduction

The tricarbonyl rhenium(I) complexes having one or two arylborane charge transfer unit(s) show intense ^{1}MLCT absorption in a broad visible region, long-lived excited state (τ^{em}) and large quenching rate constant (k_q) compared to the reference complexes as described above. All of the characteristics observed for **ReB_2phen/ReBphen** and **ReB_2bpy/ReBbpy** indicate that these complexes are very promising to act as visible-light-driven CO_2 reduction catalysts without an additional photosensitizer(s). In order to study the photocatalytic CO_2 reduction abilities of the complexes, a 4 mL DMF/TEOA (v/v = 5:1) solution containing the complex (0.05 mM) in a 17 mL test tube under CO_2 gas atmosphere was irradiated by a Hg lamp at $\lambda > 400$ nm.

As a typical example, Figure 4-5 shows the gas chromatogram of the products by the photoreactions, together with that of CO. In the gas chromatogram observed for the photoreaction mixture, a new peak was observed at the retention time of 66 min, which agreed very well with that of CO as described in the followings. H_2 was not found under the present conditions. Although HCOOH was also confirmed by capillary electrophoresis, the data were not reproducible. Therefore, the results on HCOOH formation are omitted in this thesis.

To quantify the amounts of CO produced by the photoreaction, the calibration curve for a gas chromatogram (GC) was prepared as shown in Figure 4-6, and the best fit of the calibration curve for CO was given by Eq. (4-4),

$$y = (1.42 \times 10^{-6})\, x \qquad (4\text{-}4)$$

where x is the area of the GC peak and y is the concentration of CO (%).

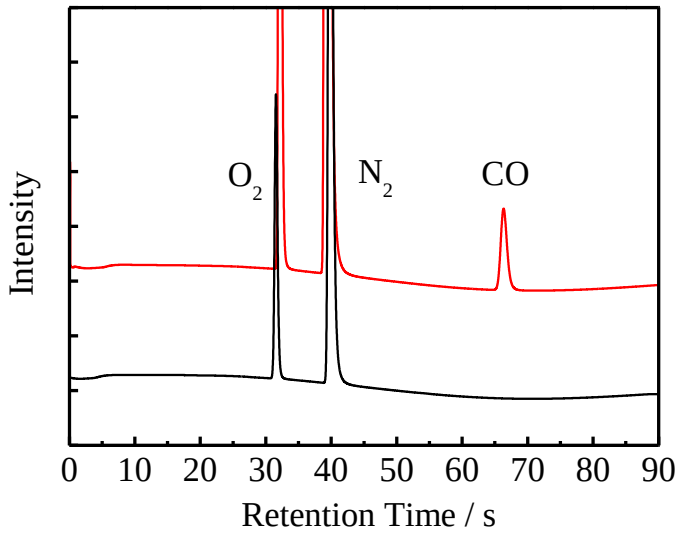

Figure 4-5 Gas chromatograms of the reaction mixtures observed for **Rebpy** in DMF/TEOA (v/v = 5/1) under CO_2 gas atmosphere with (black curve) and without photoirradiation (red curve).

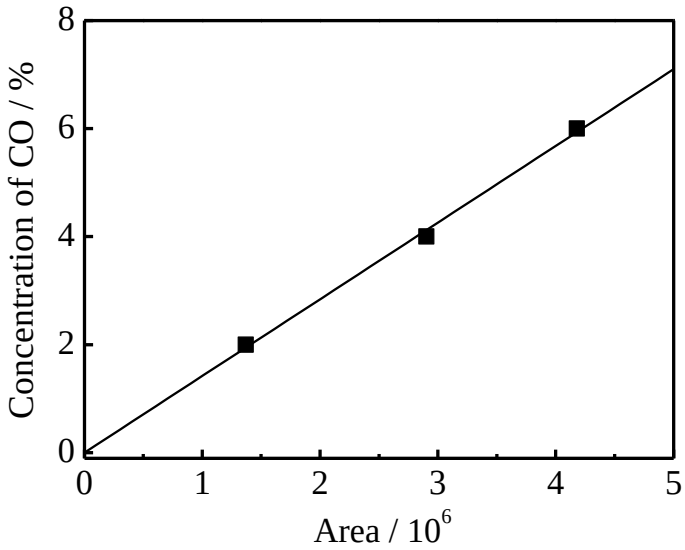

Figure 4-6 Calibration curve for CO formation determined by gas chromatography.

Figures 4-7 shows the time courses of CO formation upon light irradiation to the reactant solution. The results on quantitation of CO are summarized in Table 4-2. All of the complexes were suggested to be active CO_2 photoreduction catalysts, though the photoreduction efficiency was dependent on the complex. Figure 4-7 demonstrates that CO formation rate reaches the highest for 1 h photoirradiation and, then, levels-off for all the complexes, probably due to the transformation and/or decomposition of the Re(I) complexes under prolonged irradiation.

After photoirradiation for 10 h, the turnover number (TON) of CO formation observed for **ReB$_2$phen** or **ReBphen** (TON_{CO} = 0.42 or 1.02, respectively) was less than that of **Rephen** (TON_{CO} = 1.24). Such observations are consistent with the positive shift of the reduction potentials of the complexes and, thus, lower reducing power of **ReB$_2$phen** and **ReBphen** relative to **Rephen**. Similarly, TONs of **ReB$_2$bpy** and **ReBbpy** (TON_{CO} = 0.21 and 0.31, respectively) were much smaller than that of **Rebpy** (TON_{CO} = 3.20), indicating the low photocatalytic abilities of the complexes having an arylborane charge transfer unit(s). It is also worth noting that, with an increase in the number of the arylborane charge transfer unit in the complex, the CO formation efficiency was further decreased. Therefore, the reduction and oxidation potentials in the excited triplet state were calculated for the complexes and summarized in Table 4-2. From Table 4-2, it is clear that with an increase in the number of the arylborane charge transfer unit, the oxidation potentials in the excited triplet state increased. As a result, the reduction ability of the intermediate toward CO_2 reduction for the complexes with arylborane charge transfer units was lower than the corresponding reference complexes, respectively, which should be the primary reason for low reducing ability of **ReB**-type complexes.

These results demonstrate that all of the tricarbonyl rhenium(I) complexes act as photocatalysts for CO_2 reduction with high selectivity and the complexes exhibit two important functions simultaneously: photocatalytic and photosensitizing abilities towards CO_2 reduction.

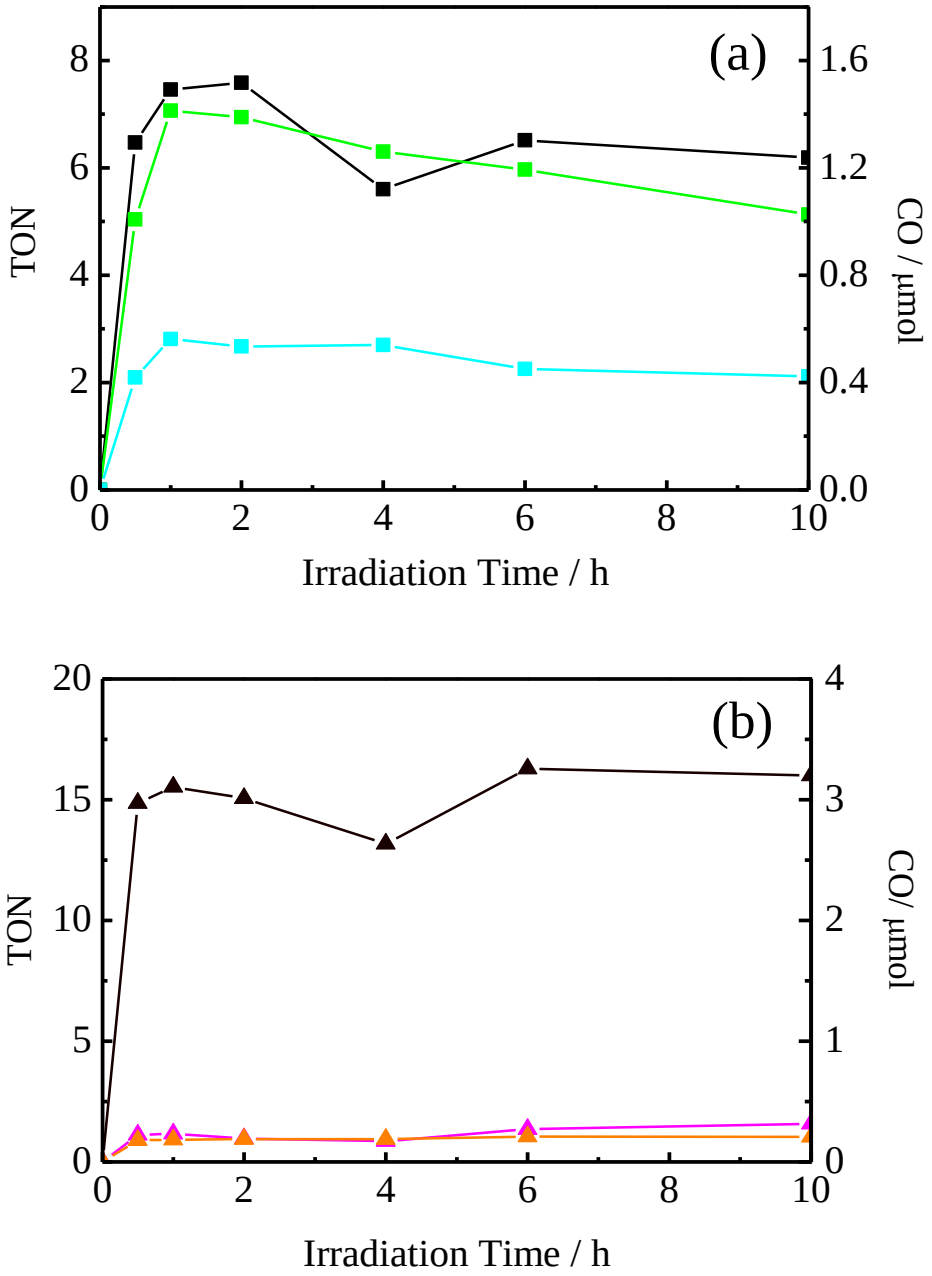

Figure 4-7 Time courses of CO formation by photoirradiation (λ > 400 nm) of (a) **ReB$_2$phen** (blue), **ReBphen** (green) and **Rephen** (black), (b) **ReB$_2$bpy** (orange), **ReBbpy** (pink) and **Rebpy** (black) in DMF/TEOA (5/1 v/v) solutions.

Table 4-2 Formation of CO for photocatalytic CO_2 reduction by the complexes.

complex	TON_{CO}[a]	CO / μmol[a]	$Re^{I/0}$ / V	$*E^{red}$ / V[c]	$*E^{ox}$ / V[d]
ReB_2phen	2.12	0.42	–1.00	0.82	n.d.[b]
ReBphen	5.13	1.02	–0.98	0.98	1.00
Rephen	6.19	1.24	–1.23	1.00	0.94
ReB_2bpy	1.03	0.21	n.d.[b]	–0.29	n.d.[b]
ReBbpy	1.57	0.31	–1.13	–0.51	–0.71
Rebpy	16.0	3.20	–1.28	–0.81	–0.81

a) irradiation for 10 h. b) not detected due to the low solubility of the complex in DMF.

c) reduction potentials in the excited triplet state. d) oxidation potentials in the excited triplet state.

4-4 Conclusions

In this chapter, the photocatalytic abilities of the tricarbonyl rhenium(I) complexes towards CO_2 reduction were studied. On the basis of emission quenching of the complexes by TEOA in DMF, the detailed quenching mechanisms were discussed in terms of the Stern–Volmer plots, calculated quenching rate constants, and the Gibbs free energy changes for the PET reactions. The quenching rate constants increased with an increase in the number of the arylborane charge transfer unit in the complex, indicating the more efficient electron transfer reactions for the complexes having multiple borane centers. Owing to the long-lived excited states and large electron-transfer quenching rate constants observed for the novel complexes having the arylborane charge transfer units, the complexes are expected to produce OER species more efficiently compared to the corresponding reference complexes. The photocatalytic activities of the six rhenium(I) carbonyl complexes towards CO_2 reduction were studied by photoirradiation ($\lambda > 400$ nm) to the DMF/TEOA solutions and the reaction products were then analyzed by gas chromatography and capillary electrophoresis. All of the complexes were shown to be active catalysts for CO_2 photoreduction, although its efficiency was dependent on the nature of the complex. Nonetheless, it was demonstrated that the complexes having an arylborane group(s) showing relatively intense visible absorption acted simultaneously as a photocatalyst and a photosensitizer for CO_2 reduction. The novel complexes having arylborane charge transfer unit(s) showed lower TON for formation of CO, in accordance with the positive shifts of the first reduction potentials of the complexes as described in Chapters 2 and 3. It will be explained by the low reducing power of the complexes as revealed by the positive shifts of their first reduction potentials as well as by the low reduction ability of the intermediate toward CO_2

reduction. The present results indicate that further optimization of the structures of the triarylborane charge transfer unit(s) in the diimine ligand of a tricarbonyl rhenium(I) complex will realize efficient photocatalytic reactions and solar–energy conversion systems.

4-5 References

1. J. Hawecker, J. -M. Lehn and R. J. Ziessel, *J. Chem. Soc. Chem. Commun.* **1983**, 536–538.
2. J. Hawecker, J. -M. Lehn and R. Ziessel, *Helv. Chim. Acta* **1986**, *69*, 1990–2012.
3. H. Hori, F. P. A. Johnson, K. Koike, O. Ishitani and T. Ibusuki, *J. Photochem. Photobiol. A: Chem.* **1996**, *96*, 171–174.
4. K. Koike, H. Hori, M. Ishizuka, J. R. Westwell, K. Takeuchi, T. Ibusuki, K. Enjouji, H. Konno, K. Sakamoto and O. Ishitani, *Organometallics* **1997**, *16*, 5724–5729.
5. P. Kurz, B. Probstand, B. Spingler and R. Alberto, *Eur. J. Inorg. Chem.* **2006**, 2966–2974.
6. H. Takeda, K. Koike, H. Inoue and O. Ishitani, *J. Am. Chem. Soc.* **2008**, *130*, 2023–2031.
7. H. Takeda, H. Koizumi, K. Okamoto and O. Ishitani, *Chem. Commun.* **2014**, *52*, 1491–1493.
8. G. Sahara and O. Ishitani, *Inrog. Chem.* **2015**, *54*, 5096–5104.
9. B. D. Rossenaar, D. J. Stufkens and A. Vlček, *Inorg. Chem.* **1996**, *35*, 2902–2909.
10. A. Juris, V. Balzani and P. Belser, *Helv. Chim. Acta* **1981**, *64*, 2175–2182.

11. H. Hukkanen and T. T. Pakkanen, *Inorg. Chim. Acta* **1986**, *114*, L43–L45.
12. R. F. Beeston, W. S. Treadway, M. C. Fitzgerald, B. A. Degraff and S. E. Stitzel, *Inorg. Chem.* **1998**, *37*, 4368–4397.
13. Z. Y. Bian, K. Sumi, M. Furue, S. Sato, K. Koike and O. Ishitani, *Inorg. Chem.* **2008**, *47*, 10801–10803.
14. A. J. Morris, G. J. Meyer and E. Fujita, *Acc. Chem. Res.* **2009**, *42*, 1983–1994.
15. C. D. Windle and R. N. Perutz, *Coord. Chem. Rev.* **2012**, *256*, 2562–2570.
16. T. Morimoto, C. Nishiura, M. Tanaka, J. Rohacova, Y. Nakagawa, Y. Funada, K. Koike, Y. Yamamoto, S. Shishido, T. Kojima, T. Saeki, T. Ozeki and O. Ishitani, *J. Am. Soc. Chem.* **2013**, *135*, 13266–13269.
17. K. Koike, S. Naito, S. Sato, Y. Sato, Y. Tamaki and O. Ishitani, *J. Photochem. Photobiol. A: Chem.* **2009**, *207*, 109–114.
18. J. Grodkowski, T. Dhanasekaran, P. Neta, P. Hambright, B. S. Brunschwig, K. Shinozaki and E. Fujita, *J. Phys. Chem. A* **2000**, *104*, 11332–11339.
19. T. Ogata, S. Yanagida, B. S. Brunschwig and E. Fujita, *J. Am. Chem. Soc.* **1995**, *117*, 6708–6716.
20. D. Behar, T. Dhanasekaran, P. Neta, C. M. Hosten, D. Ejeh, P. Hambright and E. Fujita, *J. Phys .Chem. A* **1998**, *102*, 2870–2877.
21. S. Sato, T. Morikawa, T. Kajino and O. Ishitani, *Angew. Chem. Int. Ed.* **2013**, *52*, 988–992.
22. Y. Hayashi, S. Kita, B. S. Brunschwig and E. Fujita, *J. Am. Chem. Soc.* **2003**, *125*, 11976–11987.
23. J. C. Luong, L. Nadjo and M. S. Wrighton, *J. Am. Chem. Soc.* **1978**, *100*, 5790–5795.

24. K. Kalyanasundaram, *J. Chem. Soc., Faraday Trans. 2* **1986**, *82*, 2401–2415.

25. M. R. Burke and T. L. Brown, *J. Am. Chem. Soc.* **1989**, *111*, 5185–5191.

26. H. Gan, X. Zhao and D. G. Whitten, *J. Am. Chem. Soc.* **1991**, *113*, 9409–9411.

27. M. Feliz, G. Ferraudi and J. Altmiller, *J. Phys. Chem.* **1992**, *96*, 257–264.

28. T. Ito and S. E. Rokita, *J. Am. Chem. Soc.* **2004**, *126*, 15552–15559.

29. A. Ito, Y. Kang, S. Saito, E. Sakuda and N. Kitamura, *Inorg. Chem.* **2012**, *51*, 7722–7732.

30. M. Wrighton and D. L. Morse, *J. Am. Chem. Soc.* **1974**, *96*, 998–1003.

31. G. J. Kavarnos, *Fundamentals of Photoinduced Electron Transfer, VCH, Weinheim,* **1993**.

32. P. Kurz, B. Probst, B. Spingler and R. Alberto, *Eur. J. Inorg. Chem.* **2006**, *15*, 2966–2974.

33. P. Thanasekaran, R. -T. Liao, B. Manimaran, Y. -H. Liu, P. -T. Chou, S. Rajagopal and K. -L. Lu, *J. Phys. Chem. A* **2006**, *110*, 10683–10689.

34. S. S. Sun and A. J. Lee, *J. Am. Chem. Soc.* **2000**, *122*, 8956–8967.

35. K. Kalyanasundaram, *Coord. Chem. Rev.* **1982**, *46*, 159–244.

36. N. Kitamura, H. -B. Kim, S. Okano and S. Tazuke, *J. Phys. Chem.* **1989**, *93*, 5750–5756.

37. N. Kitamura, Y. Kawanishi and S. Tazuke, *Chem. Phys. Lett.* **1983**, *97*, 103–106.

Chapter 5. Conclusions

In the present thesis, four novel tricarbonyl rhenium(I) complexes with one or two arylborane charge transfer unit(s) were synthesized (Scheme 5-1) and, the spectroscopic, photophysical and photochemical properties of the complexes in solution were studied in detail. A large number of the studies on tricarbonyl rhenium(I) complexes with various ligands have been reported in the past decades aiming at efficient photocatalytic CO_2 reduction. It is also well known that the photocatalytic CO_2 reduction efficiency by a tricarbonyl rhenium complex is controllable by its electronic structures. Since the ground- and excited-state properties of the complex are very sensitive to the coordinating ligand(s) as well as the microenvironments around the complex, chemical modification and derivatization of the complex is absolutely necessary for further advances in the relevant research fields. Thus, this thesis explored to develop new tricarbonyl rhenium(I) complexes toward future construction of an efficient photocatalytic CO_2 reduction system.

The principal experimental results and conclusions are as follows.

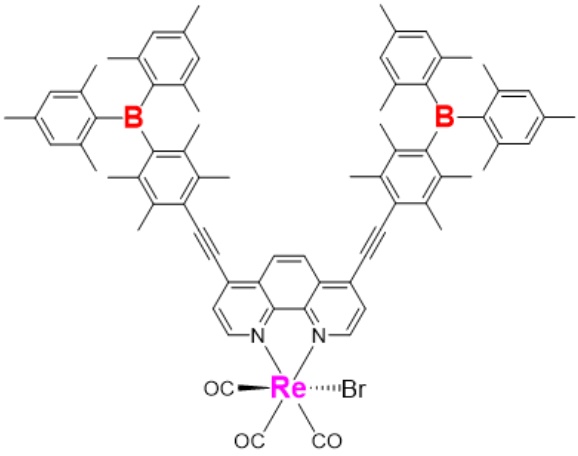

ReB_2phen

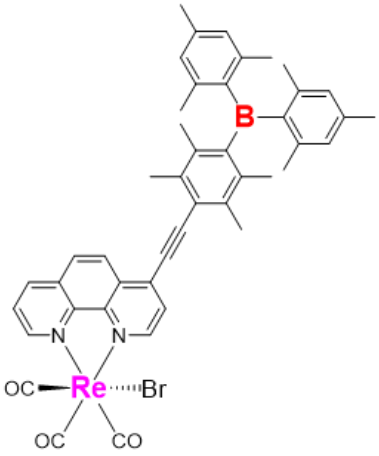

ReBphen

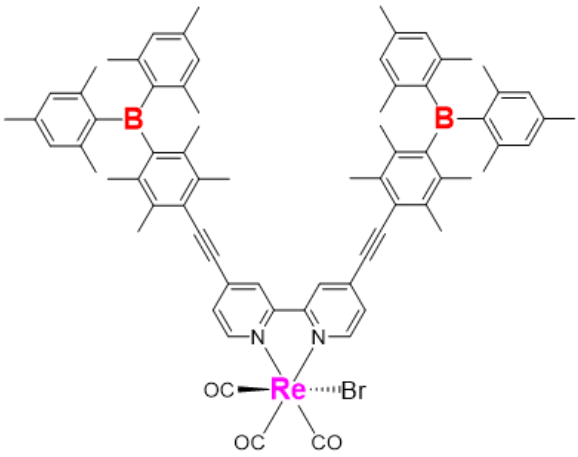

ReB_2bpy

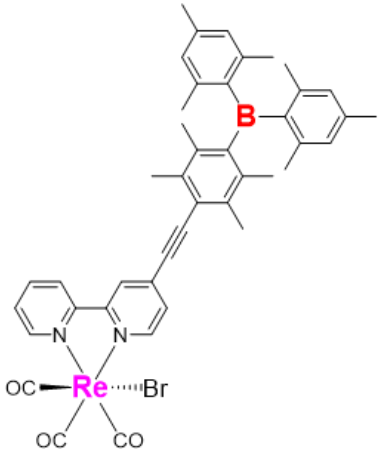

ReBbpy

Scheme 5-1 Chemical structures of novel tricarbonyl rhenium(I) complexes developed in this thesis.

In Chapter 2, two novel tricarbonyl rhenium(I) complexes having an arylborane charge transfer unit, **ReBphen** and **ReBbpy**, were synthesized and the spectroscopic/photophysical properties were studied in detail. It was demonstrated that **ReBphen** and **ReBbpy** showed low-energy/intense absorption and low-energy/long-lived excited states compared to the corresponding reference complexes without an arylborane unit: **Rephen** and **Rebpy**, respectively. TD-DFT calculations supported the assignment of the lowest-energy absorption bands of **ReBphen** and **ReBbpy** to the synergistic MLCT and π(aryl)-p(B) CT transitions. Frank-Condon analysis of the emission spectra of the complexes demonstrated that the excited ^{3}MLCT states of **ReBphen** and **ReBbpy** interact with solvent molecules more strongly than those of **Rephen** and **Rebpy**, respectively, owing to the participation of the synergistic MLCT/π(aryl)-p(B) CT interactions in the former complexes.

Temperature (*T*) dependences of the emission lifetimes of **ReBphen** and **ReBbpy** revealed the contribution of the thermal activation from the emissive ^{3}MLCT excited states to the non-emitting higher-energy lying (fourth) MLCT excited states and subsequent fast nonradiative decay to the ground state. The larger thermal activation barriers (Δ*E*) observed for **ReBphen** and **ReBbpy** compared to those of **Rephen** and **Rebpy**, respectively, demonstrated smaller contributions of the 4th MLCT excited states to excited-state decay of the complexes and, as a result, the emission lifetimes of **ReBphen** and **ReBbpy** were less sensitive to *T* compared to those of **Rephen** and **Rebpy**, respectively. These were due to the stabilization of the ^{3}MLCT excited state energies of **ReBphen** and **ReBbpy** by the synergistic MLCT/π(aryl)-p(B) CT interactions as supported by the redox, spectroscopic, and TD-DFT calculation studies.

The studies on **ReBphen** and **ReBbpy** demonstrated explicitly that an introduction of the DBDE group to the periphery of the diimine ligand in $[Re(CO)_3LX]$ can commonly modulate both spectroscopic and photophysical properties of the complex. However, it is also worth pointing out that the effects of the DBDE group on the properties of the complex are different between the bpy- and phen-type complexes. **ReBphen** shows more efficient synergistic MLCT/π(aryl)-p(B) CT interactions compared to **ReBbpy**, as proved by the larger differences in the electrochemical, spectroscopic, and photophysical properties between **ReBphen**/**Rephen** and **ReBbpy**/**Rebpy**. The differences in the properties were discussed in detail on the basis of the experimental and theoretical data.

The more rigid structure of 1,10-phenanthroline (phen) than that of 2,2'-bipyridine (bpy) by the presence of the carbon atoms at the 5- and 6-positions in phen impedes nonradiative decay from the excited state of the phen complex. The larger MO population at the 4-position of phen in **Rephen** than that of bpy in **Rebpy** presumably enhances the electronic interactions between the ligand and the arylborane unit in **ReBphen**. Furthermore, the theoretical calculations on the HOMO–LUMO electronic structures of the isomeric complexes of **ReBphen** and **ReBbpy**, **3-/5-ReBphen** and **3-/5-ReBbpy**, were also conducted toward future molecular design of related complexes. The results indicated that the substituted position of a triarylborane unit in a diimine ligand played essential roles in governing the photophysical characteristics of $[Re(CO)_3LBr]$.

Since the intense absorption and relatively long-lived excited states observed for **ReBphen** and **ReBbpy** are highly advantageous for construction of an efficient photocatalytic system, further investigations and understandings of tricarbonyl

rhenium(I)-arylborane complexes are of primary importance. Therefore, another two novel tricarbonyl rhenium(I) complexes having multiple arylborane charge transfer units, **ReB$_2$phen** and **ReB$_2$bpy**, were synthesized and the effects of the number of the arylborane charge transfer unit on the redox, spectroscopic and photophysical properties of the complexes were studied in detail as described in Chapter 3. The results indicated that **ReB$_2$phen** and **ReB$_2$bpy** showed lower-energy and more intense absorption compared to **ReBphen** and **ReBbpy**, respectively, and the molar absorption coefficients of the MLCT absorption bands were largely enhanced, demonstrating that the number of the arylborane charge transfer unit influence largely the spectroscopic characteristics of the complexes.

The radiative rate constants (k_r) of **ReB$_2$phen** and **ReB$_2$bpy** were almost twice larger than the relevant values of **ReBphen** and **ReBbpy**. The large k_r values of **ReB$_2$phen** and **ReB$_2$bpy** were qualitatively or phenomenologically explained by the Strickler-Berg-type relation for the fluorescence transition of a molecule. Furthermore, the nonradiative rate constant (k_{nr}) of **ReB$_2$bpy** was larger than that of **ReBbpy** in accord with the prediction from the energy gap law. However, the k_{nr} value of **ReB$_2$phen** is larger than that of **ReBphen** despite the same emission energies of the two complexes. Therefore, *T*-controlled emission lifetime measurements were also carried out for **ReB$_2$phen** and **ReB$_2$bpy**. The results demonstrated that the emission decay profile of **ReB$_2$bpy** required two exponential functions, which might be explained by the dual emission nature of the complex. The decrease in the ΔE values of **ReB$_2$phen** and **ReB$_2$bpy** compared to those of **ReBphen** and **ReBbpy**, respectively, suggested larger contributions of the thermal activation to the 4th ^{3}MLCT excited states to excited state decay of the complexes by the presence of the two arylborane charge transfer units

in the diimine ligands.

Furthermore, **ReB$_2$bpy** displayed more effective influences of the two arylborane units on the spectroscopic/photophysical properties compared to **ReB$_2$phen**, which was also confirmed by the results by absorption/emission spectroscopy, TD-DFT calculations, and *T*-controlled emission lifetime measurements.

Due to the intense absorption ranging in the wide UV–visible wavelength region and the relatively long-lived excited states, the novel tricarbonyl rhenium(I) complexes having one or two arylborane charge transfer unit(s) are expected to act as visible-light-driven catalysts for CO_2 photoreduction. Photocatalytic CO_2 reduction by the rhenium(I) complexes were then studied in detail as described in Chapter 4. Emission quenching studies demonstrated that the excited states of the complexes were quenched efficiently by triethanolamine (TEOA) in dynamic quenching pathways. The quenching mechanisms were discussed on the basis of Stern–Volmer analysis, calculated quenching rate constants (k_q), and the Gibbs free energy changes ($\Delta G_{ET}{}^0$) for electron transfer. The k_q value of the complex increased with an increase in the number of the arylborane charge transfer unit in the complex, indicating the more efficient electron transfer reactions proceeded for the complexes having the multiple borane centers. These results demonstrated that the presence of an "electron-accepting" arylborane charge transfer unit(s) in the periphery of the diimine ligand in $[Re(CO)_3LX]$ was highly advantageous for the "reductive" electron transfer reaction from TEOA to the excited triplet ^{3}MLCT state of the complex.

Furthermore, the photocatalytic activities of the complexes towards CO_2 reduction were studied by photoirradiation (λ > 400 nm) of the complexes in DMF/TEOA solutions under CO_2 gas atmosphere and the reaction products were then analyzed by

gas chromatography and capillary electrophoresis. All of the complexes were shown to be active catalysts for CO_2 photoreduction, although its efficiency was dependent on the nature of the complex. It was demonstrated that **ReB$_2$phen**/**ReBphen** and **ReB$_2$bpy**/**ReBbpy** showing relatively intense visible absorption in the visible region acted simultaneously as a photocatalyst and a photosensitizer for CO_2 reduction. Nonetheless, these arylborane complexes showed lower turnover numbers (TON) for CO_2 formation compared to **Rephen** or **Rebpy**, which could be explained by the low reducing abilities of the complexes as revealed by the positive shifts of the first reduction potentials of the complexes and also by the low reduction ability of the intermediate toward CO_2 reduction. The present results indicate that further optimization of the structures of a triarylborane charge transfer unit(s) in the diimine ligand of a tricarbonyl rhenium(I) complex will realize more efficient photocatalytic and solar–energy conversion systems.

In this thesis, the synthesis, spectroscopic/photophysical properties and photocatalytic ability towards CO_2 reduction for the novel tricarbonyl rhenium(I) complexes having an arylborane charge transfer unit(s) were studied in detail. All of the complexes showed characteristic spectroscopic and photophysical properties ascribed to the synergistic interactions between MLCT and π(aryl)-p(B) CT. The present complexes were shown to be active for photocatalytic CO_2 reduction. However, the efficiency of CO_2 reduction was dependent on the nature of the complex, suggesting that further improvements of the photocatalytic ability were required through optimization of the structure of an arylborane unit. It is known that the photocatalytic CO_2 reduction ability by a tricarbonyl rhenium(I) complex is strongly related to its excited-state properties,

and the excited-state properties of the complex are controllable by the ligand structure. Therefore, the diimine ligand structure and the number of the arylborane charge transfer unit are the important factors determining the photocatalytic ability. For further progress in the researches on tricarbonyl rhenium(I)–arylborane complexes, more sophisticated chemical modification and functionalization of both complex and ligand are absolutely necessary, as demonstrated by the present thesis. On the basis of such approaches, a new class of rhenium(I) complexes will be developed and it is expected strongly that such rhenium(I) complexes will play important roles in solar energy conversion systems in near future.

Acknowledgement

I would like to express my sincere gratitude to Professor Noboru Kitamura for his continuous guidance and encouragement throughout the works of this thesis.

I wish to express my sincere gratitude to Dr. Akitaka Ito, Associate Professor Eri Sakuda, Dr. Sho Fujii and Associate Professor Atsushi Miura for helpful suggestions and discussion.

I am deeply grateful to Professor Masako Kato, Associate Professor Atsushi Kobayashi and Dr. Masaki Yoshida for their kind help to X-ray crystal structure analysis experiment, ^{1}HNMR measurements and invaluable discussion.

I am deeply grateful to Professor Masako Kato, Professor Yasuchika Hasegawa and Associate Professor Atsushi Kobayashi for reviewing this thesis.

I wish to thank all the members of the Analytical Chemistry Laboratory (Kitamura Laboratory), Graduate School of Chemical Sciences and Engineering, Hokkaido University for their collaborations in the researches.

Finally, I would like to express my special thanks to my family and friends for their supports.

Sapporo, Hokkaido (2016)

Yuanyuan Kang

Publication List

1. Yuanyuan Kang, Akitaka Ito, Eri Sakuda and Noboru Kitamura

   Diimine Ligand Structure Effects on Photophysical Properties of Tricarbonyl Rhenium(I) Complexes Having Arylborane Charge Transfer Units.

   Journal of Photochemistry and Photobiology A: Chemistry **2015**, Vol. 313, 107–116.

2. Akitaka Ito, Yuanyuan Kang, Shota Saito, Eri Sakuda and Noboru Kitamura

   Photophysical and Photoredox Characteristics of a Novel Tricarbonyl(I) Rehnium(I) Complex Having an Arylborane-Appended Aromatic Diimine Ligand.

   Inorganic Chemistry **2012**, Vol. 51, No. 14, 7722–7732.

3. Yuanyuan Kang

   Synthesis, Photophysical and Photochemical Properties of a Novel Rhenium(I) Tricarbonyl Complex Having Arylborane Charge Transfer Unit."

   Bulletin of Japan Society of Coordination Chemistry **2012**, Vol. 59, 2–4.

Appendix: Calculated excited states of ReBphen/Rephen and ReBbpy/Rebpy in DMF.

ReBphen		**Rephen**		**ReBbpy**		**Rebpy**	
Energy / Wavelength	Oscillator Strength	Energy / Wavelength	Oscillator Strength	Energy / Wavelength	Oscillator Strength	Energy / Wavelength	Oscillator Strength
457.46	0.2848	427.29	0.0011	453.98	0.1423	433.34	0.0017
449.16	0.3892	412.24	0.0538	438.89	0.3204	415.62	0.0490
413.68	0.5653	383.68	0.0136	402.97	0.5572	363.02	0.0003
403.8	0.0248	376.74	0.0135	389.89	0.0208	318.03	0.0000
400.45	0.0187	357.94	0.0004	384.42	0.0057	314.94	0.0008
394.67	0.0050	325.02	0.0480	374.89	0.0004	314.71	0.0316
392.12	0.0358	324.97	0.0000	362.41	0.0022	311.15	0.0129
376.00	0.0004	312.17	0.0004	361.50	0.0452	303.69	0.063
371.61	0.0018	301.36	0.0205	356.58	0.2950	302.96	0.0042
369.72	0.0033	299.27	0.0004	352.67	0.0004	297.37	0.0019
367.97	0.0637	297.87	0.0344	343.72	0.0045	295.92	0.014
361.80	0.0004	296.80	0.0272	342.81	0.1366	290.30	0.0072
345.33	0.0375	295.17	0.0004	338.02	0.0019	287.12	0.3545
343.35	0.0291	287.16	0.0283	330.22	0.0041	277.54	0.0001
340.22	0.0300	282.75	0.0338	324.35	0.0176	272.79	0.0089
		281.16	0.0027			269.10	0.0005

277.03	0.0128	266.81	0.0423
268.49	0.0245	259.69	0.0056
265.29	0.016	256.16	0.0101
264.48	0.0436	250.52	0.0421
263.85	0.4843	248.83	0.0881
262.20	0.0432	242.1	0.0397
255.73	0.1295	240.82	0.1122
251.41	0.0116	237.53	0.0392
243.42	0.0014	236.92	0.0493
241.42	0.0285	235.54	0.0109
240.15	0.0113	235.52	0.0278
236.44	4E-4	233.15	0.0016
236.16	0.0024	232.62	0.0029
235.04	8E-4	231.02	0.014
234.94	0.0016	226.48	0.0229
231.5	0.0104	226.41	0.0013
230.83	0.0227	224.99	0.0089
230.35	0.0885	224.25	0.0064
224.75	0.0172	223.09	0.0094
223.51	0.0539	221.28	0.0023
223.17	0.0809	220.31	0.0214
221.23	0.0011	219.02	0.0131
220.58	0.0133	218.07	0.0431

220.49	0.0075	218.01	0.0142
219.45	0.1	217.14	0.0014
217.5	0.0018	215.74	0.0054
215.75	7E-4	215.54	0
212.83	0.0359	213.38	0.0185
212.72	0.0111	209.54	7E-4
212.32	0.0735	208.94	3E-4
211.39	0.0109	208.32	0.0399
210.77	3E-4	208.07	0.0024
209.89	0.0046	207.04	0.0098
209.01	0.0396	205.97	0.0013

Appendix: X-ray Structures of ReB_2phen

Table A-1. Atomic Coordinates of **ReB_2phen**

atom	x	y	z	Uani
B1	0.3897(6)	0.0983(5)	1.2698(4)	0.0547(18)
B2	0.0531(6)	0.2439(5)	1.6242(5)	0.063(2)
Br1	0.47639(9)	0.31415(8)	0.97797(7)	0.0643(4)
Re1	0.37664(2)	0.425543(17)	0.878024(14)	0.05332(11)
N1	0.2153(4)	0.3721(3)	0.9395(3)	0.0525(13)
N2	0.3086(4)	0.4780(3)	0.9589(2)	0.0443(11)
O1	0.4558(5)	0.3370(4)	0.7734(3)	0.0888(17)
O2	0.5947(4)	0.5129(3)	0.8089(3)	0.0821(16)
O3	0.2392(9)	0.5551(6)	0.7663(5)	0.073(3)
C1	0.1709(5)	0.3195(4)	0.9284(4)	0.0611(17)
C2	0.0662(6)	0.2902(4)	0.9697(4)	0.0680(19)
C3	0.0033(5)	0.3147(4)	1.0250(4)	0.0561(16)
C4	0.0474(5)	0.3708(3)	1.0383(3)	0.0468(14)
C5	0.1547(4)	0.3981(3)	0.9936(3)	0.0397(12)
C6	0.3543(5)	0.5306(4)	0.9691(3)	0.0501(14)
C7	0.3036(5)	0.5619(4)	1.0226(4)	0.0577(17)
C8	0.1971(5)	0.5391(4)	1.0689(3)	0.0516(15)
C9	0.1461(5)	0.4824(4)	1.0605(3)	0.0498(14)
C10	0.2033(4)	0.4540(4)	1.0055(3)	0.0432(13)
C11	-0.0085(5)	0.4011(4)	1.0935(4)	0.0570(17)
C12	0.0368(5)	0.4543(4)	1.1057(3)	0.0536(15)
C13	0.4277(5)	0.3705(4)	0.8121(4)	0.0590(17)
C14	0.5138(5)	0.4786(4)	0.8344(4)	0.0598(17)
C15	0.290(2)	0.5074(15)	0.8086(12)	0.038(4)
C16	0.1418(5)	0.5728(4)	1.1223(4)	0.0585(17)
C17	0.0995(6)	0.6046(5)	1.1642(4)	0.0644(19)
C18	-0.0582(5)	0.3572(4)	1.7843(4)	0.0585(17)
C19	-0.1321(5)	0.3087(4)	1.7820(4)	0.0609(17)
C20	-0.0965(5)	0.2725(4)	1.7317(4)	0.0603(17)
C21	0.0150(5)	0.2839(4)	1.6809(4)	0.0577(17)
C22	0.0854(5)	0.3340(5)	1.6842(4)	0.0631(18)

C23	0.0513(5)	0.3689(5)	1.7360(4)	0.0638(18)
C24	-0.2497(6)	0.2950(5)	1.8354(4)	0.081(2)
C25	-0.1796(6)	0.2236(5)	1.7280(5)	0.081(2)
C26	0.1281(6)	0.4239(5)	1.7368(5)	0.086(3)
C27	0.2052(6)	0.3472(6)	1.6333(5)	0.089(3)
C28	0.0785(5)	0.2941(4)	1.5403(4)	0.0546(15)
C29	0.1768(6)	0.2715(4)	1.4931(4)	0.0609(17)
C30	0.1970(6)	0.3143(5)	1.4198(5)	0.082(2)
C31	0.1252(8)	0.3795(6)	1.3882(5)	0.102(3)
C32	0.0295(7)	0.4042(5)	1.4339(5)	0.092(3)
C33	0.0058(6)	0.3625(4)	1.5092(4)	0.0664(19)
C34	0.2637(6)	0.1995(5)	1.5197(4)	0.077(2)
C35	0.1458(10)	0.4274(8)	1.3062(6)	0.170(6)
C36	-0.1053(7)	0.3942(5)	1.5528(5)	0.088(3)
C37	0.0624(5)	0.1514(4)	1.6518(4)	0.0600(17)
C38	0.1220(6)	0.1024(5)	1.7092(5)	0.079(2)
C39	0.1299(7)	0.0212(6)	1.7332(6)	0.108(3)
C40	0.0785(8)	-0.0151(6)	1.7055(7)	0.119(4)
C41	0.0201(6)	0.0335(5)	1.6474(6)	0.092(3)
C42	0.0112(5)	0.1143(4)	1.6210(4)	0.0605(17)
C43	0.1851(7)	0.1374(7)	1.7447(5)	0.107(3)

Table A-2. Bond Distances (Å) of **ReB$_2$phen**.

atom1	atom2	distance	atom1	atom2	distance
N2	C6	1.33(1)	C29	C28	1.41(1)
N2	C10	1.389(6)	C29	C34	1.51(1)
N2	Re1	2.151(5)	C29	C30	1.37(1)
N1	C5	1.358(9)	C69	C74	1.51(2)
N1	C1	1.33(1)	C67	C72	1.39(1)
N1	Re1	2.182(5)	C11	H11	0.95
C5	C4	1.413(7)	C11	C12	1.36(1)
C5	C10	1.42(1)	C71	C72	1.396(8)
C8	C16	1.42(1)	C71	C76	1.50(1)
C8	C9	1.41(1)	C6	H6	0.949
C8	C7	1.393(8)	C72	C75	1.52(1)
C16	C17	1.18(1)	C21	C22	1.41(1)
C68	C69	1.413(8)	C21	B2	1.55(1)
C68	C67	1.39(1)	C12	H12	0.951
C68	C73	1.51(1)	C37	C42	1.41(1)
C4	C3	1.41(1)	C37	C38	1.42(1)
C4	C11	1.41(1)	C37	B2	1.57(1)
C20	C21	1.444(8)	C28	C33	1.392(9)
C20	C19	1.38(1)	C28	B2	1.57(1)
C20	C25	1.51(1)	C22	C23	1.39(1)
C9	C10	1.39(1)	C22	C27	1.523(9)
C9	C12	1.439(8)	C19	C24	1.524(9)
C65	C66	1.188(8)	C1	H1	0.951
C65	C3	1.429(8)	C1	C2	1.383(9)
C66	C67	1.443(8)	C75	H75A	0.98
C7	H7	0.951	C75	H75B	0.979
C7	C6	1.39(1)	C75	H75C	0.981
C70	C69	1.39(1)	C34	H34A	0.98
C70	C71	1.41(1)	C34	H34B	0.979
C70	B1	1.597(9)	C34	H34C	0.981
C3	C2	1.37(1)	C30	H30	0.949
C18	C17	1.43(1)	C30	C31	1.35(1)
C18	C19	1.41(1)	C33	C36	1.53(1)
C18	C23	1.406(8)	C33	C32	1.40(1)

C42	C45	1.50(1)	C43	H43A	0.98
C42	C41	1.37(1)	C43	H43B	0.979
C24	H24A	0.979	C43	H43C	0.98
C24	H24B	0.98	C43	C38	1.55(2)
C24	H24C	0.98	C26	H26A	0.98
C76	H76A	0.981	C26	H26B	0.98
C76	H76B	0.98	C26	H26C	0.979
C76	H76C	0.98	C36	H36A	0.979
C45	H45A	0.981	C36	H36B	0.979
C45	H45B	0.98	C36	H36C	0.98
C45	H45C	0.98	C32	H32	0.95
C73	H73A	0.98	C74	H74A	0.981
C73	H73B	0.981	C74	H74B	0.979
C73	H73C	0.981	C74	H74C	0.981
C39	H39	0.95	C27	H27A	0.981
C39	C38	1.38(1)	C27	H27B	0.98
C39	C40	1.35(2)	C27	H27C	0.979
C25	H25A	0.981	C40	C44	1.53(2)
C25	H25B	0.98	C44	H44A	0.98
C25	H25C	0.98	C44	H44B	0.98
C35	H35A	0.98	C44	H44C	0.98
C35	H35B	0.98	Re1	C13	1.917(9)
C35	H35C	0.98	Re1	C14	1.904(6)
C35	C31	1.53(1)	Re1	Br1	2.585(1)
C2	H2	0.949	Re1	C15	1.94(2)
C23	C26	1.52(1)	O2	C14	1.153(8)
C41	H41	0.95	O1	C13	1.14(1)
C41	C40	1.42(2)	C15	O3	1.15(2)
C31	C32	1.39(1)			

Table A-3. Bond Angles (deg) of **ReB$_2$phen**.

atom	atom	atom	angle	atom	atom	atom	angle
C6	N2	C10	116.5(5)	C71	C70	B1	120.5(6)
C6	N2	Re1	127.9(4)	C4	C3	C65	121.1(6)
C10	N2	Re1	115.6(4)	C4	C3	C2	118.4(6)
C5	N1	C1	118.2(6)	C65	C3	C2	120.5(7)
C5	N1	Re1	114.6(4)	C17	C18	C19	118.0(7)
C1	N1	Re1	127.1(5)	C17	C18	C23	121.4(7)
N1	C5	C4	122.4(5)	C19	C18	C23	120.6(7)
N1	C5	C10	117.9(5)	C28	C29	C34	122.7(7)
C4	C5	C10	119.7(5)	C28	C29	C30	120.9(7)
C16	C8	C9	121.5(6)	C34	C29	C30	116.4(7)
C16	C8	C7	120.6(6)	C68	C69	C70	121.1(7)
C9	C8	C7	117.9(6)	C68	C69	C74	117.3(7)
C8	C16	C17	176.0(8)	C70	C69	C74	121.6(7)
C69	C68	C67	118.4(7)	C16	C17	C18	175.1(9)
C69	C68	C73	119.9(6)	C68	C67	C66	117.8(6)
C67	C68	C73	121.6(7)	C68	C67	C72	121.7(7)
C5	C4	C3	117.6(6)	C66	C67	C72	120.5(7)
C5	C4	C11	118.1(5)	C4	C11	H11	118.5
C3	C4	C11	124.2(6)	C4	C11	C12	123.0(6)
C21	C20	C19	121.1(7)	H11	C11	C12	118.5
C21	C20	C25	120.1(7)	C70	C71	C72	120.6(7)
C19	C20	C25	118.7(7)	C70	C71	C76	121.6(7)
C8	C9	C10	118.3(6)	C72	C71	C76	117.8(7)
C8	C9	C12	122.5(6)	N2	C6	C7	124.1(6)
C10	C9	C12	119.2(6)	N2	C6	H6	118
C66	C65	C3	177.6(8)	C7	C6	H6	117.9
C65	C66	C67	177.0(8)	C67	C72	C71	119.2(7)
C8	C7	H7	120	C67	C72	C75	119.8(7)
C8	C7	C6	119.9(6)	C71	C72	C75	120.9(7)
H7	C7	C6	120.2	C20	C21	C22	117.4(7)
C69	C70	C71	118.9(7)	C20	C21	B2	120.6(6)
C69	C70	B1	120.6(6)	C22	C21	B2	121.9(7)

N2	C10	C5	115.9(5)	C28	C33	C36	123.5(7)
N2	C10	C9	123.3(6)	C28	C33	C32	120.0(7)
C5	C10	C9	120.7(6)	C36	C33	C32	116.4(7)
C9	C12	C11	119.3(6)	C37	C42	C45	122.7(7)
C9	C12	H12	120.3	C37	C42	C41	119.5(7)
C11	C12	H12	120.4	C45	C42	C41	117.8(7)
C42	C37	C38	117.6(7)	C19	C24	H24A	109.5
C42	C37	B2	121.5(7)	C19	C24	H24B	109.4
C38	C37	B2	120.9(7)	C19	C24	H24C	109.5
C29	C28	C33	117.2(7)	H24A	C24	H24B	109.4
C29	C28	B2	121.0(7)	H24A	C24	H24C	109.6
C33	C28	B2	121.8(7)	H24B	C24	H24C	109.5
C21	C22	C23	121.6(7)	C71	C76	H76A	109.4
C21	C22	C27	120.1(7)	C71	C76	H76B	109.4
C23	C22	C27	118.2(7)	C71	C76	H76C	109.5
C20	C19	C18	119.6(7)	H76A	C76	H76B	109.4
C20	C19	C24	120.0(7)	H76A	C76	H76C	109.6
C18	C19	C24	120.4(6)	H76B	C76	H76C	109.6
N1	C1	H1	118.7	C42	C45	H45A	109.5
N1	C1	C2	122.7(7)	C42	C45	H45B	109.5
H1	C1	C2	118.6	C42	C45	H45C	109.6
C72	C75	H75A	109.5	H45A	C45	H45B	109.5
C72	C75	H75B	109.5	H45A	C45	H45C	109.4
C72	C75	H75C	109.4	H45B	C45	H45C	109.4
H75A	C75	H75B	109.4	C68	C73	H73A	109.5
H75A	C75	H75C	109.4	C68	C73	H73B	109.5
H75B	C75	H75C	109.5	C68	C73	H73C	109.5
C29	C34	H34A	109.5	H73A	C73	H73B	109.5
C29	C34	H34B	109.4	H73A	C73	H73C	109.5
C29	C34	H34C	109.5	H73B	C73	H73C	109.4
H34A	C34	H34B	109.6	H39	C39	C38	119
H34A	C34	H34C	109.4	H39	C39	C40	119
H34B	C34	H34C	109.5	C38	C39	C40	122(1)
C29	C30	H30	118.5	C20	C25	H25A	109.4
C29	C30	C31	122.8(9)	C20	C25	H25B	109.5
H30	C30	C31	118.6	C20	C25	H25C	109.5

H25A	C25	H25B	109.4	H36A	C36	H36B	109.6
H25A	C25	H25C	109.5	H36A	C36	H36C	109.5
H25B	C25	H25C	109.5	H36B	C36	H36C	109.3
H35A	C35	H35B	109	C33	C32	C31	121.8(8)
H35A	C35	H35C	109	C33	C32	H32	119.1
H35A	C35	C31	110	C31	C32	H32	119.2
H35B	C35	H35C	109	C69	C74	H74A	109.4
H35B	C35	C31	109	C69	C74	H74B	109.5
H35C	C35	C31	109	C69	C74	H74C	109.5
C3	C2	C1	120.6(7)	H74A	C74	H74B	109.5
C3	C2	H2	119.7	H74A	C74	H74C	109.5
C1	C2	H2	119.7	H74B	C74	H74C	109.5
C18	C23	C22	119.6(7)	C22	C27	H27A	109.5
C18	C23	C26	120.2(7)	C22	C27	H27B	109.4
C22	C23	C26	120.1(7)	C22	C27	H27C	109.5
C42	C41	H41	118.7	H27A	C27	H27B	109.4
C42	C41	C40	122.5(9)	H27A	C27	H27C	109.5
H41	C41	C40	119	H27B	C27	H27C	109.5
C30	C31	C35	123(1)	C37	C38	C39	120.7(8)
C30	C31	C32	117.3(9)	C37	C38	C43	121.5(8)
C35	C31	C32	119.2(9)	C39	C38	C43	117.7(8)
H43A	C43	H43B	109	C39	C40	C41	117(1)
H43A	C43	H43C	109	C39	C40	C44	123(1)
H43A	C43	C38	109.5	C41	C40	C44	119(1)
H43B	C43	H43C	110	C40	C44	H44A	110
H43B	C43	C38	109.6	C40	C44	H44B	109
H43C	C43	C38	109.4	C40	C44	H44C	109
C23	C26	H26A	109.4	H44A	C44	H44B	109
C23	C26	H26B	109.5	H44A	C44	H44C	109
C23	C26	H26C	109.5	H44B	C44	H44C	109
H26A	C26	H26B	109.4	C21	B2	C37	118.9(7)
H26A	C26	H26C	109.5	C21	B2	C28	121.1(7)
H26B	C26	H26C	109.5	C37	B2	C28	120.0(7)
C33	C36	H36A	109.5	N2	Re1	N1	75.9(2)
C33	C36	H36B	109.5	N2	Re1	C13	174.3(3)
C33	C36	H36C	109.4	N2	Re1	C14	96.1(3)

N2	Re1	Br1	84.8(1)
N2	Re1	C15	92.7(8)
N1	Re1	C13	98.7(3)
N1	Re1	C14	171.9(3)
N1	Re1	Br1	85.3(1)
N1	Re1	C15	90.4(8)
C13	Re1	C14	89.3(3)
C13	Re1	Br1	92.9(2)
C13	Re1	C15	89.3(8)
C14	Re1	Br1	93.1(2)
C14	Re1	C15	91.0(8)
Br1	Re1	C15	175.4(8)
Re1	C13	O1	178.5(7)
Re1	C14	O2	177.5(6)
Re1	C15	O3	178(2)

Table A-4. Torsion Angles (deg) of **ReB$_2$phen**.

atom1	atom2	atom3	atom4	angle
C10	N2	C6	H6	180
Re1	N2	C6	C7	-179.5(5)
Re1	N2	C6	H6	0.6
C6	N2	C10	C5	-179.5(5)
C6	N2	C10	C9	-0.1(9)
Re1	N2	C10	C5	-0.0(7)
Re1	N2	C10	C9	179.3(5)
C6	N2	Re1	N1	-179.9(6)
C6	N2	Re1	C13	-160(2)
C6	N2	Re1	C14	-0.9(6)
C6	N2	Re1	Br1	-93.4(5)
C6	N2	Re1	C15	90.4(9)
C10	N2	Re1	N1	0.7(4)
C10	N2	Re1	C13	21(3)
C10	N2	Re1	C14	179.7(4)
C10	N2	Re1	Br1	87.2(4)
C10	N2	Re1	C15	-89.0(9)
C1	N1	C5	C4	-0.4(9)
C1	N1	C5	C10	-179.5(6)
Re1	N1	C5	C4	-179.1(4)
Re1	N1	C5	C10	1.8(7)
C5	N1	C1	H1	-179.6
C5	N1	C1	C2	0(1)
Re1	N1	C1	H1	-1
Re1	N1	C1	C2	178.7(5)
C5	N1	Re1	N2	-1.3(4)
C5	N1	Re1	C13	-179.4(4)
C5	N1	Re1	C14	-8(2)
C5	N1	Re1	Br1	-87.1(4)
C5	N1	Re1	C15	91.3(9)
C1	N1	Re1	N2	-179.9(6)
C1	N1	Re1	C13	2.1(6)

C1	N1	Re1	C14	173(2)
C1	N1	Re1	Br1	94.4(6)
C1	N1	Re1	C15	-87.2(9)
N1	C5	C4	C3	0.2(9)
N1	C5	C4	C11	-179.6(6)
C10	C5	C4	C3	179.3(6)
C10	C5	C4	C11	-0.5(9)
N1	C5	C10	N2	-1.2(8)
N1	C5	C10	C9	179.4(6)
C4	C5	C10	N2	179.7(5)
C4	C5	C10	C9	0.3(9)
C9	C8	C16	C17	157(11)
C7	C8	C16	C17	-23(12)
C16	C8	C9	C10	-177.9(6)
C16	C8	C9	C12	1(1)
C7	C8	C9	C10	1.6(9)
C7	C8	C9	C12	-179.6(6)
C16	C8	C7	H7	-2
C16	C8	C7	C6	177.7(6)
C9	C8	C7	H7	178.3
C9	C8	C7	C6	-2(1)
C8	C16	C17	C18	61(18)
C67	C68	C69	C70	-3(1)
C67	C68	C69	C74	178.7(7)
C73	C68	C69	C70	179.3(7)
C73	C68	C69	C74	1(1)
C69	C68	C67	C66	-176.3(7)
C69	C68	C67	C72	4(1)
C73	C68	C67	C66	2(1)
C73	C68	C67	C72	-178.0(7)
C69	C68	C73	H73A	-172
C69	C68	C73	H73B	-52
C69	C68	C73	H73C	68
C67	C68	C73	H73A	10
C67	C68	C73	H73B	129.9
C67	C68	C73	H73C	-110.1

C5	C4	C3	C65	179.0(6)
C5	C4	C3	C2	0.3(9)
C11	C4	C3	C65	-1(1)
C11	C4	C3	C2	-180.0(7)
C5	C4	C11	H11	-179.3
C5	C4	C11	C12	1(1)
C3	C4	C11	H11	1
C3	C4	C11	C12	-179.1(7)
C19	C20	C21	C22	-1(1)
C19	C20	C21	B2	-179.2(7)
C25	C20	C21	C22	176.2(7)
C25	C20	C21	B2	-2(1)
C21	C20	C19	C18	-0(1)
C21	C20	C19	C24	-179.4(7)
C25	C20	C19	C18	-177.3(7)
C25	C20	C19	C24	4(1)
C21	C20	C25	H25A	112.1
C21	C20	C25	H25B	-8
C21	C20	C25	H25C	-127.8
C19	C20	C25	H25A	-71
C19	C20	C25	H25B	169.2
C19	C20	C25	H25C	49
C8	C9	C10	N2	-0.7(9)
C8	C9	C10	C5	178.7(6)
C12	C9	C10	N2	-179.6(6)
C12	C9	C10	C5	-0.2(9)
C8	C9	C12	C11	-178.5(6)
C8	C9	C12	H12	1
C10	C9	C12	C11	0(1)
C10	C9	C12	H12	-179.7
C3	C65	C66	C67	-9(31)
C66	C65	C3	C4	158(18)
C66	C65	C3	C2	-23(19)
C65	C66	C67	C68	33(15)
C65	C66	C67	C72	-147(14)
C8	C7	C6	N2	1(1)

C8	C7	C6	H6	-179
H7	C7	C6	N2	-179
H7	C7	C6	H6	1
C71	C70	C69	C68	0(1)
C71	C70	C69	C74	179.2(7)
B1	C70	C69	C68	179.8(7)
B1	C70	C69	C74	-2(1)
C69	C70	C71	C72	0(1)
C69	C70	C71	C76	-179.1(7)
B1	C70	C71	C72	-178.9(7)
B1	C70	C71	C76	2(1)
C4	C3	C2	C1	-0(1)
C4	C3	C2	H2	179.7
C65	C3	C2	C1	-179.2(7)
C65	C3	C2	H2	1
C19	C18	C17	C16	-32(10)
C23	C18	C17	C16	147(10)
C17	C18	C19	C20	178.3(7)
C17	C18	C19	C24	-3(1)
C23	C18	C19	C20	-0(1)
C23	C18	C19	C24	178.9(7)
C17	C18	C23	C22	-176.6(7)
C17	C18	C23	C26	-1(1)
C19	C18	C23	C22	2(1)
C19	C18	C23	C26	177.5(7)
C34	C29	C28	C33	179.0(7)
C34	C29	C28	B2	-1(1)
C30	C29	C28	C33	-2(1)
C30	C29	C28	B2	178.4(8)
C28	C29	C34	H34A	82
C28	C29	C34	H34B	-38
C28	C29	C34	H34C	-158.2
C30	C29	C34	H34A	-97.4
C30	C29	C34	H34B	142.5
C30	C29	C34	H34C	22
C28	C29	C30	H30	179.3

C28	C29	C30	C31	-0(1)
C34	C29	C30	H30	-1
C34	C29	C30	C31	178.9(8)
C68	C69	C74	H74A	-166.6
C68	C69	C74	H74B	-47
C68	C69	C74	H74C	73
C70	C69	C74	H74A	15
C70	C69	C74	H74B	134.7
C70	C69	C74	H74C	-105.3
C68	C67	C72	C71	-3(1)
C68	C67	C72	C75	-179.1(7)
C66	C67	C72	C71	177.1(7)
C66	C67	C72	C75	1(1)
C4	C11	C12	C9	-1(1)
C4	C11	C12	H12	179.4
H11	C11	C12	C9	179.4
H11	C11	C12	H12	-1
C70	C71	C72	C67	1(1)
C70	C71	C72	C75	176.9(7)
C76	C71	C72	C67	-179.7(7)
C76	C71	C72	C75	-4(1)
C70	C71	C76	H76A	-14
C70	C71	C76	H76B	106.1
C70	C71	C76	H76C	-133.9
C72	C71	C76	H76A	166.6
C72	C71	C76	H76B	-73
C72	C71	C76	H76C	47
C67	C72	C75	H75A	-135.2
C67	C72	C75	H75B	-15
C67	C72	C75	H75C	104.9
C71	C72	C75	H75A	49
C71	C72	C75	H75B	168.7
C71	C72	C75	H75C	-71
C20	C21	C22	C23	2(1)
C20	C21	C22	C27	178.7(7)
B2	C21	C22	C23	-179.1(7)

B2	C21	C22	C27	-3(1)
C20	C21	B2	C37	-58(1)
C20	C21	B2	C28	120.2(8)
C22	C21	B2	C37	123.6(8)
C22	C21	B2	C28	-58(1)
C38	C37	C42	C45	176.9(7)
C38	C37	C42	C41	0(1)
B2	C37	C42	C45	-3(1)
B2	C37	C42	C41	-179.1(8)
C42	C37	C38	C39	1(1)
C42	C37	C38	C43	177.7(8)
B2	C37	C38	C39	-180.0(8)
B2	C37	C38	C43	-3(1)
C42	C37	B2	C21	131.9(8)
C42	C37	B2	C28	-46(1)
C38	C37	B2	C21	-48(1)
C38	C37	B2	C28	134.3(8)
C29	C28	C33	C36	179.0(7)
C29	C28	C33	C32	2(1)
B2	C28	C33	C36	-1(1)
B2	C28	C33	C32	-178.0(8)
C29	C28	B2	C21	137.0(8)
C29	C28	B2	C37	-45(1)
C33	C28	B2	C21	-43(1)
C33	C28	B2	C37	135.2(8)
C21	C22	C23	C18	-3(1)
C21	C22	C23	C26	-178.7(7)
C27	C22	C23	C18	-179.3(7)
C27	C22	C23	C26	5(1)
C21	C22	C27	H27A	117.5
C21	C22	C27	H27B	-2
C21	C22	C27	H27C	-122.4
C23	C22	C27	H27A	-66
C23	C22	C27	H27B	174.1
C23	C22	C27	H27C	54
C20	C19	C24	H24A	-69

C20	C19	C24	H24B	171
C20	C19	C24	H24C	51
C18	C19	C24	H24A	111.9
C18	C19	C24	H24B	-8
C18	C19	C24	H24C	-127.9
N1	C1	C2	C3	0(1)
N1	C1	C2	H2	-179.9
H1	C1	C2	C3	-179.9
H1	C1	C2	H2	0
C29	C30	C31	C35	-179.2(9)
C29	C30	C31	C32	2(1)
H30	C30	C31	C35	1
H30	C30	C31	C32	-177.5
C28	C33	C36	H36A	-55
C28	C33	C36	H36B	-175.1
C28	C33	C36	H36C	65
C32	C33	C36	H36A	122.1
C32	C33	C36	H36B	2
C32	C33	C36	H36C	-117.8
C28	C33	C32	C31	-0(1)
C28	C33	C32	H32	179.8
C36	C33	C32	C31	-177.5(9)
C36	C33	C32	H32	3
C37	C42	C45	H45A	69
C37	C42	C45	H45B	-52
C37	C42	C45	H45C	-171.5
C41	C42	C45	H45A	-114.8
C41	C42	C45	H45B	125.1
C41	C42	C45	H45C	5
C37	C42	C41	H41	-179.4
C37	C42	C41	C40	1(1)
C45	C42	C41	H41	4
C45	C42	C41	C40	-176.2(9)
H39	C39	C38	C37	177.5
H39	C39	C38	C43	0
C40	C39	C38	C37	-2(2)

C40	C39	C38	C43	-180(1)
H39	C39	C40	C41	-177
H39	C39	C40	C44	1
C38	C39	C40	C41	3(2)
C38	C39	C40	C44	-179(1)
H35A	C35	C31	C30	20
H35A	C35	C31	C32	-161
H35B	C35	C31	C30	-100
H35B	C35	C31	C32	79
H35C	C35	C31	C30	140
H35C	C35	C31	C32	-41
C18	C23	C26	H26A	119.5
C18	C23	C26	H26B	0
C18	C23	C26	H26C	-120.5
C22	C23	C26	H26A	-65
C22	C23	C26	H26B	175.3
C22	C23	C26	H26C	55
C42	C41	C40	C39	-2(2)
C42	C41	C40	C44	180(1)
H41	C41	C40	C39	178
H41	C41	C40	C44	0
C30	C31	C32	C33	-2(1)
C30	C31	C32	H32	178.1
C35	C31	C32	C33	179.6(9)
C35	C31	C32	H32	-1
H43A	C43	C38	C37	72
H43A	C43	C38	C39	-111
H43B	C43	C38	C37	-48
H43B	C43	C38	C39	129
H43C	C43	C38	C37	-168.5
H43C	C43	C38	C39	9
C39	C40	C44	H44A	41
C39	C40	C44	H44B	-79
C39	C40	C44	H44C	161
C41	C40	C44	H44A	-141
C41	C40	C44	H44B	99

C41	C40	C44	H44C	-21
N2	Re1	C13	O1	-27(27)
N1	Re1	C13	O1	-7(25)
C14	Re1	C13	O1	174(25)
Br1	Re1	C13	O1	-93(25)
C15	Re1	C13	O1	83(25)
N2	Re1	C14	O2	25(14)
N1	Re1	C14	O2	32(16)
C13	Re1	C14	O2	-157(14)
Br1	Re1	C14	O2	110(14)
C15	Re1	C14	O2	-68(14)
N2	Re1	C15	O3	171(76)
N1	Re1	C15	O3	95(77)
C13	Re1	C15	O3	-4(76)
C14	Re1	C15	O3	-93(77)
Br1	Re1	C15	O3	115(73)

Table A-5. Anisotropic displacement parameters

atom	U11	U22	U33	U12	U13	U23
Re1	0.0491(15)	0.068(2)	0.0483(17)	-0.033(14)	0.0121(10)	-0.021(12)
B1	0.048(4)	0.059(5)	0.054(5)	-0.020(4)	-0.001(3)	-0.012(3)
B2	0.043(4)	0.078(6)	0.079(6)	-0.050(5)	0.008(3)	-0.010(3)
Br1	0.0504(6)	0.075(8)	0.0548(7)	-0.0194(6)	0.0006(5)	-0.0051(5)
O1	0.093(4)	0.103(5)	0.087(4)	-0.070(4)	0.012(3)	-0.014(3)
O2	0.056(3)	0.111(5)	0.081(4)	-0.039(3)	0.012(2)	-0.040(3)
O3	0.080(6)	0.079(7)	0.059(6)	-0.023(5)	-0.008(4)	-0.022(5)
N1	0.045(3)	0.059(3)	0.056(3)	-0.031(3)	0.009(2)	-0.015(2)
N2	0.048(2)	0.057(3)	0.034(3)	-0.022(2)	-0.003(19)	-0.015(2)
C1	0.054(3)	0.061(4)	0.067(5)	-0.029(4)	0.010(3)	-0.019(3)
C2	0.066(4)	0.062(5)	0.077(5)	-0.033(4)	0.009(3)	-0.024(3)
C3	0.048(3)	0.048(4)	0.062(4)	-0.015(3)	0.002(3)	-0.011(3)
C4	0.042(3)	0.041(3)	0.044(3)	-0.008(3)	-0.002(2)	-0.002(2)
C5	0.038(3)	0.040(3)	0.034(3)	-0.010(3)	-0.004(2)	-0.003(2)
C6	0.052(3)	0.060(4)	0.044(4)	-0.029(3)	0.000(2)	-0.009(3)
C7	0.051(3)	0.071(5)	0.060(4)	-0.036(4)	-0.007(3)	-0.009(3)
C8	0.047(3)	0.061(4)	0.049(4)	-0.029(3)	-0.007(3)	0.003(3)
C9	0.049(3)	0.057(4)	0.041(3)	-0.018(3)	-0.007(2)	-0.003(3)
C10	0.036(3)	0.053(4)	0.039(3)	-0.020(3)	0.000(2)	-0.006(2)
C11	0.038(3)	0.067(5)	0.052(4)	-0.019(3)	0.004(3)	-0.001(3)
C12	0.046(3)	0.062(4)	0.043(4)	-0.023(3)	0.008(2)	0.000(3)
C13	0.053(3)	0.064(5)	0.057(4)	-0.030(4)	0.009(3)	-0.012(3)
C14	0.052(3)	0.079(5)	0.052(4)	-0.036(4)	0.006(3)	-0.013(3)
C15	0.042(8)	0.040(7)	0.034(5)	-0.019(5)	-0.002(5)	-0.005(5)
C16	0.053(3)	0.071(5)	0.057(4)	-0.037(4)	-0.004(3)	0.000(3)
C17	0.057(4)	0.089(6)	0.062(5)	-0.045(4)	-0.013(3)	-0.002(3)
C18	0.049(3)	0.081(5)	0.055(4)	-0.041(4)	-0.002(3)	-0.007(3)
C19	0.051(3)	0.074(5)	0.065(5)	-0.044(4)	0.006(3)	-0.009(3)
C20	0.050(3)	0.067(5)	0.067(5)	-0.039(4)	0.008(3)	-0.010(3)
C21	0.057(3)	0.069(5)	0.056(4)	-0.036(4)	0.002(3)	-0.014(3)
C22	0.048(3)	0.086(5)	0.065(5)	-0.048(4)	0.006(3)	-0.009(3)
C23	0.052(3)	0.086(5)	0.065(5)	-0.045(4)	-0.002(3)	-0.008(3)
C24	0.064(4)	0.106(7)	0.080(6)	-0.064(5)	0.028(4)	-0.019(4)

C25	0.063(4)	0.114(7)	0.088(6)	-0.069(6)	0.016(4)	-0.030(4)
C26	0.059(4)	0.128(8)	0.108(7)	-0.082(6)	-0.007(4)	-0.018(4)
C27	0.059(4)	0.134(8)	0.098(6)	-0.082(6)	0.024(4)	-0.029(4)
C28	0.062(4)	0.048(4)	0.054(4)	-0.026(3)	0.002(3)	-0.010(3)
C30	0.069(4)	0.069(5)	0.072(6)	-0.015(5)	0.019(4)	0.001(4)
C31	0.093(6)	0.095(7)	0.082(7)	-0.019(6)	0.034(5)	-0.029(5)
C32	0.091(6)	0.076(6)	0.091(7)	-0.025(5)	0.004(5)	-0.009(4)
C33	0.067(4)	0.056(5)	0.071(5)	-0.030(4)	0.010(3)	-0.014(3)
C34	0.067(4)	0.083(6)	0.063(5)	-0.035(4)	0.014(3)	0.006(4)
C35	0.140(9)	0.15 (12)	0.105(9)	0.016(9)	0.039(7)	-0.002(8)
C36	0.085(5)	0.084(6)	0.085(6)	-0.046(5)	0.000(4)	0.019(4)
C37	0.054(3)	0.066(5)	0.058(4)	-0.030(4)	0.004(3)	-0.005(3)
C38	0.065(4)	0.075(6)	0.072(6)	-0.015(5)	0.002(4)	-0.005(4)
C39	0.071(5)	0.103(8)	0.142(10)	-0.026(7)	-0.040(6)	-0.004(5)
C40	0.075(6)	0.071(7)	0.190(13)	-0.032(8)	-0.033(7)	0.009(5)
C41	0.059(4)	0.068(6)	0.138(9)	-0.035(6)	-0.008(5)	-0.009(4)
C42	0.055(3)	0.057(4)	0.058(4)	-0.026(4)	0.010(3)	-0.002(3)